Co-locating geodetic reference points

On the design and performance of an Integrated Geodetic Reference Station

J. (Jurjen) C. Kamphuis

Technische Universiteit Delft

TU Delft Delft University of Technology

Challenge the future

Co-locating geodetic reference points

On the design and performance of an Integrated Geodetic Reference Station

by

J. (Jurjen) C. Kamphuis

in partial fulfilment of the requirements for the degree of

Master of Science

in Applied Earth Sciences

at the Delft University of Technology,

to be defended publicly on April 5, 2019 at 14:30.

Student number:	4030230	
Project duration:	August 22, 2017 – April 5, 2019	
Thesis committee:	Prof. dr. ir. R. F. Hanssen,	TU Delft
	Dr. ir. H. van der Marel,	TU Delft
	Dr. I. V. Smal,	TU Delft

TU Delft Delft University of Technology

Abstract

Geodesists use multiple methods to monitor surface deformation. This gives the opportunity to integrate complementary data for better interpretation of deformation processes. The integration of data has to deal with: (1) spatio-temporal differences in sampling methodologies, meaning that observed objects are not the same and thus observed processes may stem from different sources; and (2) physical differences in the methodologies leading to different kinds of coordinate reference systems with possibly different datums. This makes integration of data challenging.

In this thesis, we address one of the fundamental roots to this integration problem, by developing co-located reference points for multiple geodetic monitoring methods. This will ensure that, for multiple geodetic monitoring methods, one common deformation process is observed. This eliminates interpolation between observations. I show the main requirements for an Integrating Geodetic Reference Station (IGRS), present a design for a fully functional IGRS and describe its performance. Furthermore, the protocols for deployment and operational use are given. Benchmarks for InSAR, GNSS, levelling, LiDAR, and gravimetry are present on the IGRS. From field tests, it is found that presented radar reflectors have a 1-σ measurement precision of <0.5 mm in the Line-of-Sight of the radar. This includes both the structural stability as the influence due to clutter. Furthermore, it is shown that the GNSS antenna has mm precise performance, similar to standard monitoring GNSS set-ups.

The developed IGRS can be deployed to create a local datum connection between datasets. Ideally IGRSs, either the design presented in this thesis or similar, are deployed where integration, validation and calibration of data, especially InSAR data, is needed.

Preface

With this thesis I conclude a study period at the TU Delft, which felt like undergoing a whole geological era. However, people often say their study period has been their best time of their life, so for most parts of it, I do not really mind. My journey in Delft started with some years of Mechanical Engineering. A wise, well spoken man at Mechanical Engineering stated that his beloved study stood at the basis for everything in modern day life. Rebellious as I was, I felt that this basis, although it included "everything", did not fulfil my needs. The doubter as I was (or am?), it took me 3 years to find my spot at Applied Earth Sciences or, as some may prefer, Mining Engineering. The insights which helped me understand why I had only seen loose material below my feet during my early years growing up in the Netherlands, and why I had seen magnificent big chunks of solid rock elsewhere during my travels abroad, opened my eyes.

With my eyes fully opened, I tumbled into the master track Geoscience & Remote Sensing (GRS). Shortly said, it has been a challenge converting observations into mathematical models, especially when my physical understanding of processes lacked behind the mathematical proofs on which simulations are build. On the other hand, learning about: the spherical harmonics in the global tides, possibilities to classify land use based on its reflective spectrum, feedback mechanisms in climate studies, the shapes of the clouds which are real-time visualizations of certain atmospheric boundary condition related to e. g. temperature and humidity, and many other subjects - has been enormously interesting throughout.

For my thesis, I decided to look for a (for me) interesting process rather than for a (for me) interesting subject. This led to my work in the design study on an Integrated Geodetic Reference System (IGRS) under the supervision of Prof. dr.ir. R.F. (Ramon) Hanssen, which I am grateful for giving my the opportunity to be part of the joined team of the TU Delft, NAM and 06-GPS. This team has been responsible for the full development of the IGRS, including design, manufacturing, testing and deployment of 30 Integrated Geodetic Reference Stations in Groningen. Not many GRS-graduating projects include 3D-drawing, engineering and leading the outsourced manufacturing work of 30 large size instruments.

I would like to thank Shizhuo Liu from NAM for letting me, as a thesis student, collaborate in an actual project. This gave me lots of motivation to finish the design within the set deadlines. I would like to thank Frank Dentz from 06-GPS for leading the deployment campaigns and piloting us around the whole province of Groningen from site to site with only short peeks on Google Maps. I would like to thank Dr. I.V. (Ihor) Smal for carefully proofreading my thesis.

To end this project as a graduation project, the thesis that you are now reading had to be written. I think I can easily say that without the patient guidance of Dr. ir. H. (Hans) van der Marel this work would not have passed the test (easily). His honest feedback on both the process and the content have helped me to grow enormously with my writing skills. Not to forget the many useful MATLAB script made by Hans which have been used extensively throughout this thesis.

Last but not least, I would like to thank anyone who reads this for their interest in this thesis, but moreover for their contribution in any form. From being a sound board in the process of writing this thesis to being someone who motivated me to: run the extra mile; climb the extra tree; swim the extra canal (no not them actually); grab the extra rope; explore the extra mountain; kiss the extra cheek (Liz's to be precise); and share the extra thought, tear or laughter.

J. (Jurjen) C. Kamphuis
Delft, April 2019

Contents

List of Figures

List of Tables

1

Introduction

1.1. Motivation

The geodetic interpretation of deformation estimates derived from spatio-temporal location measurements obtained by multiple geodetic observation techniques is limited by the differences in their sampling methods of physical processes. This work is a design study, aimed to develop a method to co-locate reference points for multiple geodetic techniques. This method will lead to one common set of observations which ensures one common process is interpreted.

1.2. Introduction to the problem statement

In geodesy, deformation processes are those processes that cause change in the shape of the earth's surface [1][2]. They include (1) slow movements like subsidence, uplift due to post glacial rebound, horizontal movements due to plate tectonics or (2) rapid movements due to eruptions, seismic activity and land slides. Monitoring the position of a point in space over time results in a time series representing the deformation of this point. Different monitoring techniques are in frequent use, ranging from local terrestrial measurements such as levelling[3] and tachymetry[4], to spaceborne techniques with global coverage, such as GNSS[5] and InSAR[6].

Global Navigation Satellite Systems (GNSS) are mainly used for geo-spatial positioning. Multiple satellites forming a constellation emit signals encoded with orbital parameters and a time stamp. Receivers on the earth are used to determine the distance, or *range*, between the receiving and sending antenna. When at least 4 ranges to 4 satellites are found, trilateration is used to determine the 3D geo-spatial position of the receiving antenna[1]. A deformation process is monitored by recording the geo-spatial position of a specific point in space over time. For high precision estimates, complex processing is required[5].

For *Interferometric Synthetic Aperture Radar* (InSAR), one of the main functionalities is monitoring deformation. Differences in range (wrapped as phase values) between two 2D radar images are used to form a 2D deformation map of the earth surface. Images are made from opportunistic reflections from natural or man-made scatterers. The reflections are sampled with a given resolution resulting in pixel values representing a 2D area.

Where GNSS data is available as point values of a GNSS antenna as a known physical source, InSAR is available as spatially spread data without exact information about the source. This difference is one of the problems related to the integrations of seemingly common deformation trends. As the sources are different, interpretation will always be effected by some sort of interpolation. Two other examples of differences are: (1) GNSS deformation trends are known in 3D, whereas InSAR deformation trends are strictly 1D; but more importantly, (2) GNSS deformation trends are often measured from stable monuments deeply founded in the subsurface of the earth whereas InSAR measures surface deformation only. Overall, these differences may lead to comparing apples to oranges.

[1] The fourth satellite is used to determine the clock error of the receiver

A fundamental solution to the problem would be to force a pixel value in the InSAR deformation image to represents the exact deformation of the GNSS antenna. In doing so, it is ensured that observations for both the InSAR and the GNSS measurement stem from the same origin. As a result, deformation estimates can be translated to a common datum and can be interpreted together correctly. The materialization of this solution is the Integrated Geodetic Reference Station (IGRS). This geodetic station houses reference points for GNSS, (In)SAR, levelling, LiDAR and total stations.

So, the main objective of an IGRS is to provide co-located reference points for levelling, GNSS and InSAR, such that observations of multiple geodetic techniques represent the same physical process. Consequently, time series represent the same deformation characteristics, which is an essential aspect in the interpretation of measurements stemming from different sensors or monitoring methodologies.

In scientific literature, methods have been proposed and implemented to co-located InSAR targets and GNSS antenna's [7][8][9]. However, these methods are: (1) based on the implementation of complex instruments called active radar transponders [7], which are not yet available at commercial levels; (2) based on placing reference points on separate foundations which is not preferable in a country as the Netherlands which is lacking bedrock availability[9]; (3) not including a method for integration of airborne LiDAR data[8]; or (4) not well suited for areas facing rain, snow and small wind driven debris. Therefore, developing a new design is desirable.

1.3. Objective and contributions of this work

The objective of this work is *to develop the concept of an Integrated Geodetic Reference Station and to describe its performance to aid its implementation.*

Achievement of this objective can at least contribute to better interpretation of physical deformation processes due to the use of complementary data. The IGRS helps the validation of geodetic datasets during quality control as the differences due to methodologies are split from the differences due to different sources. Furthermore, the known location of the IGRS in a well defined global coordinate reference system and in the radar image can lead to calibrated deformation time series and better geolocation estimates for (In)SAR scatterers. To summarize, the IGRS is at least able to link geodetic datums, validate methodologies and calibrate InSAR time series.

1.4. Research question

The research question stems from the objective of this work, which includes the development of the first design for an IGRS into deployable version. For it to be applicable and deployable in the field, the performance should be within set requirements.

This leads to the general research question addressed in this work:

How to design a device, that couples InSAR, GNSS, levelling and preferably other geodetic measurements, with the main goal to integrate InSAR measurements into a well defined geodetic datum?

This question leads to four sub questions:

i. What are the requirements for the device such that it can fulfil its main goal?

ii. What is a good and practical design for such an instrument that fulfil the requirements?

iii. What is the error budget and performance of this design?

iv. Which strategies and procedures should be followed for deployment of this design?

1.5. Outline and Research Methodology

This thesis contains 8 chapters, with 5 chapters in its core body embracing the 4 sub questions belonging to the main research question. The first chapter is an introduction to the work, the second one gives both background information on the essential subjects for reading this thesis, as a literature review on similar projects.

The third chapter states the requirements an IGRS should meet, made with a rational decision process based on literature and prior experience of stakeholders in the project. Chapter four describes the design and design process of the IGRSs that are presented in this thesis. Chapter five elaborates on the experiments done to validate and further improve the design of the IGRS. While doing so, focus is given on the RCS and interferometric phase stability. The sixth chapter describes the deployment and operational use of an IGRS, partly based on a project of deploying 24 IGRSs in and around the Groningen gas field in the north of the Netherlands.

In the seventh chapter, a synthesis is given combining multiple aspects of both design, deployment and operational use to present their relationships. Finally, this thesis is closed off with conclusions and recommendations in which an outlook on future development of the IGRS is included.

1.6. Introduction to the Groningen field study

Throughout this thesis, references to the Groningen field study will be made. This field study is a project in which 30 IGRS stations are deployed in and around the province of Groningen to monitor the surface deformation with high quality standards. The project is spun around the 'Study and Data Acquisition Plan' of NAM[2] in which plans are made to better understand the deformation characteristics due to gas extraction[10]. Although NAM has been the project leader throughout whole project, the TU Delft has been responsible for the research and development process of the deployed stations.

A main goal presented in the 'Study and Data Acquisition Plan' is to install 30 GNSS stations to densify the current GNSS monitoring network and to be able to have better monitoring capabilities on the rim of the deformation regime. A second goal is to connect other monitoring techniques to this GNSS monitoring network in the physical world. The IGRSs have been deployed to reach these goals.

At the moment of writing 24 stations have been installed.

[2]Nederlandse Aardolie Maatschappij - Dutch exploration and production company

2

Background theory and literature study

This chapter starts with a basic explanation of the geodetic principles of coordinate reference systems. It continues with an overview on popular methods for deformation monitoring while keeping the coordinate reference systems in mind. The problems linked to the integration of data stemming from the different monitoring methods are given together with state of the art solutions. Furthermore, this chapter gives the reader some more background information about the radar signal used for InSAR applications.

2.1. Basic concepts of coordinates, geodetic datums and measuring networks

The location of a point on Earth can be expressed by coordinates in a chosen *coordinate reference system* (CRS). For example the location of the Prometheus statue on the TU Delft campus has a set of coordinates (52.001434°N, 4.373135°E) in the *World Geodetic System 1984* (WGS 84) CRS. The choice of CRS can be quite arbitrary, the same point can be expressed by different coordinate values that belong to another CRS. CRSs have a *geodetic datum* that defines the origin, orientation and scale of the coordinate axis. Other parameters that define a non-Cartesian CRS are the ellipsoid and/or map projections used for its reference surface[11].

A collection of linked measurements is often referred to as a *network*. A network of which the observational data are insufficient to determine either its position, orientation or scale, is called a *free network* [12]. The link between a network and a measurement providing a geodetic datum, is called a *datum connection*.

Example Campus specific datum

Instead of using a common coordinate reference system to express the location of the faculties on the campus, one could express their location by their distance North and East from an iconic statue on the TU Delft campus; the Prometheus statue. See Fig. 2.2. In this newly made-up coordinate system, the coordinates of the statue are (0m N, 0m E). The datum defining this system is given by an origin, orientation and scale which are arbitrarily chosen in favour of this example. They are defined as follows:

- The Location of the statue is defined as the origin.
- The north axis follow the magnetic north at the location of the statue. The up axis is the normal vector of the equipotential gravitational surface. The east axis is pointing orthogonal to the other axis.
- The unit of length on the axis is meter.

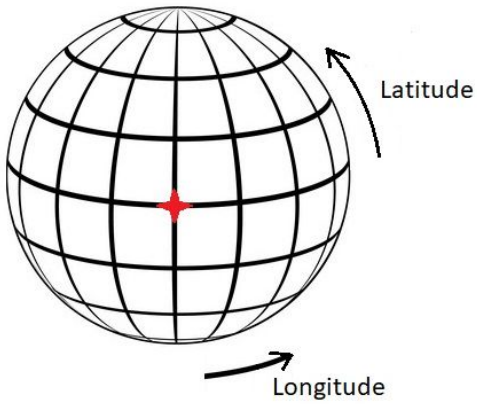

Figure 2.1: Simplistic representation of a global latitude-longitude grid on a sphere. The red cross represents the origin of the grid.

Figure 2.2: Orthogogal grid on campus representing the campus-datum example sketched in the text. The red cross represents the location of the Prometheus statue, which is the origin of this hypothetical grid.

With the newly made-up datum on the TU Campus in mind, a student would be able to measure the distance in north and east direction between two buildings. If he or she is really eager, distances between all faculties could be measured resulting in a network of measurements relative to each other. This set of measurements, in which distances between faculties are known would be a free network since the position of the whole network relative to the statue is unknown. Figure 2.3 visualizes this example. Green lines represent measured north and east distance measurements. The location of each building is known with respect to the other buildings, but not with respect to the campus-datum.

In our campus experiment, the statue is defined as the origin of the coordinate system. If we include the statue in the network of measurements, the free network is connected to a datum. We know the coordinates of the statue in the WGS84 coordinate system are (N52.001434°, E4.373135°). Therefore - keeping in mind the differences in north definition and linearising the relation between degrees and meters for the location of the statue - we can also compute the location of all faculties in the global datum by using the connection between the local and global datum made at the statue's location.

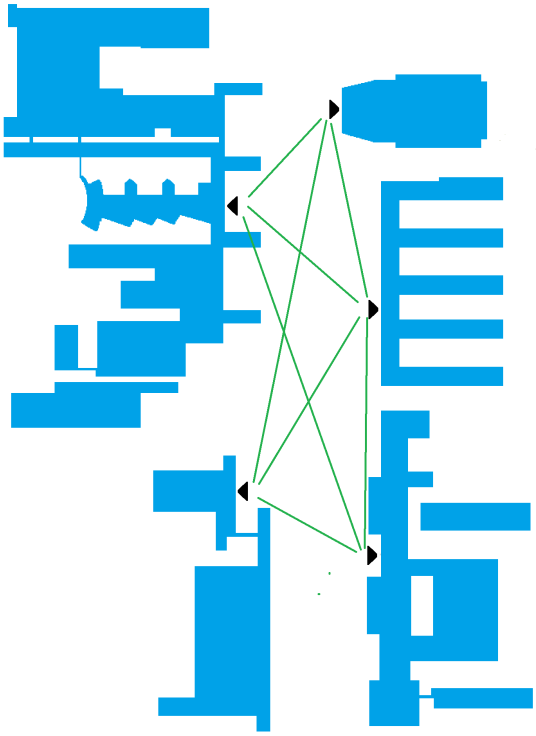

Figure 2.3: Green lines are distance measurements between buildings. In the example sketched in the text, each location of a building's entrance is known with respect to the other entrances (black arrow). As no link is made to an object with a known position in the campus-datum, this network of measurements represents a free network.

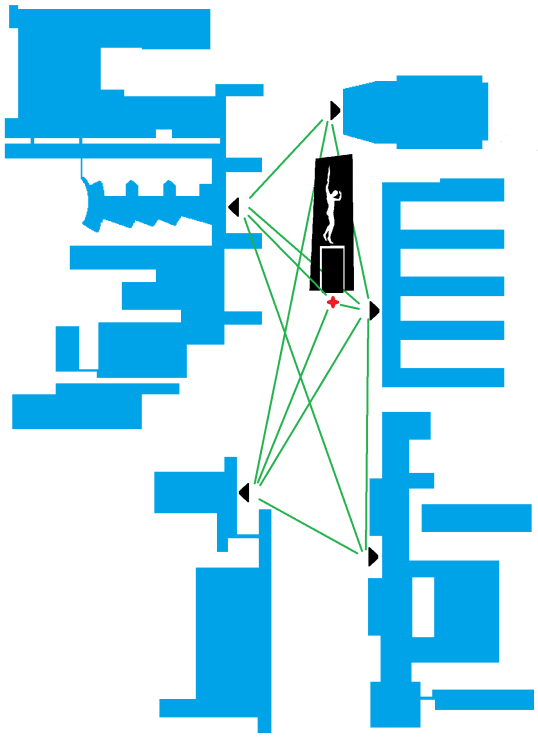

Figure 2.4: The free network from Figure 2.3 is connected with a object with known coordinates; the statue of Prometheus. With this connection a datum connection is made turning the free network in a fixed network

2.2. Geodetic deformation monitoring

This section is an overview of the main monitoring techniques which are included in the IGRS requirements. Their basic principles together with their common observations and estimated parameters are given.

2.2.1. Levelling

Geodetic levelling is a traditional surveying technique to determine relative height differences between control points. It is widely used to measure geodetic heights in regional measurement campaigns. For the Netherlands large areas are generally only levelled once every 5 to 10 years [13].

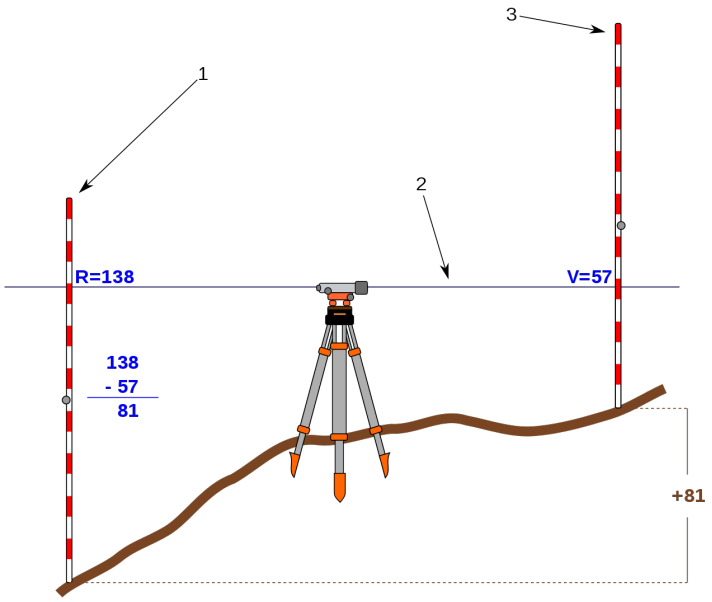

Figure 2.5: Principle of levelling. 1 and 3 show levelling rods, 2 is the Line-of-Sight through the levelling instrument which should be perfectly horizontal. [14]

Principle Being a traditional method, the principles of geodetic levelling can be found in many sources. A geodetic textbook covering the technique is by G. Bomford in [1]. More information can be found in [3] and [15]. The main principle is presented in Figure 2.5.

The figure shows a levelling instrument placed on the tripod in between two levelling rods. By looking trough the viewer of the levelling instrument, a surveyor can read a height on the rod By turning the instrument towards the other rod, its height on this rod can be read as well. The difference between these two relative heights readings is the height difference between two points.

For the measurement to be accurate, the levelling instrument should be perfectly levelled. Within the instrument there is a special mechanism to ensure a level Line-of-Sight, with a constant instrument bias for the full 360 horizon. When the distance towards each rod is similar, the instrument error drops out of the equation. Measurements are taken twice, when the mean value is taken as a result, the possible error due to settlement of the rod is minimized.

Levelling rods can be placed at a distance in the order of tens of metres, meaning that multiple steps have to be made to survey points further apart. The error associated with modern levelling instruments is given by

$$\sigma_l[\text{mm}] = c_0 + c_1 \cdot \sqrt{L} \tag{2.1}$$

with L the horizontal distance in km. c_0 is given by an initial error not related to baseline length and has

values between 0 and 2 mm[3][13]. c_1 is a constant giving a measure for the influence of the baseline length on the error. Values between 0.2mm and 1.29mm are given in consulted literature[3][13].

Reference point and observed process Reference points for levelling, or *benchmarks*, are generally small round headed bolts that are secured to stable objects, often with a published height value in a national height reference framework. The round head will ensure the same point will be measured every acquisition. Examples of levelling reference points are given in Figures 2.6 and 2.7. The observed process depends on the deformation process of the benchmark, which is site specific.

Frequently used reference frame In the Netherlands, benchmarks can be part of the national height reference framework (NAP), or be part of a local densification of this network for particular applications. In 2004, the NAP was represented by 362 subsurface benchmarks which are anchored in the Pleistocene layers[16]. These 362 subsurface benchmarks are assumed to be stable and checked once every 20 to 25 years. During this time, 35000 secondary benchmarks are used to shorten the routine levelling campaigns by providing a reasonable stable reference point in close proximity. These secondary benchmarks are checked every 5 -10 years[13]. Data is given as orthometric height in NAP at a certain time epoch.

Estimated parameters Deformation can be observed by computing differences between two epochs. With levelling we can only observe height differences between points, the primary observable for deformation analysis will be single differenced height. For instance, suppose we have observed a levelling network consisting of N points at an epoch, then, from multiple observations, we can estimate N-1 unrelated height differences. If the same points are observed a second time (epoch 2) we have a new set of estimated height differences. For monitoring change, this would result in only N-1 double differences with the change in height differences with respect to epoch 1. Note that these double difference heigths include the height change of the reference point. So, all height differences are given with respect to the first epoch and the common reference point. For monitoring change in absolute sense, either we have to assume the common reference point is stable, or we have to be given the height change in the reference point from a different source.

Figure 2.6: Example of a geodetic control point, USA.

Figure 2.7: Example of a NAP control point, Vlissingen, NL. (Photo D.Bruin)

2.2.2. Global Navigation Satellite Systems

The term *Global Navigation Satellite System* (GNSS) is a generic name for multiple satellite-based positioning systems. The widely known *Global Positioning System* (GPS) has been the first satellite-based system to enable quick and global determination of position and time [5]. The system has been developed for the US Department of Defence. The Russian counterpart to GPS is the Global Navigation Satellite System (GLONASS) and the EU, with ESA, has developed the Galileo system. The

Chinese government has developed Beidou and for special applications there are several correction based augmentation systems.

Principle GNSSs are based on the geometric principle of trilateration in which 3 distances from 3 known points fix a location in 3D space. Figure 2.8 shows a representation of one receiver and one satellite. The distance ϱ is measured as the time it takes for the signal to travel from a satellite to the receiver. The observed time difference includes an unknown clock error t_r [s] resulting in a offset $\delta(t_r)$ [m] . Therefore, observed ranges are so called *pseudo* ranges. In the pseudo-range equation[5], ϱ [m] is given by

$$\varrho = \|\boldsymbol{\varrho^s} - \boldsymbol{\varrho_r}\| + \delta(t_r), \tag{2.2}$$

in which $\boldsymbol{\varrho^s}$ is a vector describing the location of the satellite and $\boldsymbol{\varrho_r}$ is a vector describing the location of the receiver, both in 3D Cartesian space. The ephemeris of the satellite is modulated on its signal and can be used to compute the location of the satellite. For GPS, data is provided in the WGS84 *coordinate reference system* (CRS) making this CRS popular, especially among users of consumer grade GPS devices. The location of the receiver is a vector of 3 unknowns. Therefore, an inverse model with 4 unknowns has to be be solved. This requires at least 4 pseudo-ranges. As a consequence, a total of 4 GNSS satellites is theoretically enough to determine the location of the receiver.

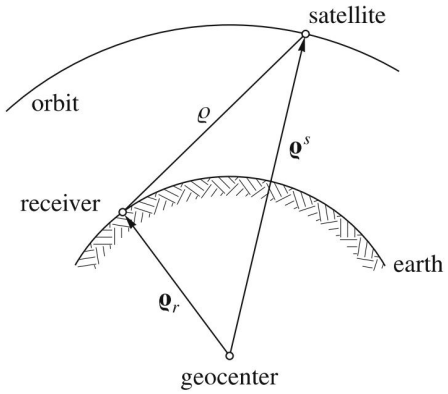

Figure 2.8: Geometry of the pseudo-range equation. (Forward model representation) [5]. Geometrically in this example, $\delta(t_r)$ = 0.

This process of determining the pseudo-ranges to the satellites can be used to estimate the location of a GNSS receiver with a accuracy up to ~1-2 meter horizontally and ~3-5 meter vertically , which is not sufficient for surveying and deformation monitoring. However, more accurate methods have been developed to obtain an up to cm to mm accuracy[5]. These methods use relative measurements between two receivers and exploit the possibility to measure the phase of the carrier signal which has much higher frequencies than the signal itself.

There are multiple methods for the use of GNSS for geodetic monitoring. They have one common principle: relative measurements over a baseline from a base station, with known coordinates in the CRS of the satellite orbits, to an unknown station, which is often called a *rover*. In this set up, the primary parameters to be estimated are not the coordinates of the receiver, but the differences in coordinates between the receivers on the rover and base station. Figure 2.9 shows a set-up of two GNSS receivers. They receive signals from i, j, k,... satellites. The difference in observed phase between station 1 and station 2 ($\varphi_2^i - \varphi_1^i$) is a function of their different location, the clock error (δt), the difference in tropospheric delay (ΔT) and an integer amount of full phase cycles (A_1^i). $\Delta x_{12}, \Delta y_{12}$ and Δz_{12} are identical for every satellite used. This leads to the phase observation equation

$$\varphi_2^i - \varphi_1^i = F(\Delta x_{12}, \Delta y_{12}, \Delta z_{12}, \delta t, \Delta T, A_1^i). \tag{2.3}$$

In the phase observations equation, $\Delta x_{12}, \Delta y_{12}$ and Δz_{12} can be determined by solving a set of equations when signals from 4 or more satellites are simultaneously received. $\Delta x_{12}, \Delta y_{12}$ and Δz_{12} are used to determine the location of receiver 2, the rover, with respect to the known location of receiver 1, the base station.

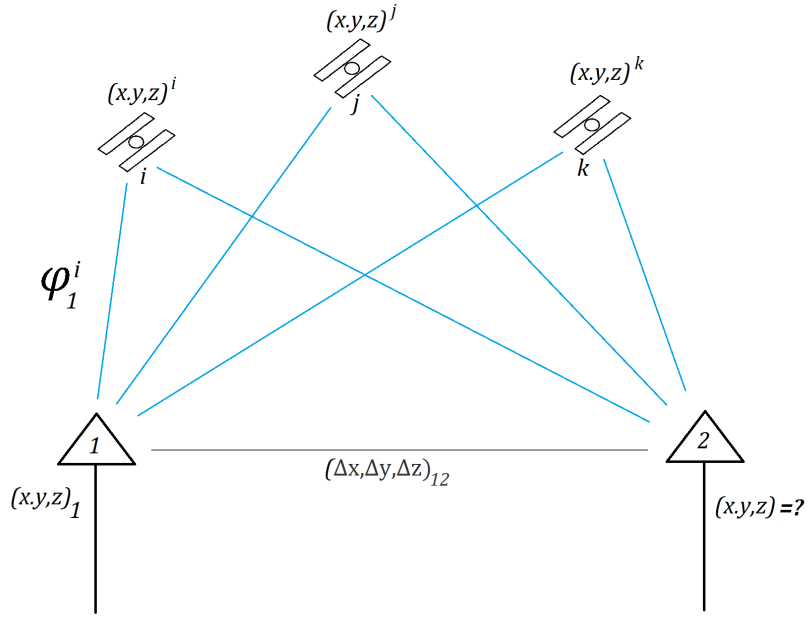

Figure 2.9: Short baseline relative GNSS measurements. Three satellites i, j,and k, are shown together with two receivers. The signal from a satellite is both received by receiver 1 and 2. From the differences in the signal received by receiver 1 and 2, the local offsets between the two locations can be estimated. Based on the offsets and the known location of receiver 1, the location of receiver 2, which is the unknown of interest, can be computed.

The location of receiver 1 is a given in the scenario given in figure 2.9. In practise, the coordinates need to be available in the same CRS with roughly the same accuracy as the satellite orbits which is in the order of metres. This accuracy can be obtained by processing long time series, or by using an external source for its coordinates. However, the user can be freed from the task of setting up a base station and getting base station coordinates by using an existing GNSS *continuously observing reference station* (CORS).

This station might be one of the base stations of the *International GNSS Service* (IGS) network (like the ones in Figure 2.10 and 2.11). This is a global network of high quality GNSS receivers which form a measurement network covering the whole globe. An optimal solution for their position in the *International Terrestrial Reference Frame of 2014* (ITRF2014) is determined by the IGS.

From Fig. 2.9 one may believe that the primary observable from GNSS for deformation analysis are double differences in the three coordinate directions. However, unlike levelling, GNSS networks span the whole globe, and unlike levelling the precision is only weakly sensitive to the baseline length. Therefore, GNSS may also directly provide coordinates in an *Earth-Centred, Earth-Fixed* (ECEF) reference frame, such as the ITRF2014.

ITRF2014 is a geometrical reference frame based on two sets of seven parameters. The first three give the location of the origin of the x,y and z-axis, the second three give the orientation of these three axis. These first six parameters are estimated based on the network solution of the IGS GNSS stations. The seventh parameter determines the scale of the reference frame based on among others Satellite Laser Ranging (SLR). The second set of seven parameters are the change rates of the first seven.

Post-processing of raw data from continuous GNSS stations based on the network solution of the IGS produces mm precise estimates for the x, y, z and $V(x, y, z)$ in ITRF2014. $V(x, y, z)$ gives the velocity of the station in 3D space. Deformation rates of the continuous GNSS stations can be estimated from

GNSS measurement time series.

Further work on the fundamentals of GNSS for further information can be found in [5].

Reference point and observed process The reference point for a GNSS measurement is either the antenna itself, or a benchmark with known offsets to the antenna. GNNS instruments, consisting out of an antenna and receiver, range in quality and size. They go from small integrated sensors in personal mobile devices with real time processing for easy navigational tasks to dedicated continuous GNSS stations for monitoring work. The latter have calibrated offsets to a specific reference point and their location estimates are enhanced by post-processing. Figure 2.10 and 2.11 show such continuous GNSS stations. Continuous GNSS stations are often fixed to bedrock or founded on stable subsurface layers which determine the observed deformation process.

Figure 2.10: Example of a Continuous GNSS station. This station is located in Delft, Netherlands. (Photo: ©TU Delft)

Figure 2.11: Example of a EUREF GNSS station. This station is located in Hetta, Finland. (Photo: ©Royal observatory of Belgium)

2.2.3. InSAR

Interferometric Synthetic Aperture Radar (InSAR) and more specific *Persistent Scatterer InSAR* (PSI) is a common, satellite-based deformation monitoring technique, providing a dense spatial distribution of millimetre resolution deformation estimates. Both commercial and governmental organisations provide raw data which is used by third parties to compute and deliver deformation estimates.

Principle The InSAR principle is covered in great detail in [6], [17], PSI in [18]. A short summary is presented here.

For common geodetic InSAR applications, measurements are taken by satellite-based radar instruments. A single radar measurement starts when a short radio pulse is emitted by the instrument. The pulse travels as a wave-front towards the earth, reflects, and comes back to the instrument resulting in a time delay between emitting and receiving the signal. This time delay is a measure for the range between the antenna and the reflecting object.

The radar instrument is mounted at an angle to reduce ambiguous reflections, which would otherwise occur at equal range but on the opposing sides of the satellite's ground track. As the wave-front travels the surface of the earth, reflections of the wave continuously return towards the instrument. Objects returning the signal are called *scatterers*. By repetitive sampling the incoming return signal, samples at increasing time delay and thus increasing range are taken. Each sample leads to a pixel in the later described radar image. The sampling frequency determines the spacing between measurements in the range direction (perpendicular to the flight's azimuth direction). However, for real aperture

radar, the range resolution[1] of those measurements is determined by the length of the pulse[6].

While the radar instrument travels along its flight path, the process of emitting and receiving pulses as described above repeats itself. The frequency in which pulses are emitted determines the spacing of the measurements along the azimuth direction. The azimuth resolution is determined by the size of the antenna.

To increase performance, signal processing principles are used to mimic large antennas (Synthetic Aperture Radar) and short pulses (chirp signals) which result in high resolution measurements[6].

Large numbers of radar measurements are represented as images in 2D space. The image pixels are indexed by the range and azimuth sample numbers. These pixels contain a complex signal which represent the radar measurement data. The magnitude of the complex signal is dependent on the physical and electrical properties of the reflective object, the radar signal and the geometry of the scene. The phase of the complex signal depends on the time it takes for the signal to travel the path between instrument and the objects in the resolution cell and the scattering characteristics. The time depends on the range and the propagation speed of the signal. The range is a result of the geometry of the scene and the propagation speed is influenced by atmospheric conditions[6].

Two radar images, taken at different times from approximately the same position can be combined into an *interferogram*. An interferogram is created by multiplying the pixel-values of a so-called *master* image with the complex conjugate of the corresponding pixel-values of a so-called *slave* image. Interferograms made with very short baselines[2] show differences among pixels in phase due to effects in the line-of-sight (LOS) of the radar. These effects include surface deformation and differences in atmospheric conditions between the master and slave image.

Each pixel of an interferogram represents a difference in phase between the master and a slave pixel. The difference between two pixels within the interferogram shows the difference of these differences. Therefore, again, we have double differences as the primary observable for deformation analysis.

Figure 2.12: Example of a radar reflector. This one is located in Surat Basin, Queensland, AU. (Photo: ©Geoscience Australia)

Figure 2.13: Example of a radar reflector. This one is located in Rosamond Dry Lake Bed, California, USA. (Photo: ©Jet Propulsion Laboratory)

Measurements points and the observed process InSAR is an active remote sensing technique. Therefore, it depends on scatterers; the objects or structures on the earth surface that reflect the radar signal leading to measurements. Measurement are only helpful if they are interpretable. The interferometric phase of a pixel in a interferogram is not interpretable if the object or scatterer changed in such a way that its signal in the slave image is not representative for the signal in the master image. If this happens, *coherence* is lost. Scatterers with high coherence and thus with interpretable interferometric phase characteristics are called persistent scatterers. Besides natural or opportunistic

[1] the distance in range direction at which two objects can be observed separately
[2] distance between satellites positions at the time of acquisition

man made scatterers, dedicated objects with high reflective properties can show up in the radar image. If their phase centre is known, they can be used as a reference point in the radar image. Common reflectors are trihedral corner reflectors, which are thoroughly described in [19] and shown in figure 2.12 and 2.13. Whereas dedicated objects can be both identified in the radar image as in the physical world, natural scatters are often only well identifiable in the radar image. This makes interpretation of the observed process of such a scatterer difficult. Depending on the origin of the signal, observed processes may be linked to shallow subsurface processes like peat compaction or linked to deep subsurface processes like gas extraction. This problem is shown in Figure 2.14.

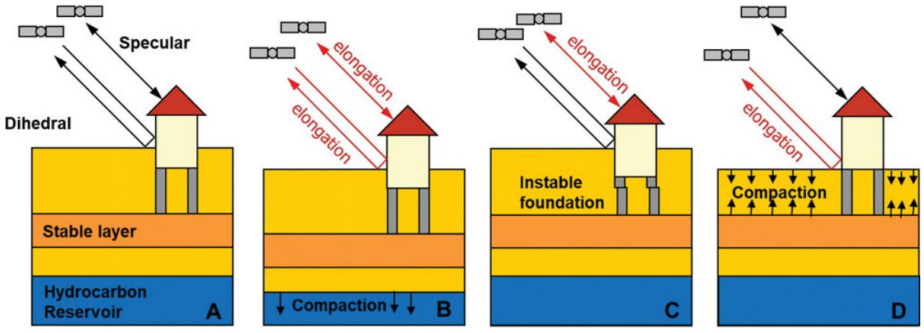

Figure 2.14: Sensitivity of PSI measurements for different deformation regimes. (A) Dihedral wall-surface reflections are sensitive to motion of the surface layer and deeper layers, whereas, in case of deep foundations, specular reflections from objects are only sensitive to motion of the foundation layer due to deep processes. (B) The effect of deep compaction, measured by both the dihedral and specular reflections. (C) The effect of an unstable foundation, only measured by the specular reflections. (D) The effect of shallow compaction, only measured by the dihedral reflections. [20]

Frequently used reference frame and estimated parameters Depending on the step within the processing pipe line, the coordinate reference system of the radar data changes. The data is observed in the radar datum, which is defined as a 2D datum spanned by two axis presenting the pixel and line numbers of the observation which are based on time. The origin of the datum lays in the pixel and line number one, which corresponds to the first sample of the radar image. The direction of the two axis depend on the flight geometry of the satellite. After the process of geocoding, the radar datum is transformed to a global, geometrical 3D reference frame like ITRS2014, or a ellipsoidal reference frame like WGS84. However, estimation errors in the order of meters to decimetres are involved in this process [21]. Therefore, for monitoring applications, data is presented as highly accurate data on deformation in the *Line-of-Sight* (LoS) of the satellite (~sub mm/year) with a rough estimate on geolocation of the signal's origin (~m to ~dm).

2.2.4. Laser altimetry, Gravimetry and Total station measurements

Levelling, GNSS and InSAR are the main techniques to design the IGRS for as these are the conventional techniques which can lead to high precision deformation measurements over reasonable spatial scale. Other techniques to monitor or measure surface deformation which are included in the IGRS are gravimetry and laser altimetry. Total station measurements are typically used for the mapping or the monitoring of local sites, therefore it can be regarded as a complementary technique.

These three techniques are not covered in detail in this thesis, but are incorporated in the design of the IGRS and therefore presented in Table 2.1. More information on gravimetry can be found in [22], on laser altimetry in [23] and an introduction to total stations can be found in [4].

Table 2.1: Overview of common measuring techniques used to monitor surface deformation. [13]

Technique	Platform	Spatial density	Sampling frequency	Precision	Measurement points	Sensitivity direction	Height type	Common datum
Levelling	Terrestrial	~1 p/km^2	~yearly	~mm	Benchmark	Vertical	Orthometric	NAP
Continuous GNSS	Spaceborne	~1 p/900 km^2	~daily	~mm	Fixed receiver	3D	Geometric	ITRS2014
InSAR (Deformation)	Spaceborne	~1000 p/km^2	~weekly	~mm	Natural reflection point or man-made scatterer	Radar line-of-sight	Geometric	Radar datum
InSAR (Geolocation)				~dm to ~m		3D	Geometric	ITRS2014
Gravimetry	Terrestrial	~1 p/10.000 km^2	~yearly	~mm	Benchmark	Vertical	Orthometric	NAP
Laser altimetry	Airborne	~20 p/m^2	~yearly	~dm	Natural reflection point	Vertical	Geometric	RD-NAP
Total Station	Terrestrial	Custom	Custom	~mm	Benchmark	3D	Geometric	Local XYZ

2.3. Data integration

A fundamental question for any measurement is whether the measurement is representing the signal of interest. Understanding the inconsistencies and possible complementaries in when, where, what and how the different measurements techniques sample is a continuation to this question.

The previous section has given an overview on the measurement techniques of interest. Table 2.1 gives a summary of the given techniques, clearly showing an inconsistency in the spatial density and sampling frequency of measurement points. Furthermore, the datasets are acquired in different datums, of which some are orthometric and some geometric which makes direct integration of the data without any processing steps impossible or non-valuable. However, the data is complementary, meaning that a correct combination of the data will give more information than one individual set. Therefore, integration of the multiple datasets is desirable.

For deformation, integration parameters of interest are: displacement series, showing repetitive measurements; mean velocities (linear trend through the displacement series); and higher order effects (acceleration, discontinuities, harmonics).

These parameters are valuable in a well defined (ECEF) reference frame. The parameters need to be determined from double differenced LoS InSAR measurements, GNSS coordinates (or differences in coordinates) and double difference height measurements from levelling. This leads to the following three challenges for data integration:

i. Each observation system has its own datum.

ii. Observations are not coincident in time.

iii. Observed objects are not the same, therefore observed processes may stem from different sources.

Integration of data has to deal with these challenges.

Parameter integration Integration based on a parameter that can be estimated with multiple techniques, like linear deformation rate, is one of the possibilities. Caro Cuenca et al. performed such an integration on levelling, GNSS, InSAR and gravimetry data for the Netherlands [24]. The inconsistency in sampling frequencies is solved by using the linear deformation rates. The different spatial distribution

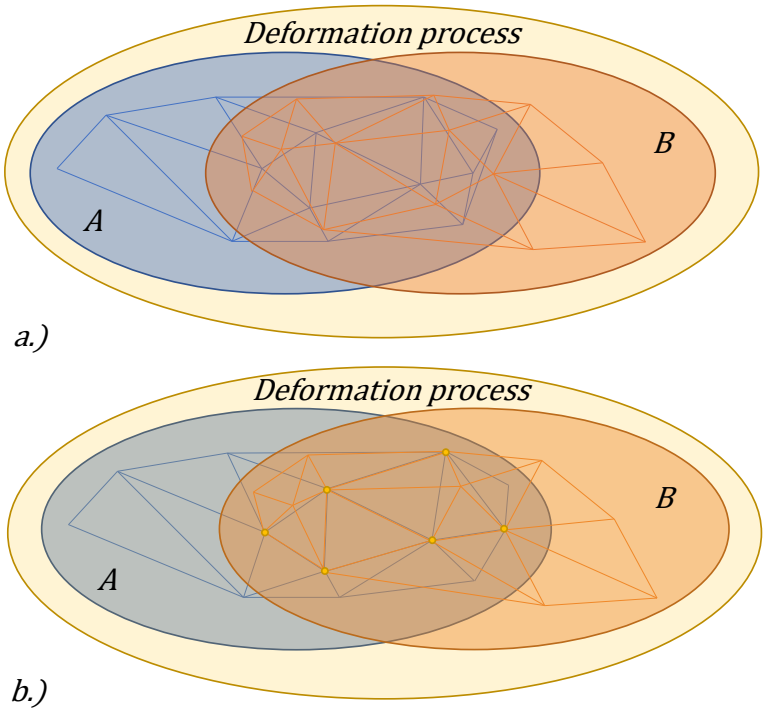

Figure 2.15: Abstract visualisation of the data integration options. The biggest ellipse represents a deformation process. Part of this deformation process is only available to A, part is available to B. By interpreting A and B together, the interpreter will get more information on the total deformation process. The lines represent when and where measurements are taken. for a.) these do not coincide. A form of interpolation of measurements is needed to coincide the data points. For b.) the two techniques include some coinciding measurement points, which make a combination of A and B possible without interpolation.

of measurement points are equalized using kriging interpolation to a common grid. By using kriging, also a precision estimate could be derived for every grid cell. To cope with the different deformation mechanisms, each dataset was divided in a subset of observations with, and a subset without a deep foundation. The result of this work is seen in Figure 2.16 and 2.17.

This method is based on multiple steps; what starts as a deformation process, is (1) observed in a certain way, (2) these observations are modelled in a simplistic model of linear deformation, (3) this model of linear deformation is than interpolated spatially to be combined with a similar set of estimated parameters. These steps leave lots of room for interpolation error in both space and time and the whole method is based on the assumption of observing similar deformation processes. To remove the interpolation from the process and to make sure similar deformation processes are observed, a method where observations are linked is desirable.

Observation integration The fundamental step for any method with the goal of linking observations is co-locating reference points in the physical world. The theory behind co-locating reference points for terrestrial techniques with fixed benchmarks like levelling and gravimetry measurements is trivial and only asks for proper planning; linking observations can be done by taking measurements of the same benchmark at similar epochs. Co-locating techniques without clear benchmarks and fixed acquisition times, such as InSAR, requires more sophisticated methods.

Such methods are described by Garthwaite et al. in [9], by Parker et al. in [25], by Fuhrmann in [8] and by Mahapatra in [7]. The first three describe work done for Geoscience Australian, which is part of the Australian government. They show two methods, of which one extensively. In this method they use trihedral corner reflectors mounted on concrete foundations, placed in close proximity of continuous GNSS stations. Horizontal movement is estimated to be non existent and vertical movement is checked with repeated levelling acquisitions. Hardware used on one of these sites is presented in Figures 2.18

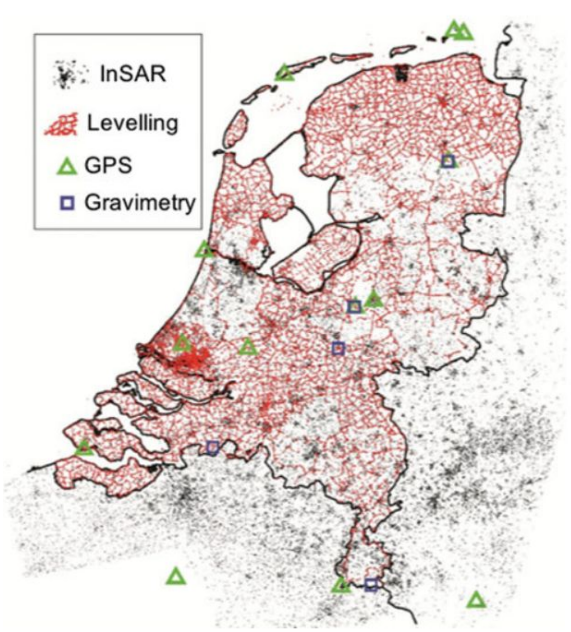

Figure 2.16: Spatial distribution of measurements points for data integration by Caro Cuenca et al.[24]

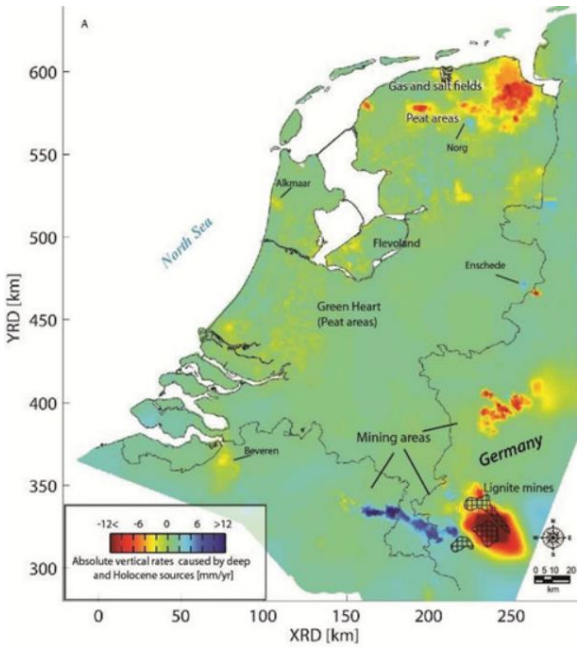

Figure 2.17: Linear deformation rates over the whole of the Netherlands by Caro Cuenca et al.[24]

till 2.20. The second method presented in figure 2.22 shows a set up with two corner reflectors fixed to a GNSS station, ensuring equal motion is monitored without the need for a second foundation and repeated levelling surveys. Mahapatra et al. describe a similar method, but in this method active radar transponders are used to collocate observations. Similar projects have started in Scandinavia, although no information on these projects can be found in scientific literature (yet). Figure 2.24 shows a Norwegian project where two corner reflectors have been integrated into one system, which is mounted on a 2-m pole to be sure measurements can be made year round without interference of built up snow [26].

Figure 2.18: Continuous GNSS antenna placed on concrete monument used by Parker et al. in [25].

Figure 2.19: GNSS supporting hardware. [25]

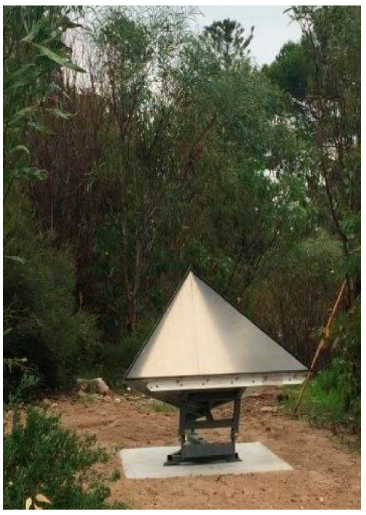

Figure 2.20: CR on a concrete foundation used by Parker et al. in [25].

Figure 2.21: Experimental set up of a continuous GNSS antenna equipped with CRs by Fuhrmann et al. in [8].

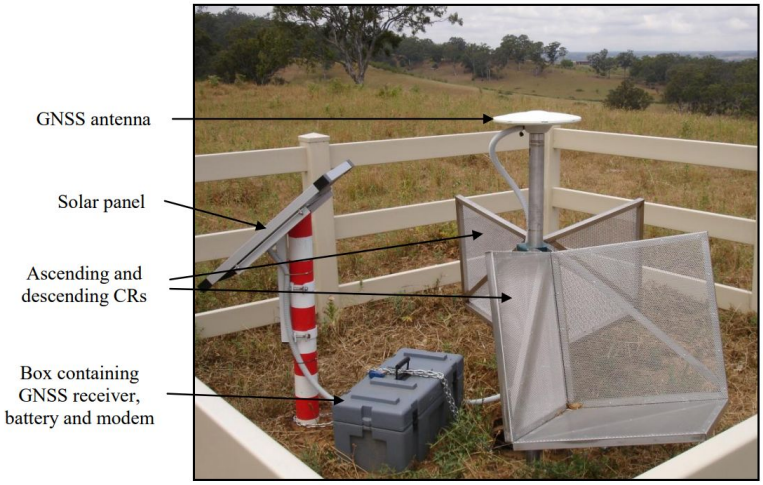

Figure 2.22: Monitoring set up of a continuous GNSS antenna equipped with CRs by Fuhrmann et al. in [8].

Figure 2.23: Monitoring set up of a continuous GNSS antenna equipped with a transponder by Mahapatra et al. in [7].

Figure 2.24:]
Co-located corner reflector system (front) in close proximity of a continuous GNSS station (back) in Norway by the Geological survey of Norway (NGU). (Photo: ©NGU)

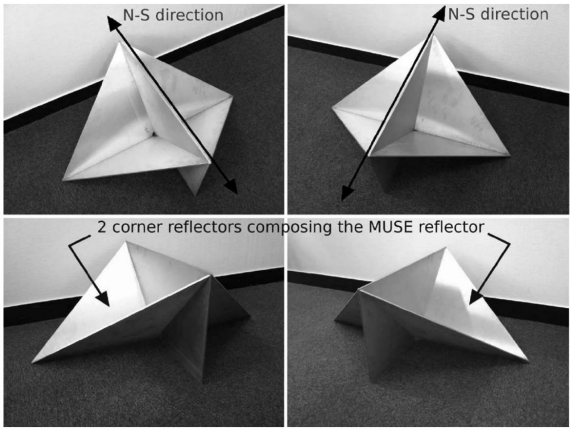

Figure 2.25: Multipass scatter equipement (MUSE) corner reflectors developed in 2013 by Quin and Loreaux. Developped for 3D deformation monitoring with the help of multiple SAR tracks. [27]

Figure 2.26: Collocated corner reflector system including levelling benchmarks (side) and GNSS mount (top). In use by the Agency for Data Supply and Efficiency in Sweden (SDFE). Designed by: SDFE, Lemvig Water & Wastewater and DTU Space. (Photo: ©SDFE)

Opportunities for improvement and alternative approaches for observation integration These examples partly show solutions for the design of an IGRS. However, some room for different approaches are present. For the IGRS, no active transponders will be used as these were not yet widely available at full developed levels at the start of this project. This means that some form of passive reflector shall be used. The presented corner reflectors still have a clear disadvantage related to debris or water build up. This is shown in e.g. [28] and [29] where both groups have some bad results because of precipitation. The project in Australia opted for perforated plate material as seen in Figure 2.22. The Norwegian group clearly have other weather characteristics including lots of snow. So, a radome preventing regular snow built up is mounted on the reflectors despite the negative effect on the signal quality. For the Netherlands, rain, leaves, debris and snow are all possible to encounter. Mounting the reflectors in downward pointing manner proved to be a solution as presented in further chapters in this report. Integration of a surface for airborne laser altimetry campaigns is not yet present in one of these examples. Furthermore, the integration of all benchmarks on one foundation is still not one of the standard methods while this is favourable for placement of stations in soft soil underground like commonly found in the Netherlands.

2.4. Radar signal theory

A major part in designing the IGRS is the design and handling of the radar reflectors. This sections elaborates on the basic theory associated with radar corner reflectors.

2.4.1. Definitions and background information on radar signal theory

Signal to Clutter ratio (SCR) The precision of an interferometric SAR measurement of a persistent scatterer, such as a corner reflector, depends on the power of the signal returned by the corner reflector and the power of the (background) signal returned by other scatterers in the same resolution cell. This background signal is known as *clutter* and can be regarded as random noise. The ratio between the reflector's signal and the clutter, the *Signal-to-Clutter Ratio* (SCR), can be used to estimate the standard deviation of the phase. The standard deviation in the Line-of-Sight σ_{LOS}, which is directly related to the phase standard deviation, is defined in [30] and [31] as

$$LOS_{\text{error}}\ [\text{m}] = \sigma_{\text{LOS}} = \frac{\lambda}{4\pi}\sigma_{\text{phase}} = \frac{\lambda}{4\pi}\frac{1}{\sqrt{2SCR}}, \tag{2.4}$$

with λ the wavelength of the signal (0.0555 m for Sentinel-1). This relation is shown in Figure 2.27.

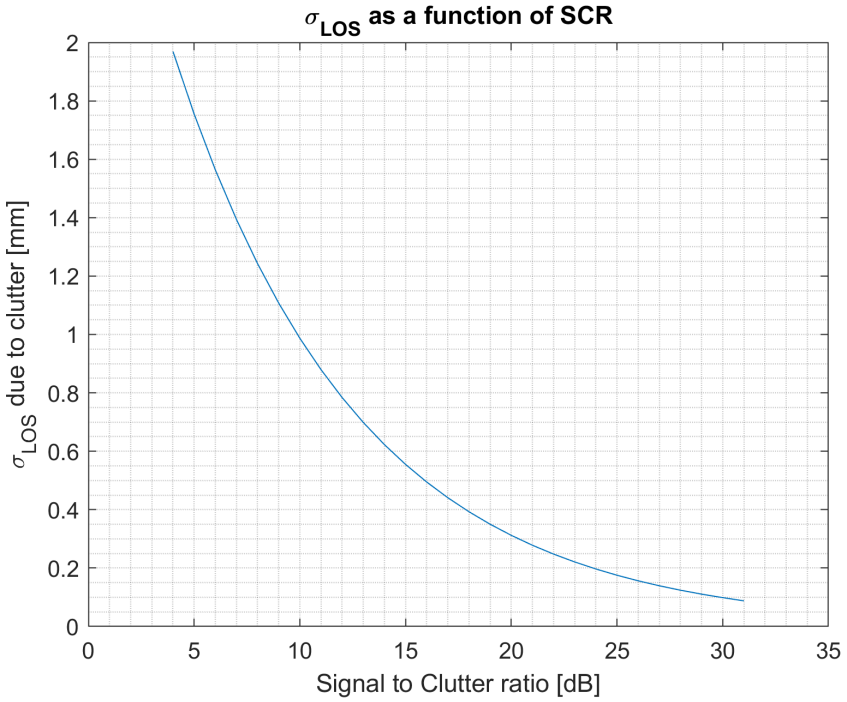

Figure 2.27: Standard deviation of the error in the Line-of-Sight with respect to the Signal-to-Clutter ratio.

The SCR is given by [31] and [19] as

$$SCR\ [-] = \frac{s^2}{c^2} = \frac{RCS_{cr}}{\beta_0\ A_{res}}. \tag{2.5}$$

The symbol c denotes the clutter amplitude whereas s denotes the signal amplitude. Alternative to amplitudes the SCR can be expressed as signal strength. For the signal of interest this leads to RCS_{cr} which is the radar cross section of the corner reflector $[m^2]$. $\beta_0 \cdot A_{res}$ is a measure for the clutter strength. The clutter strength is a product of the (average) dimensionless backscatter coefficient (in the Line-of-Sight), β_0 and the area $[m^2]$ of the resolution cell, A_{res}.

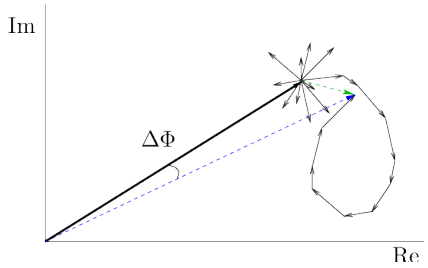

Figure 2.28: A PS (thick black arrow) plotted in the Re-Im space as part of a pixel value (blue dotted) of a resolution cell containing multiple scatterers (light arrows). [31]

Eq. 2.5 is closely linked to the *signal model*. In the signal model, used for PSI presented by [31] and [30], each captured signal of the radar image is a complex summation of multiple return signals of separate scatterers. High power persistent scatterers such as a corner reflectors dominate the signal, as can be seen in Fig. 2.28. The thick black arrow represents a high power scatterer, the small arrows represent some low power scatterers which add up to the green dotted arrow. The captured signal, represented by the blue dotted line, clearly has a similar magnitude and phase as the signal of the corner reflector.

In a time series of a persistent scatterer, the signal represented by the black arrow can be regarded as a constant, while the clutter represented by the green arrow has a 2D Gaussian distribution in both imaginary (I) and real (Q) axis. This kind of distribution can be described by a 2 parameter Rice distribution.

Due to the random phase of the clutter, the mean of $\Delta\Phi$ (shown in Fig 2.28) in a time series is zero. The standard deviation of $\Delta\Phi$, σ_ϕ, gives a quality measure of the PS. Although the analytical stochastic error propagation of the rician distribution of the clutter on $\Delta\Phi$ is a non-linear function, Ketelaar shows in [31] that for a PS with a SCR of at least 8, $\Delta\Phi$ has an approximate normal distribution. Therefore, the phase values of PSs with a SCR of at least 8 can be characterized by a Gaussian curve with a mean and a standard deviation. With the mean clutter being 0, the mean of $\Delta\Phi$ is also 0. The variance is given by Ketelaar as [31]

$$\sigma_\phi^2 = \frac{1}{2\ SCR}, \tag{2.6}$$

which was already implicitly shown in eq. 2.4.

In the same way it is possible set up an equation for the standard deviation of the signal magnitude due to clutter. The standard deviation is given by [30] as

$$\sigma_{\text{RCS}} = \frac{m_a}{\sqrt{2\ SCR}}. \tag{2.7}$$

The mean amplitude of the measured signal is given by m_a. For $s >> c$, $M_a \approx s$. If we take $SCR = s^2/c^2$ from Eq. 2.5, σ_{RCS} turns into

$$\sigma_{\text{RCS}} = \frac{s}{\sqrt{2\ SCR}} = \frac{s}{\sqrt{2 \cdot \frac{s}{c^2}}} = \frac{1}{\sqrt{2}} \cdot c. \tag{2.8}$$

The influences of a CR on SCR The RCS of a corner reflector is given in [32] as

$$RCS_{\text{cr}}\ [\text{m}^2] = 4\pi \cdot \frac{A_{\text{eq}}^2}{\lambda^2}, \tag{2.9}$$

with A_{eq} the equivalent flat plate area of the corner reflector. The equivalent area A_{eq} can be computed for a corner reflector knowing its shape and its orientation to the signal. This is discussed in more detail in [32].

In the dB scale we can formulate Eq. 2.5 and 2.9 as

$$SCR\ [\text{dB}] = RCS_{\text{cr}} - (\beta_0 + A_{\text{res}}) \tag{2.10}$$

$$RCS_{\text{cr}}\ [\text{dBsm}] = 2A_{\text{eq}} + (4\ + \pi - 2\lambda). \tag{2.11}$$

If we take these formula's together we get

$$SCR\ [\text{dB}] = 2A_{\text{eq}} - \beta_0 + C. \tag{2.12}$$

This shows the direct influence of β_0 on the SCR (linked to σ_{LOS}) and thus the importance of choosing a location with a low value as described in Section 6.1. Further more it shows the influence of a large equivalent area for the radar reflector.

The constant C is given by $C\ [\text{dB}] = 4 + \pi - 2\lambda - A_{\text{res}}$, which is only influenced by the choice in satellites system.

The equivalent area A_{eq} and thus the SCR depend on the orientation of the corner reflector with respect to the signal. The equivalent area is at a maximum at the so-called boresight of the corner reflector. When the signal is not at boresight one can write

$$SCR_{\text{loss}}\ [\text{dB}] = SCR_{\text{boresight}} - SCR_{\text{apparent}} = 2(A_{\text{eq boresight}} - A_{\text{eq apparent}})\ , \tag{2.13}$$

in which SCR_{loss} gives the loss in SCR (in dB) due to the fact that the signal is not at the boresight of the corner reflector. In this equation the system constant C and β_0 conveniently drop out. Eq. 2.11 proves that if expressed in dB, the change in RCS for a corner reflector is similar to the change in SCR. This gives the opportunity to study the effect of alignment on the radar signal without dealing with site and CR specific parameters. Results on such a study can be found in section 6.2, influence off the alignment on RCS of a corner reflector is given in the next paragraph.

Alignment The theory behind RCS loss of a reflector due to alignment bias can be found in [32], [33] and [34]. For a trihedral CR to stay below a 1 dB change in RCS/SCR, the azimuth offset should be between $\pm$ 12.17 degree. The incidence angle offset should be between -11.92 and +11.91 degree. The full contour combining azimuth and incidence angle offset is given in Fig. 2.29. The individual components of azimuth and incidence angle can be found in Figure 2.30 and 2.31

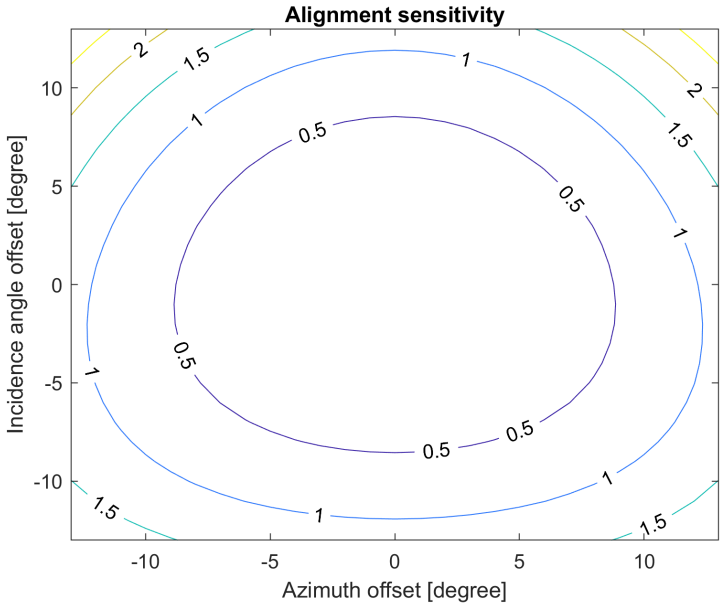

Figure 2.29: Alignment sensitivity for DBF90T-GNSS. Contour lines show RCS or SCR loss in dB due to misalignment.

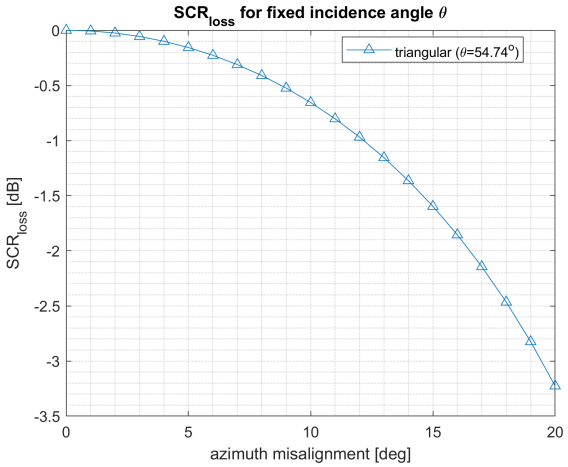

Figure 2.30: SCR_{loss} due to misalignment in the azimuth direction [32][34][35] (with an axis of symmetry in the optimum angle).

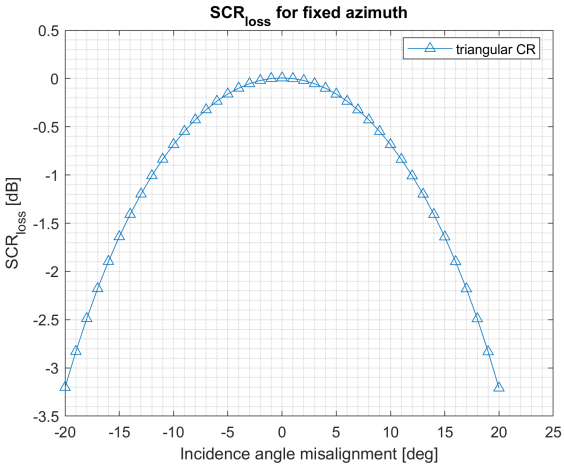

Figure 2.31: SCR_{loss} due to misalignment in the vertical plane [32][34][35] (without an axis of symmetry in the optimum angle)

Error propagation of phase error in the interferometric phase The previous paragraphs only present a measure of the theoretical phase quality of a single reflector. However, the results shown in this report are results for double difference measurements. The interferometric phase is a result of the difference between the master and slave phase, hence error propagation occurs. Furthermore, interferometric observations show a difference between the phase of a PS or reflector of interest and that of a reference PS/reflector. So again, error propagation occurs at this step. When it is assumed that the master, the slave and both PSs/reflectors are uncorrelated, this results in the following equation for the variance of the double difference method [31]:

$$\sigma^2_{\varphi^{m-s}_{\text{PS-ref}}} = \sigma^2_{\phi^m_{\text{PS}}} + \sigma^2_{\phi^s_{\text{PS}}} + \sigma^2_{\phi^m_{\text{ref}}} + \sigma^2_{\phi^s_{\text{ref}}} \tag{2.14}$$

in which $\sigma^2_{\phi^m_{\text{PS}}}$ is the variance of a PS of interest in the master image, the other three follow in the same way.

2.4.2. Radar system Geometry

The radar system geometry describes the geometrical relation between the earth, the SAR satellite platform, the SAR signal, and the region of interest. Figure 2.32 shows a satellite platform following a near polar orbit around the earth. As the satellite circles the near poles, the earth spins underneath its circular path. The part shown in the figure are the *ascending* tracks of the satellite, travelling from southern to northern hemisphere. The view on the *descending* tracks, where the satellite travels from the northern to the southern hemisphere is blocked by the earth in this figure. When a satellite orbits the earth in a *sun-synchronous* orbit, it orbits in such a way that each satellite overpass happens at the same time of the day after a fixed period of day, as its repeat pass frequency of the satellite is in sync with the repeat pass frequency (1 day) of the sun.

The orbital inclination of the satellite's orbit determines the shape of the ground track. The orbital inclination of Sentinel-1 is 98.18°[36]. As the orbit falls in a plane tilted with respect to the earth's equator, it seems to have a constant flight direction. However, if projected on a Mercator map, which shows true cardinal directions, a trajectory is shown which changes heading throughout the orbit.

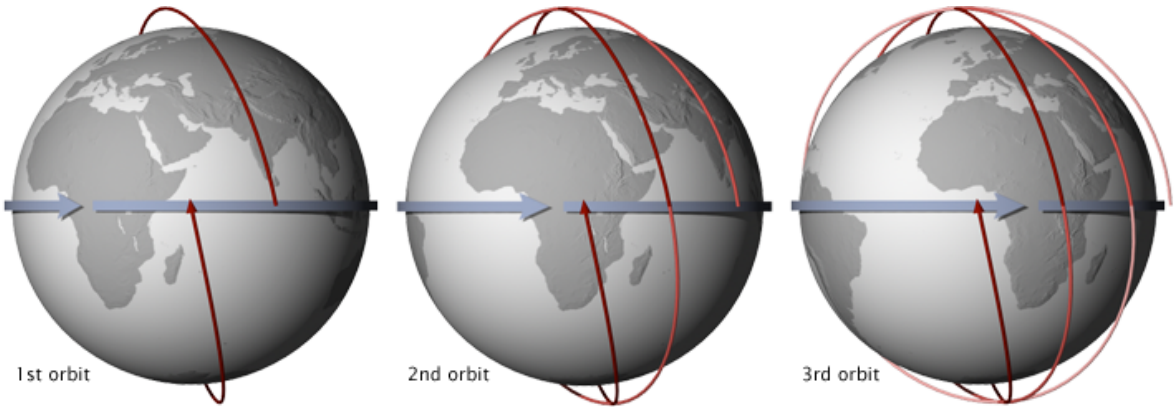

Figure 2.32: Three revolutions of a near polar, sun-synchronous orbit. (Figure courtesy of NASA)

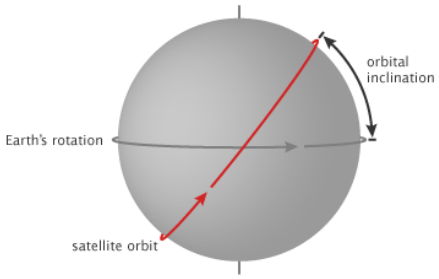

Figure 2.33: Orbital inclination of a satellite orbit. (Figure courtesy of NASA)

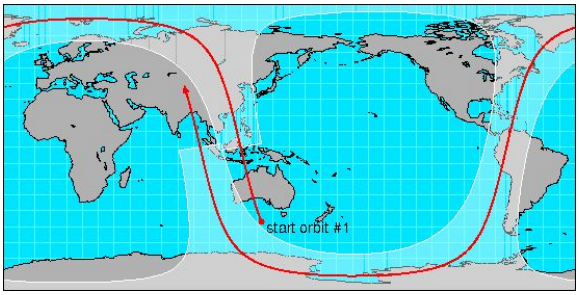

Figure 2.34: Ground track of a near polar orbit. showing the different heading along different latitudes. (Figure courtesy of San Francisco State University)

The geometry of the radar the signal is shown in 2.35. It shows a right looking satellite traversing the earth's surface in the direction from 1 to 2 following the red line shown in figure 2.33 and 2.34. Geometrical parameters shown are H_{sat}, which is roughly 693km, and the off-nadir angle θ ranging from 26° to 40.40° both for Sentinel-1[36]. Further explanation of parameters shown in the figure can be found in [6].

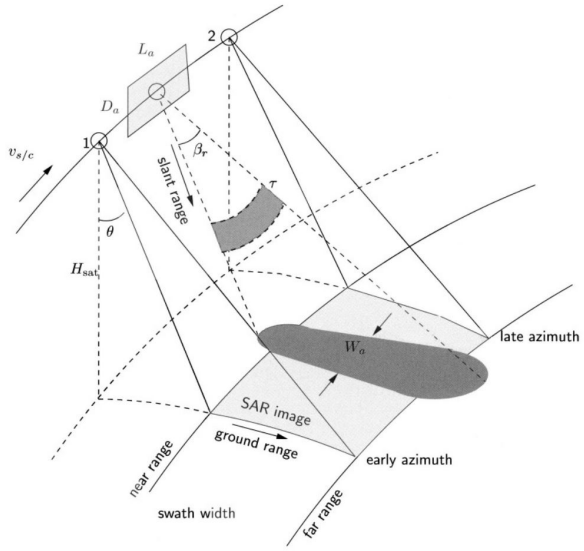

Figure 2.35: Signal geometry of a SAR satellite. [6]

Figure 2.36 shows the differences in seemingly similar angles. The off-nadir angle might be inter-

preted as similar to the incidence angle, but the figure exaggeratedly shows the difference caused by non parallel nadir and zenith directions. The look angle for simple SAR systems is perpendicular to the heading. The heading is given with respect to the North direction by the metadata of the SAR data, this may be used to determine the azimuth of the signal towards the ground. However, this azimuth is not the same azimuth that is used at the ground station to determine the azimuth towards the satellite. This effect is also shown by the convergence of meridians.

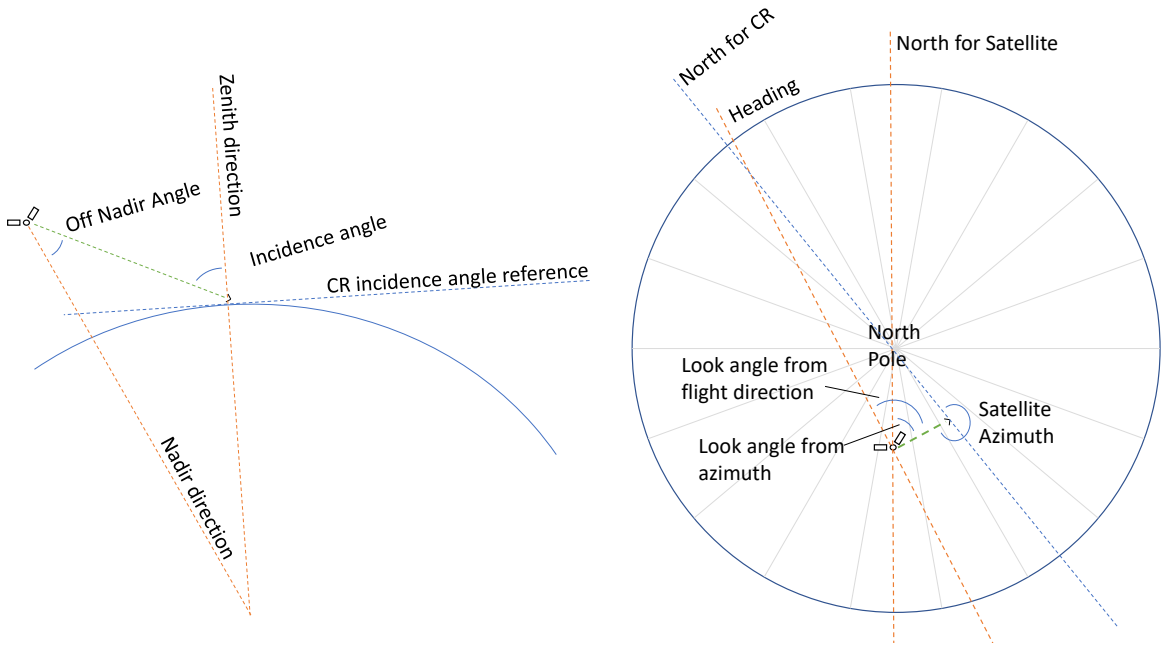

Figure 2.36: Differences in geometry between the perspective of the satellite and a ground station.

2.4.3. Aligning a corner reflector to the radar geometry

The alignment of the boresight of an reflector with respect to the incoming signal has an impact on the RCS and thus the SCR of the CR. Both the alignment in the vertical as in the horizontal plane is discussed in the following paragraphs.

Azimuth and Incidence angles The direction of the incoming signal can be described by two parameters. The azimuth and the incidence angle. The Azimuth is an angle describing a direction in the horizontal plane. The reference is the true North direction (WGS84). It is measured clockwise from this reference. For the case of the Groningen field study, the azimuth of the signal is more of less the same for the whole deployment area; it is 100° and 260° for descending and ascending tracks respectively.

The Incidence angle is a parameter describing the direction of the signal in the vertical plane. The reference is the zenith axis, running perpendicular from the reference ellipsoid towards the sky. The incidence angle depends on the acquisition geometry. Because of the north-south oriented path of radar satellites, it shows a strong correlation with longitude. This can be seen in figure 2.37. The figure shows the incidence angles for Sentinel-1 satellites for locations spread over the province of Groningen, the Netherlands. The data shows a spread of roughly 12°, most notably because each location is visible from two different satellite tracks in ascending as well as in descending direction. Within a specific track, the spread of the incidence angle is a little less than 4° within the area.

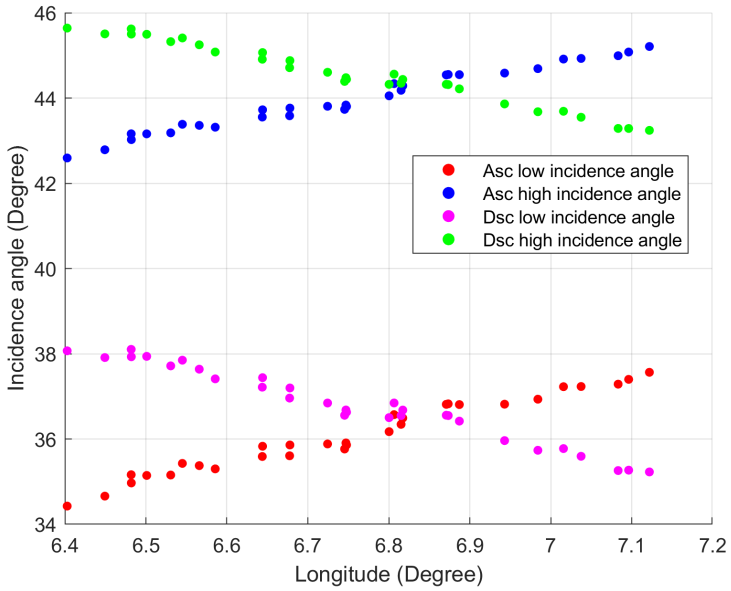

In

Figure 2.37: All incidence angles with respect to their longitude for IGRSs in the Groningen field study. The incidence angel is clearly related to the longitude as seen by the trends in the data. The slight deviations from a straigth line running through the points are given by the different latitudes of the locations.

Boresight axis of a trihedral corner reflector The boresight of a corner reflector is given by the direction of maximum signal reflection. The boresight axis is shown in figure 2.38 in which the CR is placed in a local XYZ reference system. A corner reflector will only reflect a fraction of the incoming signal depending on the aperture of the CR. The aperture depends on the orientation of the reflector with respect to the incoming signal. The axis of maximum aperture is the boresight. For a trihedral corner reflector the boresight can be represented by the vector [1, 1, 1]. The angle made from the z axis to the boresight is called θ and has a value of $\arctan(\sqrt{2}) \approx 54.74°$. The angle between the vertical plane of the boresight and the x axis is called ϕ and has a value of $45°$. Different shaped reflectors have different values for θ and ϕ[32].

Perfect alignment When the boresight axis of the reflector has the same orientation as the signal, it is called a perfect alignment. Both a misaligned and a perfectly aligned corner reflector are shown in figure 2.39. A misaligned reflector will still reflect the signal but with a lower signal strength since its effective aperture is smaller[32].

Apex of the corner reflector The phase centre of a reflector is the physical location which corresponds to the location represented in the return signal. For a trihedral corner reflector, the phase centre is located in its *apex*. The apex is given by the origin of the axis drawn in Fig. 2.38 and 2.39.

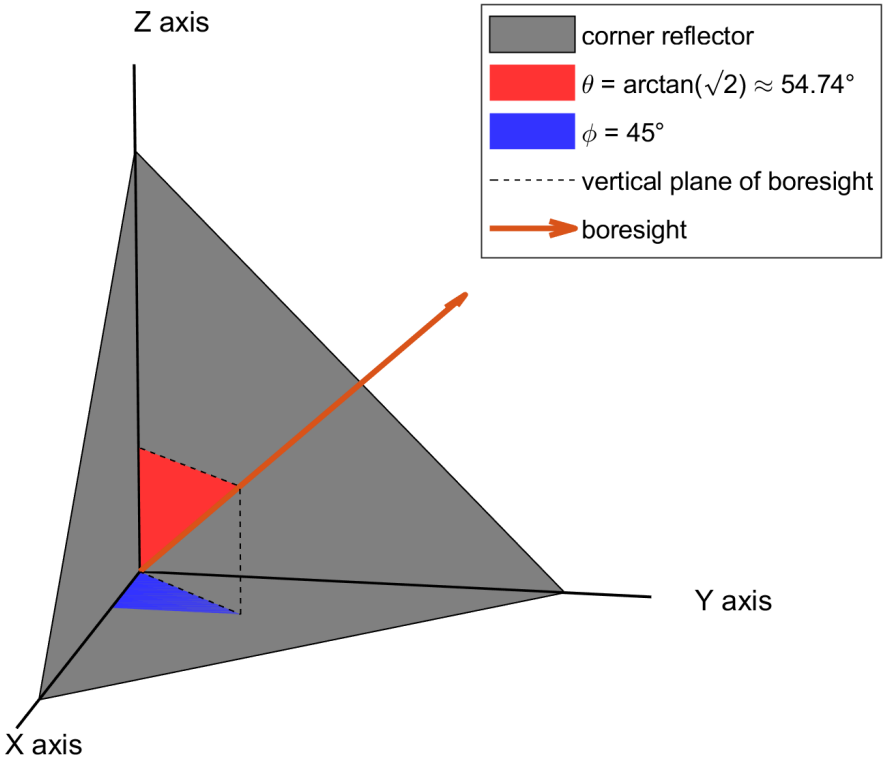

Figure 2.38: Representation of a CR with its boresight axis.

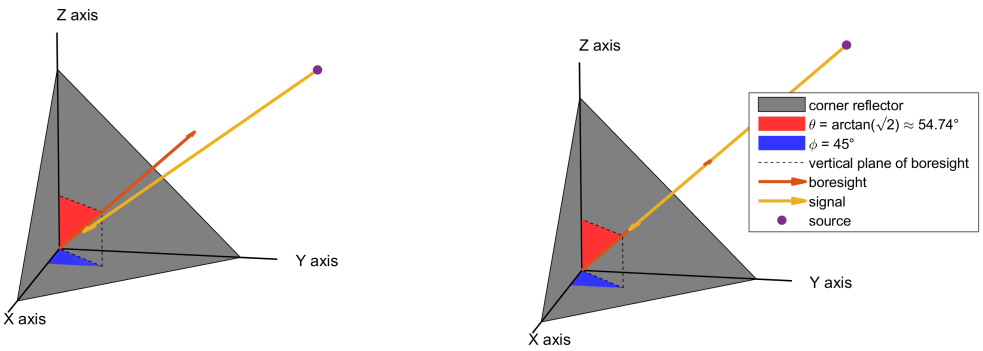

Figure 2.39: Left: A misaligned reflector. Right: A perfectly aligned reflector.

2.4.4. Actual deformation vs. Line-of-Sight displacement

From phase to LoS deformation The radar system used for InSAR measures the 2-way travel time between target and antenna. It does so in its *Line-of-Sight* (LoS) towards the target as described above in the geometry and sensitivity sections. Therefore, all deformation of a target is projected on the vector of the LoS.

The relation between phase values and LOS deformation is given by

$$LoS_{\text{deformation}}[\text{mm}] = \phi * \frac{\lambda}{4 \cdot \pi}. \tag{2.15}$$

λ is the carrier wavelength of the signal, ϕ is the interferometric phase. Eq. 2.4 implicitly presented this relationship earlier.

Sensitivity of the InSAR instrument to shifts of a target The sensitivity of the InSAR instrument to a deformation signal with components in the north, east and up direction is dependent on the LoS geometry. The forward model, going from in-situ 3D deformation to 1D LoS measurements, is given in detail in [6] and [18]. This subsection presents a simplified visual representation of this forward model to present the main message.

A deformation signal can be represented as a shift of a target in a certain direction. The sensitivity of the InSAR instrument to such a shift is visualised in a top view and a side view in Figure 2.40 and 2.41, which are based on a LoS found at the test location in Wassenaar (described in section 5.1.1).

From Fig. 2.40, showing the horizontal plane or the top view, it can be seen that InSAR is capable of picking up east-west motion with a single reflector. When combining the sensitivity of both reflectors, the most pessimistic shift in a north-south signal has a maximum detection ratio of 0.2 times the sensitivity of a measurement in the azimuth direction. This indicates that it is very poorly detected.

Figure 2.41 shows the sensitivity in the vertical plane parallel to the LOS. Strictly, all four tracks have their own vertical plane which are not parallel as they have their own LOS geometry. However, these four planes are only roughly 20 degrees apart (see Fig. 2.40). This figure shows the importance of combining the ascending and descending geometries. When both are combined, the reflector pair is sensitive to the vertical components in the deformation direction. When exclusively ascending or descending geometries are used, insensitivity occurs at an angle perpendicular to the incidence angle.

When a target reflects towards ascending and descending satellites and if it is located in the overlapping region of two tracks it can be monitored from 4 directions. With an inverse model, this would give enough information to derive the 3D deformation of a target. However, 3D results include large propagated errors due to the ill-posted nature of the LOS measurements due to their unfavourable mutual angles. Therefore, results are often shown in the easy interpretable 1D format of LoS deformation.

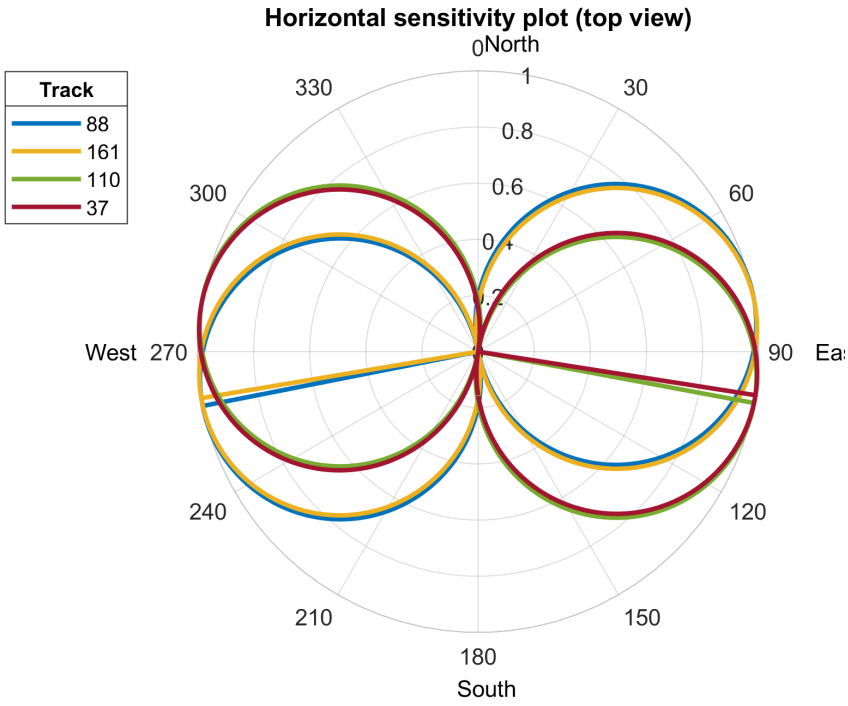

Figure 2.40: Normalized sensitivity plot in the horizontal plane. The plot shows the sensitivity to horizontal movement in any direction. The colored lines present the ratio of measured deformation over in-situ deformation for the specific direction. The straight and coloured lines are the azimuth angles of the LoS.

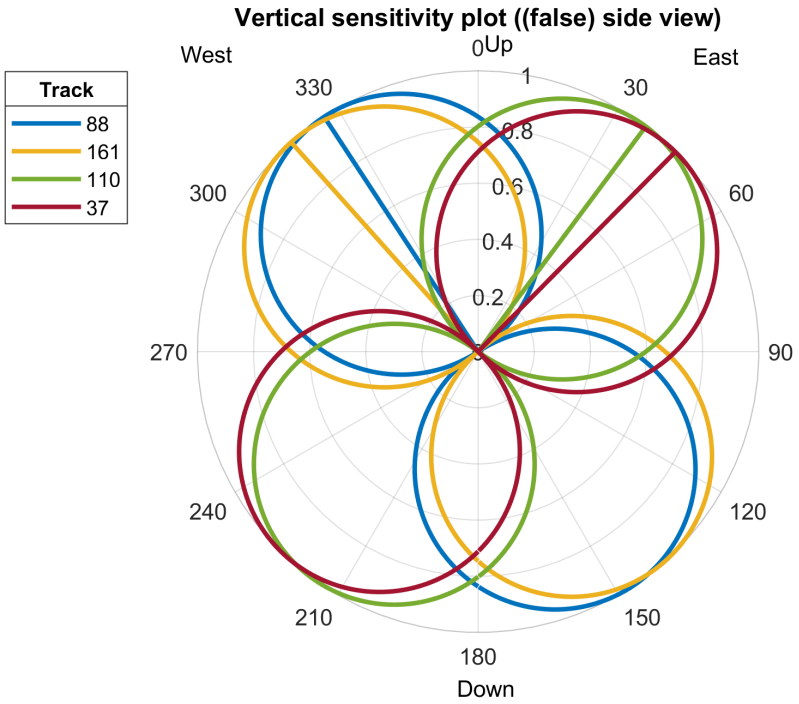

Figure 2.41: Normalized sensitivity plot in the vertical plane running parallel to the LOS azimuth (found in 2.40). The plot shows the sensitivity of the InSAR measurment to movement of a target in any direction along the vertical plane. The coloured lines give the ratio of measured deformation over in-situ deformation for the specific direction. The straight lines are the incidence angles of the LOS.

3

IGRS Requirements

The requirements for an IGRS stem from the objective of the IGRS given in the last paragraph of Section 1.2 and the data integration problem stated in 2.3. The final requirements are set by a team of the TU Delft consisting of Prof.dr.ir. R.F. (Ramon) Hanssen, Dr.ir. H. (Hans) van der Marel and J. C. (Jurjen) Kamphuis. Their motivation for these requirements is based on scientific literature describing similar projects. The main motivation of each requirement is given below the requirement. The requirements can be split in two categories. The functional requirements stating what the system should do, and the non-functional requirements stating what the system should be or to what quality standards it should meet. The performance requirements are included in the non-functional requirements.

3.1. Functional requirements

The functional requirements which can be used to develop an IGRS are listed below together with their main motivation.

The IGRS shall:

1. **receive and record GNSS signals by using a continuous operating GNSS reference station;**

   To be able to connect the IGRS to a well defined Terrestrial Reference Frame (TRF), e.g. ITRF(2014).

2. **reflect radar signals back to SAR satellite constellations (Sentinel-1, TerraSAR-x, Radarsat 2) for both ascending and descending acquisitions;**

   To be able to connect the (In)SAR measurements to the reference frame defined by the GNSS measurements.

   To be able to connect multiple (In)SAR measurements from different tracks to one single radar datum.

3. **house levelling benchmarks;**

   To be able to connect the IGRS to a national height datum by means of levelling campaigns.

   To be able to monitor the stability of the IGRS (monument stability) with respect to nearby survey markers.

   To be able to monitor the stability of the reference points on the IGRS amongst each other.

4. **house total station reference points;**

   To be able to monitor the stability of the IGRS (monument stability) with respect to a local XYZ reference frame

   To be able to monitor the stability of the individual reference points amongst each other.

5. **house a LiDAR reference surface; and**

   To be able to translate the reference frame of a regional LiDAR product to a common datum.

6. **integrate all of the above into one physical system.**

   To ensure stable collocation of observations and minimize the error in the local 3D location estimates of the individual reference points.

3.2. Non-functional requirements

The non-functional requirements can describe the minimal performance, a quality standard or any other requirement not stating the functionality of an IGRS. Our non-functional requirements are given by the following eight statements.

The IGRS shall:

1. **make use of geodetic monitoring grade GNSS equipment ensuring ~mm precision;**

   The IGRS is a research and development project and strives for a state-of-the-art solution for the collocation of reference points. This includes using the best available GNSS solutions as this is the direct link to a well defined Terrestrial Reference Frame. This means a GNSS antenna can be mounted with unobstructed view. Furthermore, housing for the GNSS receiver, power, data storage and data communication should be present.

2. **make use of radar reflectors with 1 mm double difference phase precision in the Line-of-Sight;**

   The use of trihedral corner reflectors follows from the requirements regarding manufacturability, deployability and maintenance. Active electronic transponders are not yet developed to stable and proven enough levels at the start of this project to be used as SAR reference point.

   This requirement should be specified further for proper implementation in the design. If the 1 mm double difference phase precision is a result of two IGRS reflectors, this requirement leads to a single phase precision of one reflector of 0.5 mm. This follows from Eq. 2.14. From Eq. 2.4 follows that for a one-sigma value of 0.5mm in the Line-of-Sight, a SCR of 15.9 dB is needed.

   As the SCR is depended on clutter strength, which is site specific, there is no one-size-fits-all solution. Therefore, a wisely but arbitrary chosen or site specific value can be used during the design process. 13 dB can be argued to be a likely arbitrary value for nominal clutter strength for Line-of-Sight-1 (Section 6.2.3). Using Eq. 2.10, a reflector with a RCS of 28.9 dB is needed to meet this requirement.

   Using the specific case of Eq. 2.9 for a trihedral corner reflector (given by Eq. 4.1), this leads to a corner reflector with an inner leg length of 0.87m.

3. **lead to errors associated to the relative location of reference points which are of the same order or lower than those of the individual sensor errors;**

   Collocation of observations is not possible if the relative locations of the reference points are not stable or unknown. However, collocating the reference points very precise will be overshadowed by the precision of the individual measurements.

4. **house equipment for measurement techniques, which do not significantly lower the signal quality for other measurements;**

   Any bias or noise signal caused by the IGRS itself, will degrade the transformation to a common datum.

   Items of concern are multipath in the GNSS signal caused by the radar reflector and auxiliary reflections in for InSAR from the mounting structure.

5. **be resistant to transport, handling and deployment;**

   The IGRS will inevitably be transported, handled and mounted by contractors. The design shall be designed to withstand these activities to avoid strict regulations and extreme caution.

6. **be able to withstand 20+ years of exposure to weather influence (wind, rain, corrosion) with minimum amount of maintenance;**

   An IGRS is mounted to interpret deformation processes with long time scales which implies the long term use of an IGRS. Advancements in the field of geodetic remote sensing make it plausible that different solutions for the datum connection problem will be developed reducing the need for a significantly longer lifespan which otherwise would cause problems such as corrosion and/or degradation of the active instruments.

   The IGRS shall be designed in such a way that it requires minimal maintenance as a result of weather influences. This includes mounting a radome on the GNSS antenna and implementing a downward pointing set-up for the radar reflectors leading to less downtime and minimal maintenance due to debris.

7. **be affordable, manufacturable and deployable for campaigns with multiple units; and**

   The transformation parameters between geodetic datums may be spatially variable. Therefore, multiple units are desirable for larger study areas.

8. **not lead to any hazardous situation.**

   Creating an IGRS design that does not lead to any hazardous situation once it is deployed does not inherently interfere with the core objective of an IGRS and should therefore be pursued.

4

Design of the IGRS

This chapter describes the design and the design methodology used for the development of the IGRS. The three different types are introduced and the design choices are explained

4.1. Design methodology

The design of the IGRS has been a research and development (R&D) process because no products with the same requirements exists on the market or in scientific literature yet. New knowledge on the different subjects had to be gathered and has been implemented into the design in different design cycles. Each design cycle was used as input for the next, resulting in a clear development towards a fully functional IGRS.

Every cycle in the R&D process can be expressed schematically by the design model shown in Fig. 4.3 by [37]. Although this model was not implemented from the start, it does represent the steps that were made during our process. A total of three cycles were run through in a period of 5 months resulting in 3 stages of advancement, of which the third stage got the label ”approved design”. These stages are shown in Fig. 4.1 and described below by three level of advancement and function:

i. mock-up design as a first proof of concept

ii. prototypes for full performance testing

iii. production type to deploy in the field

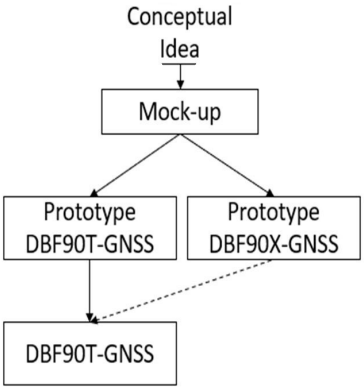

Figure 4.1: Model of the design process. The lines respresent evolved design, the dotted line represents lessons learned.

Figure 4.2: Mock-up version of a first IGRS.

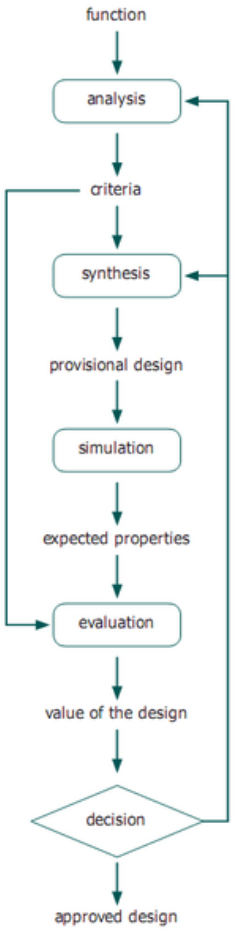

Figure 4.3: Delft design cycle representing the steps that were made in each design cycle from the mock up to the production model. [37]

4.2. Naming conventions

The names of the IGRSs are defined in the following manner: DBF#(T/X)-(GNSS/…). 'DBF': Double backflip reflector, describing the radar reflector part. '#' for inner leg length in cm. (T/X) for shape definition, T for triangular plates and X for extended plates. (GNSS/…) is a label for all active sensors on board. For example; DBF90T-GNSS is a double backflip triangular corner reflector with an inner leg length of 90 cm and mounted with a GNSS antenna.

Figure 4.4 shows the prototype DBF90T-GNSS. Figure 4.5 shows the nomenclature of all the parts.

Parts:

1. pole
2. frame
3. top/horizontal plate
4. radar reflector (2X)
5. CR tilt angle mechanism
6. GNSS antenna
7. GSM antenna
8. instrument cabinet

Figure 4.4: Prototype DBF90T-GNSS.

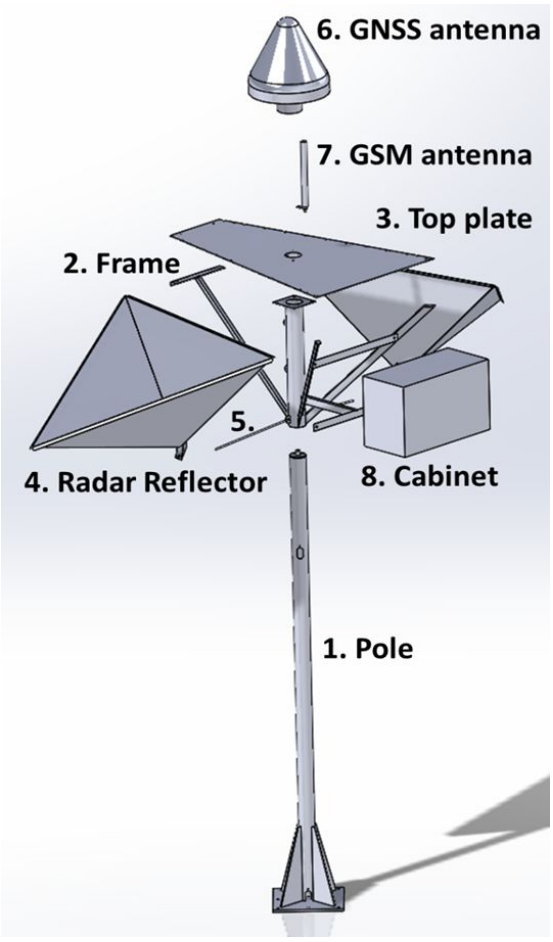

Figure 4.5: Nomenclature of the IGRS.

4.3. Cycle I. The mock-up

Three design cycles took place resulting in the mock-up, the prototypes and production model. This and the following two sections elaborate on the main goal and results of each cycle.

The first functional requirements from Chapter 3 were materialized in a first mock-up consisting of

an initial design for the two reflectors and a provisional mounting construction. This mock-up is shown in figure 4.2. The mock-up has been used for three main purposes:

i. To do an experimental verification of the DBF concept and of the predicted RCS.

ii. To find a position for the GNSS antenna on the IGRS such that the interference between GNSS and the DBF reflector, and vice-versa, is at an acceptable level.

iii. To be able to verify and improve on the structural integrity and stiffness.

Major design decisions for two other prototypes are based on this mock-up. The experimental results on RCS and GNSS antenna position are described in Chapter 5 and [38]. Conclusions from these experiments were taken as input for the development for two new prototypes. The three main purposes of the mock up resulted in three conclusions corresponding to the three main purposes described above. The three conclusions as follows:

i. The calculated RCS based on 90cm inner leg length CRs was verified. (See chapter 5.)

ii. A location for the GNSS antenna was found. (See requirement 1 in the next section.)

iii. The construction lacked stiffness and was able to be moved with little effort resulting in a vibration of the whole station. Overall, the mounting structure of the CRs was not stiff enough to ensure a stable fixation of the CRs.

Furthermore, two extra lessons were learned that were not intended but were used in the prototype design:

- The corner reflectors were produced in a way which could not ensure high quality orthogonality.
- The alignment mechanism was not user friendly for installation by one operator and had too many degrees of freedom to lead to reproducible set-ups.

4.4. Cycle II. The prototypes

The results from the experiments with the mock-up together with expert opinion from other stakeholders resulted in the following set of design requirements for the prototypes. The source of the design requirement is given in between brackets

1. (Cycle I) GNSS antenna should be on a 2.40 meter pole.

   Experiments show clear quality loss due to multipath when the GNSS antenna is placed directly above the radar reflectors [38]. A low placement with 30 cm in between the antenna and the radar reflectors led to acceptable results, but will be more likely to be influenced by structures on the horizon. A high placement of the antenna will need an existing or dedicated mounting structure. The choice has been made to use the standard height of the involved stakeholders.

2. (Original requirement) There should be both ascending and descending corner reflectors.

   To fully make use of the available Sentinel-1 radar imagery, ascending and descending corner reflectors are needed. Furthermore, integration of ascending and descending corner reflectors will give a direct link between measurements in both measurement geometries, leading to more meaningful interpretation of deformation estimates.

3. (Original requirement) The corner reflectors should be back flipped.

   By placing them with one edge in a downward position, most of the debris will slide down the reflector, which results in a reflector less likely to collect wind driven debris and water.

4. (Validated requirement) The corner reflectors should have a inner leg length of 90 cm.

   Corner reflectors with an inner leg length of around 90 cm will lead to acceptable phase precision as presented in the non-functional requirements. Corner reflectors with considerably smaller size (30-40 cm) will not have a high enough SCR to result in a precise interferometric phase. Corner reflectors considerably larger will not directly lead to a better interferometric phase. Further details are found in Chapter 5.

5. (Original requirement) The phase centre of the corner reflector should be on a stable position relative to the pole.

   The main goal is to connect reference points in the physical world. The precision in which the offsets of the measured points are known will directly propagate into the performance of the IGRS. The phase centre of the corner reflector is found in the apex. Thus, a stable position of the apex to the pole, which is stable with respect to the GNSS antenna, is needed.

6. (Original requirement) The IGRS should include a horizontal surface of about 0.5 m^2.

   This surface can be used as a reference surface in airborne laser altimetry. The Dutch airborne laser altimetry dataset AHN2 has around 10 points per square meter [39]. A horizontal surface of about 0.5 m^2 is likely to be visible in a future dataset.

7. (Original requirement) The reflectors should be orientable to Sentinel-1 satellites.

   Sentinel-1 is the preferred satellite constellation by the stakeholders because of its good spatio-temporal coverage of the Netherlands. Additionally, TerraSAR-X can still be used opportunistically due to its higher carrier frequency.

8. (Newly discovered requirement at start of Cycle II) The orientation of the radar reflectors should be done independently from orienting the GNSS antenna.

   When the orientation of the GNSS antenna and the reflectors is done independently, a readjustment of either of the two is possible, keeping the original time-series of the untouched sensor intact.

9. (Newly discovered requirement at start of Cycle II) There should be a place to mount the GNSS instrument cabinet.

   This should be either on a pole next to the IGRS, or on the IGRS. To keep both the footprint small and unwanted signal low, the instrument cabinet should be placed on an appropriate place

10. (Newly discovered requirement at start of Cycle II) There should be levelling benchmarks included on suitable reference surfaces.

    Levelling benchmarks are needed to be able to perform repeatable levelling surveys which are relatable to the other sensors or reference points.

These requirements were used to develop two prototypes. The DBF90T-GNSS and the DBF90X-GNSS.

4.4.1. Prototype DBF90T-GNSS

The design requirements result in the following design choices for the DBF90T-GNSS. See Fig. 4.5 for reference to the parts.

Pole

Because of design requirements (1) and (8), one continuous pole from the foundation to the antenna is used. The mock-up could be set in motion by hand, as the foot lacked a stiff connection between the pole and the anchoring bolts. This is solved by placing fins between the pole and the base plate, creating a much stiffer design. The new pole resembles the standard pole used by the stakeholders

involved in the project, but the wall thickness of the pipe is updated to a thickness of 3mm to cope with the extra stress due to the reflectors. Two holes are added so all cables running from antenna to receiver can be guided through the pole without the need for external mounts.

Frame

The mock-up design did not have a frame, this gave the following disadvantages: poor fixation of the reflectors, extra parts for aiming the reflector and no place to mount the cabinet. A frame was constructed to lift the weight of the reflectors which would otherwise bend the top plate (5, 6). The frame ensures a 90-degree angle between the top plate and the pole, even under and after high loads. The frame carries both reflectors, the cabinet and simple hardware to aim the reflectors (2, 3, 8, 9). The frame is mounted around a 2mm thick tube which has an incision from the bottom to just below the top. The prototype design has three welded fixation points which tighten the tube around the main pole. The production type has two off-the-shelf clamps which can handle the high tightening forces better. The frame mainly consists out of 4 mm thick 40 by 20 mm stainless steel corner profile strips. Corner strips are preferred over tubes for easy welding and mounting whilst ensuring stiffness. Using 4 mm thick hot rolled, rather than thin cold rolled profiles helps in minimizing deformation after welding.

Horizontal plate

The horizontal plate is made of 5 mm thick aluminium. Aluminium would not be the preferred material of choice in terms of GNSS multipath and laser scanning altimetry (as the smooth aluminium works as a near perfect mirror and might lead to false reflections), but from a construction point of view it is a low risk solution (6, 10). An alternative would be a non-metallic substitute for the GNSS or simply a coating for the laser scanning altimetry. The trapezium shape of the plate follows from the requirement to aim for both ascending and descending satellites (2) (corners of 79° and 101°). This implies the shape is only suitable at latitudes where satellite tracks have an azimuth direction of roughly 349 and 191 degrees north (or south). There is a midpoint marker on both the north (=wide) and south (=narrow) side of the top plate (too small to be seen on the drawing), which can be used while orienting with the help of a physical north-south line (7).

The horizontal plate can be used as a reference during levelling surveys. The procedures for levelling surveys are found in Chapter 6.5.

Radar reflector

The radar reflector has been dimensioned with the help of results from RCS calculations. Details on these calculations are given below. From the first mock-up we learned that 2mm sheet aluminium without stiffening features is moving in heavy winds and is vulnerable for deformation (5). Especially while handling and carrying the structure. The choice has been made to increase the thickness to 3mm and bend the outer edge 55 degrees creating stiffeners along the whole outer edge. The choice has been made to bend one plate in a "V" and bolt it to a second plate to minimize orthogonality errors. See figure 4.7 for en exploded view of the reflector.

RCS sensitivity on sizing The peak RCS for a trihedral corner reflector (RCS_{tcr}) is given by

$$RCS_{\text{tcr}} = \frac{4\pi a^4}{3\lambda^2}, \tag{4.1}$$

in which a represents the inner leg length of the reflector [m] and λ is the frequency of the signal [Hz][33]. Changes in a have an impact on the RCS. This impact is presented in Figure 4.8. Unintended size errors are not likely to cause large effects as one mm leg change corresponds to a change in RCS of about 0.02 dBsm for a CR with inner leg length of 90 cm and a peak RCS of 29.5 dBsm. However, just 5 cm would be sufficient for an intentional resizing leading to a 1 dBsm change.

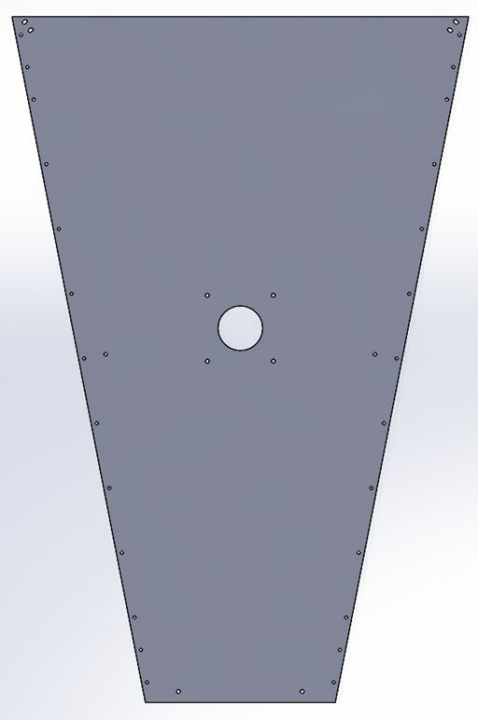

Figure 4.6: Top plate acting as part of the frame and reference surface. The long edges have a length of about 130 cm.

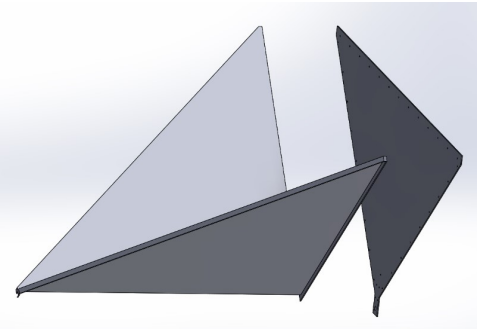

Figure 4.7: The two separate parts of the corner reflector.

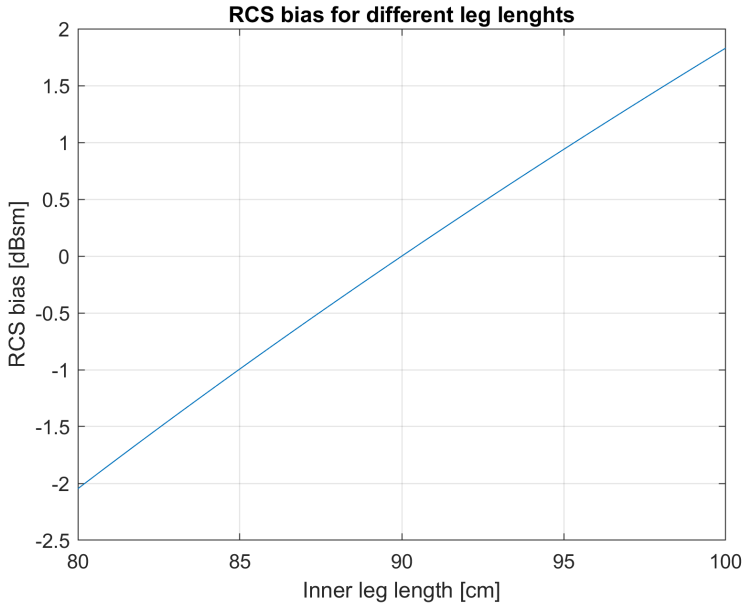

Figure 4.8: RCS sensitivity to sizing for the DBF90T-GNSS.

CR tilt angle mechanism

The aim for the corner reflector tilt angle mechanism is to have a full range of motion to tilt the CR from roughly +6 degrees to -15 (6). The mechanism is preferably far away from the hinge, to get the highest rigidity against tilting while ensuring low forces on the parts. So, because of the stability, strength and position of the apex, this is a good place for attaching the mechanism. The other attachment is chosen to be at the lower end of the frame.

The apex describes a roughly 25 cm long horizontal arc when making the 21-degree tilt. Starting from about 5 cm from the frame to about 30 cm from the frame. As the movement is mostly horizontal, a mostly horizontal fixation in any tilt-state is preferable. When using a horizontal expanding mechanism this would result in an expansion of 600% which seems unreasonable. This is why the choice has been made to go for a slider-and-rod principle. As the slider is attached to the apex, it moves in an arc. A fixed rod should be curved to allow a smooth movement of the slider. Another (easier) option is to go for a straight, but tilting, rod.

Figure 4.9 shows a simulation of such a rod and slider principle. It shows the full range of motion of the CR and the corresponding range of motion of a rod fixed with a hinge on the frame. An optimal mounting position on the frame and length of the rod is chosen based on this simulation. The optimal place is such that the rod does not interfere with the CR and does not stick out much when the CR is tilted all the way backwards.

The rod has a flat surface on one of the sides on which 50 mm marks have been made. After mounting, the distance between the bolts on the inside of the rod should be measured and noted for future reference.

Figure 4.10 gives a detailed view on the mechanism.

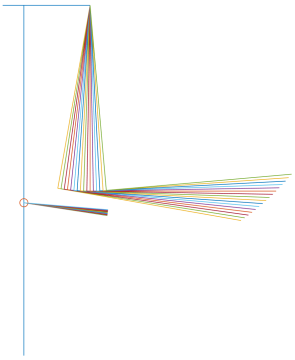

Figure 4.9: Matlab simulation of the range of motion for both reflector and rod.

Figure 4.10: Final design of the mechanism.

GNSS antenna

The top of the pole contains a 5/8 inch bolt on which the GNSS antenna adaptor can be mounted. The GNSS adaptor for this project is an off-the-shelf SECO mount. The GNSS antenna is attached to the pole with the help of the SECO mount. The GNSS antenna can be levelled and oriented north by adjusting screws on the mount.

Cabinet

The cabinet itself is an of-the-shelf product and houses all the active instruments. It is mounted on the frame so it rotates together with the corner reflectors.

Foundation

Making a foundation is beyond the scope of this report. However, the IGRS has to be connected to the foundation. Therefore, the basic requirement for the foundation is that it includes 8 M10 bolts spread around evenly on a 30 by 30 cm square, making the heart-to-heart distance between the bolts 15 cm.

4.4.2. DBF90X-GNSS

The DBF90X only differs from the DBF90T in the design of the corner reflectors. When the radar signal hits the reflector, it can be modelled as a ray bouncing of at the plates [32]. When a ray bounces subsequently at all three orthogonal plates, the return signal makes a 180-degrees turn in the 3D space. When a ray hits the first plate but never reaches the second one to bounce off, it does not contribute to the return signal as it does not make the full 180-degree turn.

Incoming rays parallel to the boresight axis (axis of maximum reflection, vector [1 1 1] if the edges of the reflector are aligned to x, y and z-axes, see Fig. 2.38) hitting the tips of the reflector, do not hit a 2nd or 3rd time. So, for a reflector who's boresight is aligned to the incoming radiation, it would not matter to remove the area at the far tips as it is not used to form a return signal. This effect is shown in figure 4.11 and 4.12.

Figure 4.11 shows the contributing area of all points hitting the blue panel first. Rays hitting the outer tips of the blue panel do not hit a 2nd of 3rd panel again so they do not contribute to the signal and are not shown. Figure 4.12 shows the total set of simulated rays that contribute to the reflection in the reflector.

The RCS of a trihedral corner reflector (RCS) is heavily dependent on the inner leg length as seen

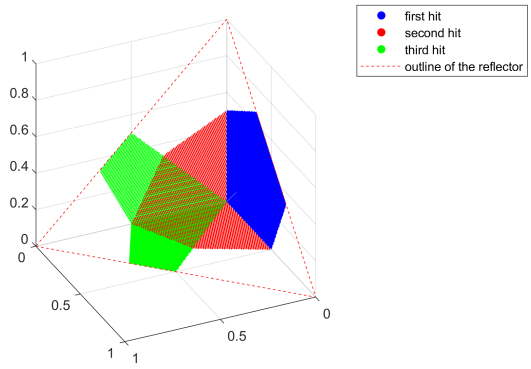

Figure 4.11: Reflection area of a corner reflector. Only the area that hits the blue panel first is shown for better interpretation of the reflection mechanics.

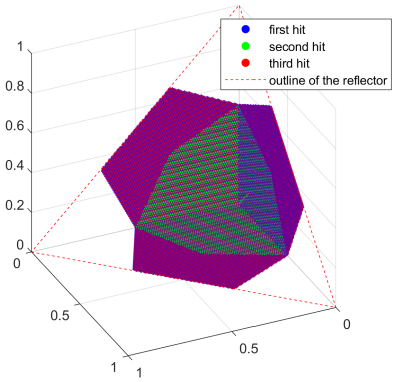

Figure 4.12: Reflection area of a corner reflector. The total reflective area is given by the summation of all colours. It can clearly be seen that the corners do not contribute to the signal.

in Eq. 4.1. So, it is beneficial to have a large inner leg length. However, with the theory above in mind, we can enlarge the effective inner leg length without changing the footprint. By extending the plates in the manner seen in figure 4.13, the RCS can be enlarged by almost 7 dB as the inner leg length for the trihedral model grows while the actual inner leg length does not change. As a consequence, the footprint stays roughly the same.

As a consequence of the adaptation, the triangular outlines which give stiffness to the reflector are not present any more. This leads to wobbly sides. This problem is solved by placing polycarbonate plates in the corners and polycarbonate strips on two diagonals. These extras give the desired stability.

Figure 4.13: Prototype DBF90X-GNSS: Descending reflector.

Figure 4.14: Prototype DBF90X-GNSS: Ascending reflector.

4.5. Cycle III. Production model for full deployment

During exploratory studies on possible deployment sites for the Groningen field study it is assumed by the main stakeholder that none of the sites are vulnerable for high background clutter. The risk and costs of the DBF90X are higher due to the more complicated manufacturing. Furthermore, there is a chance of debris built up, which might lead to even higher (maintenance) costs. Based on these considerations, it was decided to select the DBF90T-GNSS design for production during this project.

Only minor changes have been implemented for the production type. For this reason, no new name was proposed. There are 5 extra features which make up de difference between the prototype and the production model:

- full 90-degree bend of stiffening ribs on corner reflector
- the use of off-the-shelf parts to clamp the frame to the pole
- reference marks on the top plate for orienting north and levelling surveys
- making use of rivets where bolts had been used previously
- adjusted hole patterns for rivets to get higher strength at places with larger stresses

Figure 4.15: Production type DBF90T-GNSS.

4.6. Error budget of the IGRS design

The error budget of the design of the IGRS is defined by a combination of all errors for a certain application. In this thesis, the integration of InSAR time series into a well defined CRS has been the

main application of interest. However, presented in section 1.3, mulitple applications of an IGRS are possible. Therefore, depending on the application of a IGRS, different errors budgets may prevail.

The error budget for any application may consist out of one of the following sources. They can be split in errors related to sensor measurements itself, and errors related to the offset between the actual and estimated position of those sensors. The errors related to the sensor measurements are the following four errors:

1. measurement error of the corner reflectors
2. measurement error of the GNSS instrument
3. measurement error of the levelling instrument
4. measurement error of any other consulted external sensor/device

The errors related to the sensor position can be split even further into the time dependent, and time invariant errors. Whereas time dependent errors are different at the time of the master and slave acquisitions, the time invariant sensor position errors are constant over time. The time dependent errors are given by the following three sources:

5. loading (wind, snow)
6. thermal expansion
7. permanent deformation of the IGRS within the data acquisition period

If the time invariant sensor positions are based on the design parameters, errors may occur due to the following two sources:

8. geometrical production tolerances
9. permanent deformation outside the data acquisition period

If the time invariant sensor positions are based on local measurements, the errors are related to the measurement methodology that has been used. This can be seen as a 10th error, which is an alternative error to error 8 and 9.

For the integration of InSAR time series into a well defined CRS the time invariant errors, number 8, 9 and 10 are of little importance, since they will be assumed constant for both the master and slave image. Error 7, which represents large permanent deformation of the IGRS within the data acquisition period due to structural damage of the IGRS cannot be modelled, but effects of small movement on the measurement output is given later in this section. If any movement is suspected, it should be monitored/measured as will be described in Section 6.5. Simplistic models to determine errors 5 and 6 due to loading and thermal expansion are given below.

4.6.1. Errors due to loading

Wind and snow can exert forces on the IGRS which lead to strain. If the measurements are sensitive to this strain, it will end up as a bias in the data. For the calculations of the strains of the IGRS, rigorous simplifications have been made. The wind is modelled as two horizontal forces acting on the pole structure at a height of 2.4m and 1.2m. The first is representing the wind pushing to the GNSS antenna, the second one is the representation of the wind pushing to the radar reflectors. The pole is modelled as a homogeneous pipe from top to bottom, with neglecting the stiffness added by the fins in the foot and the extra material of the frame around its lower half. The assumption has been made that the foot gives a secure connection fixing all degrees of freedom for the bottom of the pipe.

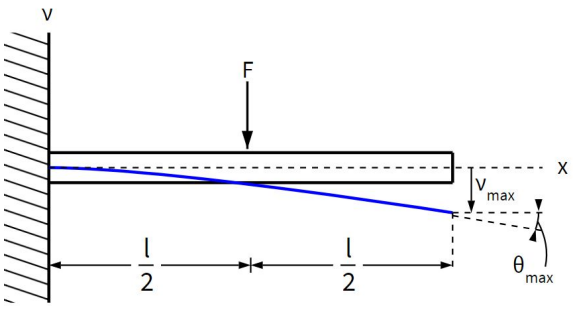

Figure 4.16: Fixed beam with loading half way [40].

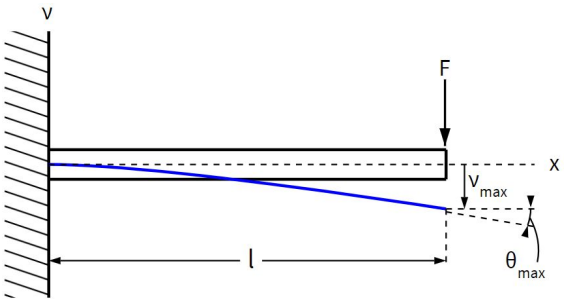

Figure 4.17: Fixed beam with loading at the loose end[41].

This leads to a combination of the load schemes in Fig. 4.16 and Fig. 4.17. This results in the equation[40][41][42]:

$$v_{\text{max}} = \frac{5l^3 \cdot F_{\text{reflector}}}{48EI} + \frac{l^3 \cdot F_{\text{Antenna}}}{3EI} \tag{4.2}$$

in which $F_{\text{reflector}}$ and F_{antenna} are the forces [N] due to wind load of the reflector and antenna, l is the length of the pole [m], E is the Young's modulus [Pa] and I the moment of inertia [m^4]. The force of the wind is given by

$$F_{\text{wind}} = 0.5AC_D\rho v_{\text{wind}}^2, \tag{4.3}$$

in which ρ is the density of air in [kg/m^3] and v_{wind} is the wind speed in [m/s], A is the frontal area of the object of interest [m^2] and C_D is the drag coefficient [-] given by the shape, roughness and frontal area definition of the object[43]. For the IGRS a C_D of 1 with a conservative estimate for the frontal area is taken to be on the safe side.

The moment of inertia of a tube is given by

$$I_{\text{tube}} = \frac{\pi(d^4 - (d-2w)^4)}{64}, \tag{4.4}$$

in which d is the outside diameter [m], and w is the wall thickness of the tube [m][42].

The full profile of displacement due to wind loading can be seen in Figure 4.18. Two empirical cumulative distributions of the wind speed in the Netherlands are included to give an idea of common wind speeds. One distribution shows the the wind speeds of the inland area, represented by weather stations in Cabauw, Eelde and Maastricht. The other distribution is based on wind speeds in coastal areas represented by Vlissingen and Vlieland. The graphs are based on 10 year long time series of hourly data from the Royal Netherlands Meteorological Institute (KNMI)[44].

A common scenario of wind speeds lower than 6 Bft. leads to a horizontal displacement of the GNSS antenna of 2mm. The actual deformation will be smaller due to the added stiffness of the fins and frame.

The displacement of the radar reflectors will be small. If the horizontal displacement of the GNSS antenna is represented by a tilt, a horizontal displacement of 2 mm (6 Bft.) would lead to a range bias for the reflector of 0.5 mm (see Fig. 4.26). However, the deformation of the pole is more of a bend than a tilt and the apexes of the reflectors are horizontally fixed to the pole just above the fins, which provide a rock solid base. Therefore, it can be assumed that the range bias of the corner reflectors is much smaller than 0.5 mm (for 6 Bft).

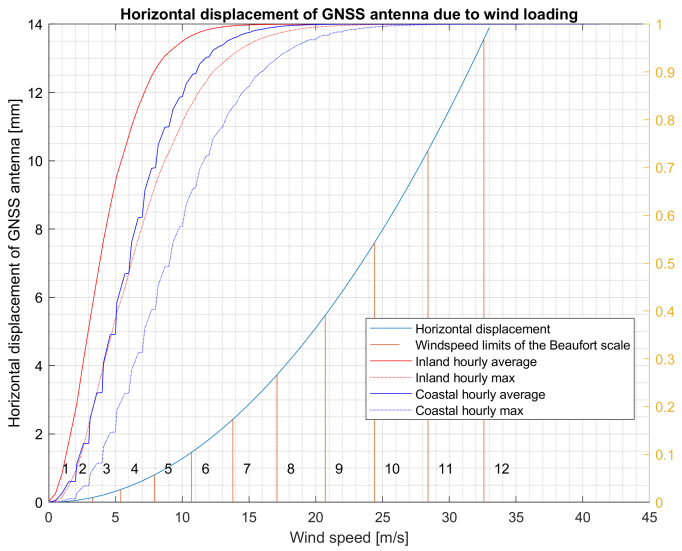

Figure 4.18: Horizontal displacement of the GNSS antenna due to wind loading of the production type DBF90T-GNSS. The right axis shows the empirical cumulative distribution of wind speeds for Cabauw, Eelde and Maastricht representing the Dutch inland area, and Vlissingen and Vlieland representing the coastal areas.

The effect of snow will be neglected, as small amounts will not exert any significant force, and large amounts will block the radar signal anyhow. Furthermore, deformation due to tilting or bending of the pole of the IGRS (if any) will only be seen in the unlikely event of a-symmetric loading of large amounts of snow.

4.6.2. Errors due to thermal expansion

When the IGRS changes its temperature, its size chances with a certain amount. This is called thermal expansion. The thermal expansion of solid materials is expressed by:

$$L = L_0 + L_0 * \alpha * dT \tag{4.5}$$

with L being the length of a material in the direction of interest, L_0 being the initial length, α being the linear expansion coefficient [m/mK] and dT being the temperature difference in $^\circ$C or K [45].

The linear expansion coefficient of 304-steel (used in the IGRS) is 17.3e-6 [m/mK] and for aluminium a range of 21 - 24e-6 [m/mK] is given[45].

A simple model for the IGRS used for calculating the effects of thermal expansion is given in Fig. 4.19 and the displacements due to thermal deformation are given in Fig. 4.20

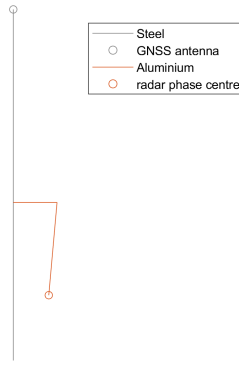

Figure 4.19: Stick figure model, in which all important elements are simplified to line elements, used for thermal expansion calculations.

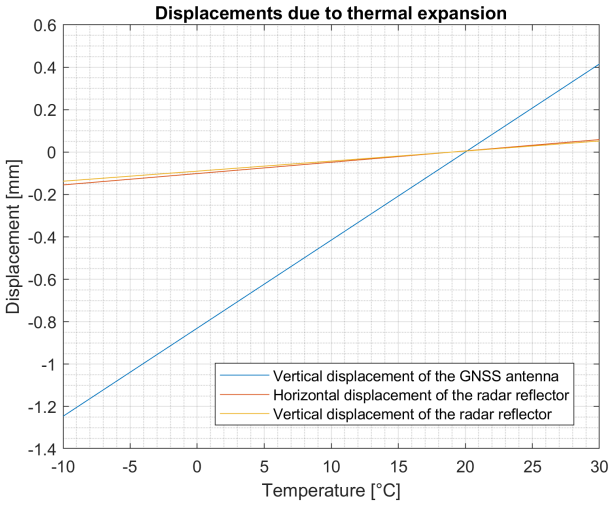

Figure 4.20: Displacements due to thermal expansion.

4.6.3. Range bias due to unintended tilt and rotation of the IGRS

These paragraphs describe the range bias due to tilt and rotation of the IGR, which is a measure of the design related measurement sensitivity towards movement or deformation of the IGRS. As the deformation sensitivity of InSAR depends on the geometry of the scene, the sensitivity is dependent on the location of the IGRS. To give the sensitivity in a general sense, a standard set-up is assumed. This set-up is based on the following four assumptions:

i. The pole is perfectly vertical, the horizontal plate is perfectly horizontal.

ii. The tilt angle of the radar reflectors is 5.1 degrees (Section 6.2).

iii. There is one incidence angle at boresight. (Section 2.4.3) This corresponds to an incidence angle of 40.4°.

iv. The azimuth angles are 101 and 259°N.

If the IGRS deforms, the most basic deformations are: a horizontal rotation of the DBF reflector around the pole, a tilt of a single reflector around its top edge, and a tilt of the IGRS as a whole. Therefore, these deformations are studied in the next paragraphs. However, it is not likely that those deformations end up in the data. This will only be the result of a unnoticed malfunctioning foundation or unreported collisions and realignments.

A rotation of the DBF reflector around the pole The rotation of the DBF around the pole results in a purely horizontal movement of the apex. The azimuth alignment changes, but the effects on RCS are neglected here. The movement is mostly perpendicular with respect to the measurement geometry for small rotations. So for small rotations, interferometric phase almost does not change. Fig. 4.21 shows the top view of the rotation geometry. Fig. 4.22 gives the range bias in mm for different degrees of rotation. A shift in the original alignment will lead to a shift of the bias profile on the y-axis in such a way that the line crosses the x-axis on the point of the baseline alignment.

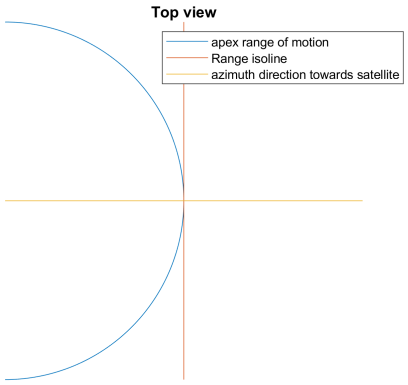

Figure 4.21: Top view of the rotation geometry. In this geometry, the reflector rotates around the pole of the IGRS

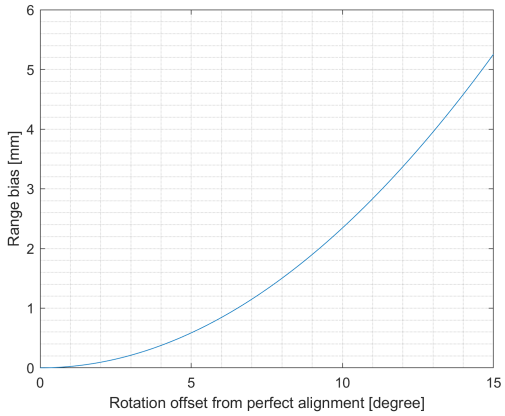

Figure 4.22: The LOS bias in mm for different degrees of rotation.

A tilt of a single reflector around its top edge A movement of the apex can occur when the tilt of the reflector changes. The tilt of the reflector can change when the bolts on the tilt angle mechanism loosen or get changed on purpose. Since the range of motion passes the iso-range line at an angle (see Fig 4.23), there is a direct effect. A tilt of 1 degree will result in about 10 mm change in LoS.

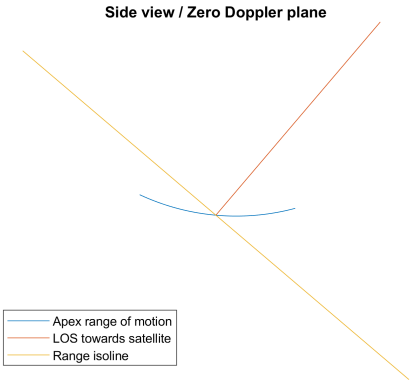

Figure 4.23: Side view of tilt geometry. In this geometry, the reflector tilts around its top edge.

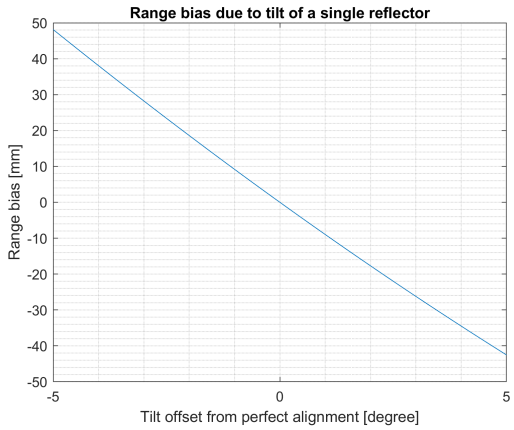

Figure 4.24: The LOS bias in mm for different degrees of tilt.

A tilt of the IGRS as a whole The IGRS is mounted on a foundation which is fixed in the subsoil. In the unlikely event of a tilt of this foundation, the IGRS will follow this tilt. Another option will be a tilt of the IGRS relative to the foundation. This can happen in the unlikely event of multiple loose nuts in the foot of the IGRS.

The largest effect will show when the tilt is in the vertical plane through the pole and one of the two apexes. For the following figures, the left part shows deformation in the plane through the ascending reflector. The right part shows deformation in the plane through the descending reflector. Main message is: the GNSS measurements will be strongly influenced in the horizontal plane. The LOS radar measurements will only pick up a minor change of about 1 mm per degree of tilt, due to the smaller distance to the turning point (taken at the foot of the IGRS) and the deformation being in line with the iso-range line.

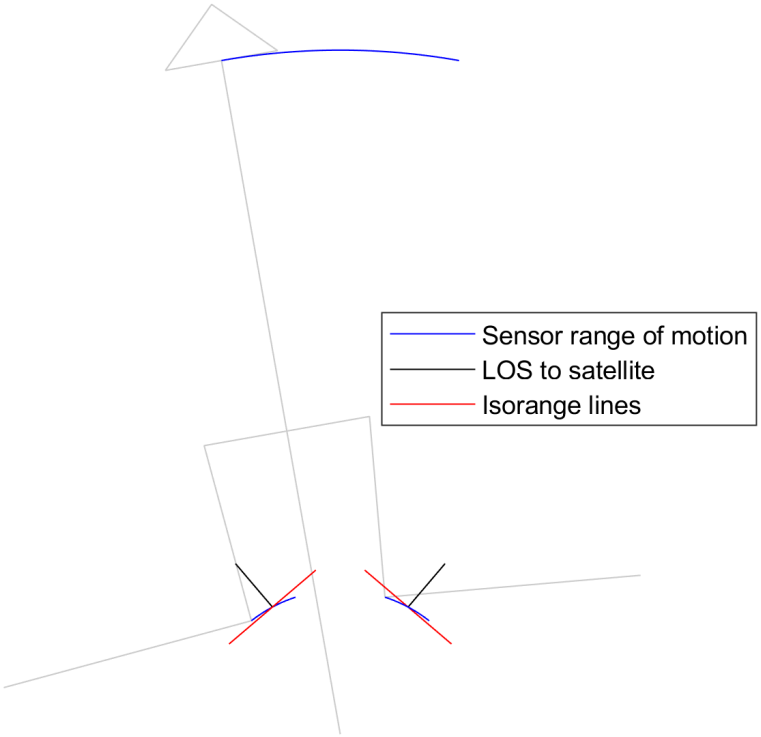

Figure 4.25: Movement geometry of the IGRS for a $\pm$ 10 degree tilt.

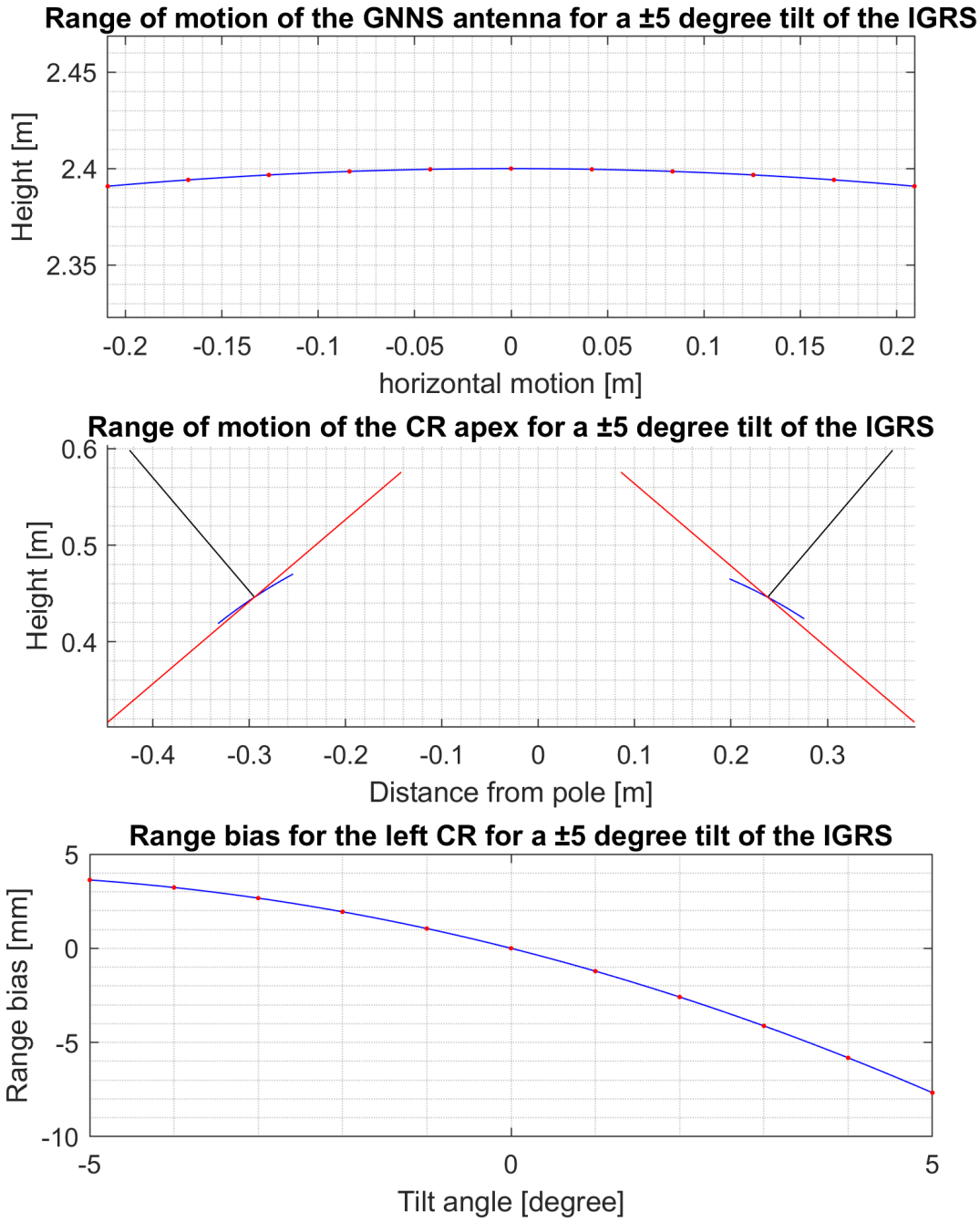

Figure 4.26: Detail plot of Fig. 4.25 for a ± 5 degree tilt.

4.6.4. Conclusions on the error budget for InSAR datum connection

To conclude, for the error budget of a single IGRS for InSAR data integration into well defined CRSs used by geodetic grade GNSS, the following 5 items items are of importance:

i. measurement error corner reflector(<0.5mm, LOS)
ii. measurement error GNSS (<3mm,<2mm,<5mm, NEU [38])
iii. loading (wind, snow) (GNSS: <2mm horizontal, InSAR: «0.5mm horizontal)
iv. thermal expansion (GNSS: <1 mm vertical. InSAR <0.2 mm vertical & <0.2 mm horizontal)
v. permanent deformation of the IGRS within the data acquisition period (Likely: ~ 0 mm in any direction. Unlikely: up to ~dm due to unreported collisions, unreported realignments etc.)

In this section it can be seen that the effect of thermal expansion and displacements due to the wind will probably be lower than the precisions of the sensor measurement. However, thermal loading will result in a slow, seasonal trend which can be modelled and subtracted from the data if needed.

The effects of wind loading will most probably result in dynamic movements, which, due to its magnitude, only is of interest winds above 6 bft. These make up less than 3% in coastal areas when hourly averages are used. The combination of the high frequency movement with respect to the short measurements make it hard to model this movement for every acquisition especially without external input data such as data from strain gauges or inertial measurement units (IMUs). However, the small magnitude of these sources of error do not justify the design of a station that does incorporate such sensors.

To conclude, no extraordinary source of errors is present in the error budget, which indicates that the resources to enhance performance are allocated evenly.

5

Radar performance of the IGRS

This chapter reports on experiments done for the development of the IGRS. It starts with an introduction of the experiments. The main objective is to present the results and share the interpretations which are used during the IGRS development.

5.1. Experiment set-up

A key aspect in the design of an IGRS is the quality of the radar signal. This chapter reports on the experiments done to get 1.) a proof-of-concept and 2.) a validation of the developed prototypes on the quality of the radar signal in terms of the stability of the reflectors phase centre and the influence of the clutter.

Figure 5.1: mock-up

Figure 5.2: DBF90T-GNSS

Figure 5.3: DBF90X-GNSS

Multiple IGRSs have been tested in a field experiment. A mock-up to perform a proof of concept experiment and assist in the design process, and the DBF90T-GNSS and the DBF90X-GNSS for validation of the design and performance before full deployment. They were installed at the TUD test site in Wassenaar. This test site houses stable concrete slabs to mount the reflectors and permanent corner reflectors, which can be used as reference reflectors. During the course of the experiments, in-active GNNS antennas were mounted on the IGRS to simulate the actual set-up. One difference with the a

fully functional setup is the absence of the instrument cabinet. However, this is not expected to cause significant effects.

Reflectors All reflectors that have been tested are part of a double backflip (DBF) corner reflector set. In total six reflectors were tested, mounted as three DBF reflector sets at three different IGRSs. Per set one reflectors is mounted on the west side of the IGRS aimed at the ascending satellite passes and one reflector is mounted on the east side and is aimed at the descending satellite passes. Three IGRSs were tested:

- The mock up shown in figure 5.1

  These reflectors are welded 2mm thick aluminium trihedral corner reflectors with an inner leg length of 90 cm.

- The DBF90T-GNSS shown in figure 5.2

  These reflectors are again aluminium trihedral corner reflectors with an inner leg length of 90 cm, but these are assembled with the help of bend edges and fasteners. The plates are made out of 3mm thick aluminium.

- The DBF90X-GNSS shown in figure 5.3

  These reflectors are bigger. They can be seen as a larger trihedral corner reflectors, of which the tips are removed. This gives them a larger aperture while their footprint is just slightly larger.

More info on the different IGRSs can be found in Chapter 4

Research question in the radar experiments In the experiments done on the radar reflectors, there have been three main research questions:

i. Does the experimental RCS match the theoretical value of 29.5 dBsm [1]?

ii. What is the experimental double difference 1-σ phase precision between an IGRS and a reference reflector keeping in mind that the theoretical derived 1-σ phase precision due to clutter around 0.25 mm in LOS [2]?

iii. What are key features that have negative influence on ease of installation and how can they be solved?

To find answers to these research questions, experiments have been done. The experiments can be divided in two sets: on one hand the experiments to get a proof of concept with the help of the mock-up, and on the other hand the experiments done to get a validation of the prototypes. The results of these experiments are presented in the main part of this chapter.

5.1.1. Wassenaar test site

The test site has been an active radar transponder/reflector test site since 2013. An overview is shown in figure 5.4. Six concrete slaps on which sensors and reflectors can be mounted are present on WASS## locations.

[1] 36.7 dBsm for DBF90X-GNSS
[2] for an estimated clutter of 4.4 dB

Figure 5.4: Google Earth image of the Wassenaar test site, showing the location of the reference Corner Reflectors CR-DSC for descending tracks and CR-ASC for ascending tracks near concrete slab WASS06. The concrete slabs WASS01 and WASS03 have been used for testing the IGRSs. LVL1 and LVL2 are the locations from where regular levelling is carried out. The electronic corner reflectors (ECR#) are installed for another project, but can used as (alternative) reference in this project. [46]

Stability The geology of the test site is a very stable former barrier beach formed in the Holocene era. The ground layers consist of Holocene sand deposits on top of pleistocene sand layers. Unlike lots of other Dutch sediment soils, this soil contains little to no clay or peat deposits (see Figure 5.5 up to 5.9). The ground water level is very stable as the controlled surface water level of the nearby canals is only 50 cm below ground level. The surface water levels in these nearby canals are managed to be within 1-2 dm of summer or winter level. The concrete slabs are installed directly on the sand sediment without any topsoil in between. Earlier experiments and regular levelling acquisitions support the stable behaviour by showing little to no relative movement between the markers. [46]

Reference corner reflectors The test site includes two large reference reflectors (see figure 5.10). One for the acquisitions of both the ascending and descending tracks. The reflectors are square based triangular corner reflectors with an inner leg length of 1.425 m. They are mounted on four 30x30cm square flat plates which are buried 25 cm below ground level. The maximum RCS at C-band (Sentinel-1 mission) is 40.65 dBm^2 which makes them more powerful than the tested IGRSs. Table 5.1 and 5.2 show the incidence angles and azimuths for a list of possible tracks. The actual RCS of the reference reflector depends both on the alignment and used frequency. Low frequencies result in a lower RCS. Therefore, the choice has been made to align the reference reflectors in favour of the Sentinel-1 tracks as they use C-band whereas CSK (COSMO-SkyMed) and TSX (TerraSAR-X), which are possible alternative radar systems, use X-band. The incidence angles are met within precision of the measurement device during installation. The azimuth values for ascending and descending have become 259.05 (259.65 intended) and 100.05 (99.73 intended) degrees north. This set-up results in a theoretical RCS of at least 40 for all used missions [46].

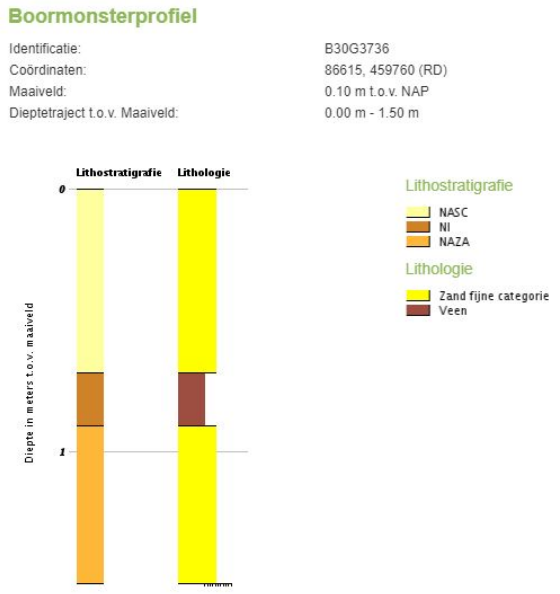

Figure 5.5: Ground profile at the test site[47].

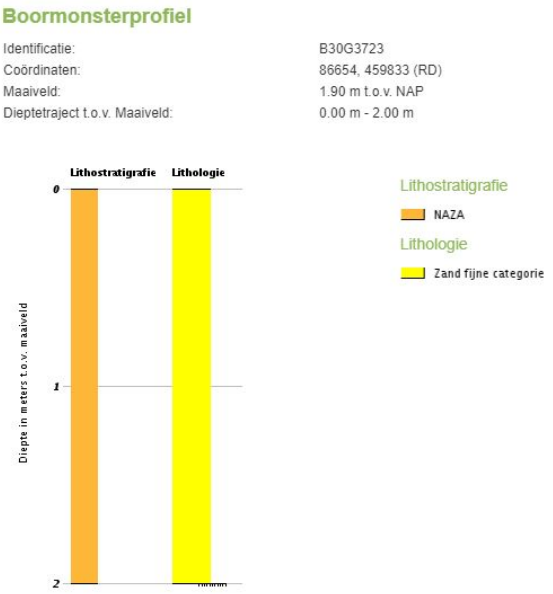

Figure 5.6: Ground profile 100m N-E of the site[47].

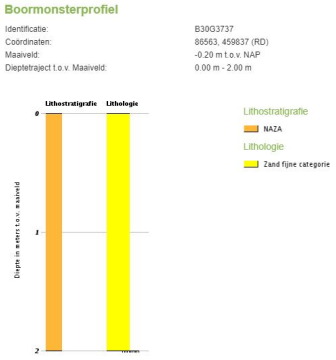

Figure 5.7: 100m N-W[47].

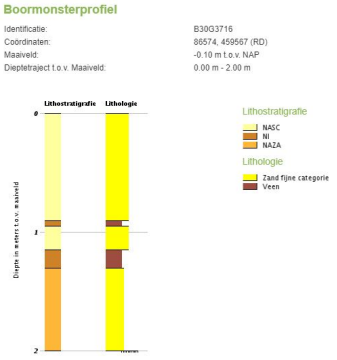

Figure 5.8: 200m S-W[47].

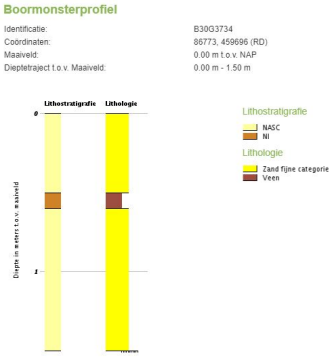

Figure 5.9: 200m S-E[47].

Figure 5.10: The two reference corner reflectors. The corner reflector in the left is used for descending tracks, the corner reflector on the right for ascending tracks. the kind of concrete slap that is used to mount reflectors at the test site can be seen in the middle.

Table 5.1: Acquisitions ascending reference reflector.

Ascending		
	Incidence	Azimuth(south of E)
CSK	29.36	11.34
TSX	39.59	10.10
S1(88)	33.24	11.16
S1(161)	41.76	9.54
S1(mean)	37.50	10.35

Table 5.2: Acquisitions descending reference reflector.

Descending		
	Incidence	Azimuth (south of W)
CSK	54.86	6.6
TSX	24.12	12.18
RS2(101)	32.79	11.39
RS2(102)	36.92	10.56
S1(37)	44.65	8.92
S1(110)	36.68	10.54
S1(mean)	40.67	9.73

Analysis of Wassenaar clutter strength Any estimate on the phase precision of a radar target is based on the background clutter it has to overrule. Therefore, it is important to have an estimate on the clutter. Literature on PS-InSAR describes two common ways on finding clutter [31][30]. First, the dispersion index method; a method exploiting the stochastic nature of the clutter in time. Second, the SCR Method; a method exploiting an assumed spatial correlation of the clutter in the radar image.

However, for this report a third method has been used. It can be argued that the time series of the expected experiments are to short for the dispersion index method. Furthermore, estimating the stochastic nature of the reflector itself is part of the experiment. The SCR method has not been used, as only sub-pixel values at the location of the IGRS are easily available after processing the data stack. Also, spatial correlation is not guaranteed, due to the concrete slab in the resolution cell of interest whereas the surrounding resolution cells are purely filled with meadow. As an alternative, 212 clutter intensity samples of the concrete foundations before the IGRSs were installed are used as empirical data to to fit a distribution to. When it is assumed that distribution does not change over time, it can be used to make a likely estimate for a standard clutter strength.

The 212 clutter samples are represented by a Rayleigh distribution in Figure 5.11. A most likelihood estimate can be found at the maximum of its probability density function. For Sentinel-1 at the Wassenaar test site, this corresponds to 4.4 dB . However, the cumulative distribution function shows that the maximum likelihood estimate corresponds with the 40 percentile of all clutter samples. This means that if this estimate is used in Signal-to-Clutter ratio (SCR) estimates, only 40% of the measurements have a SCR higher than estimated and 60% has a SCR lower than estimated. Therefore, if the estimated clutter strength is used as a design parameter, it is better to use a more pessimistic estimate for the clutter strength such as the 75 percentile highlighted in the figure.

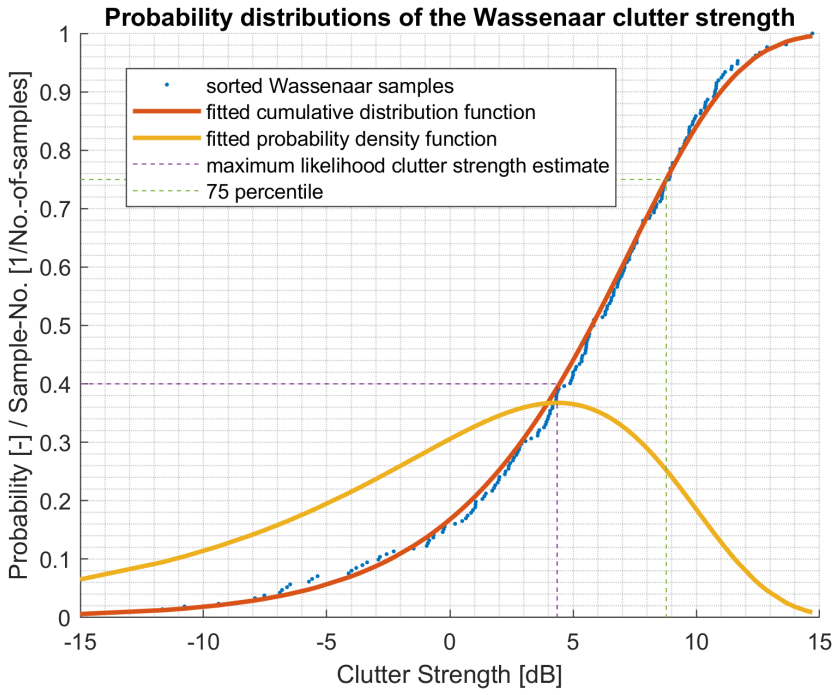

Figure 5.11: Distributions of the Wassenaar clutter strength. The label shows the 75 percentile.

Relevance of tests on an InSAR test site The interferometric phase ($\varphi_{\text{interferogram}}$) already corrected for the radar geometry is given by[17]

$$\varphi_{\text{interferogram}} = W\{\varphi_{\text{orb}} + \varphi_{\text{dtopo}} + \varphi_{\text{defo}} + \varphi_{\text{atmo}} + \varphi_{\text{clutter}} + \varphi_{\text{noise}}\}, \tag{5.1}$$

in which φ_{orb} is phase contribution due the orbital error, φ_{dtopo} is the contribution due to the errors in the digital elevation model (DEM), φ_{defo} is due to deformation, φ_{atmo} is due to the atmosphere, φ_{clutter} is

due to clutter and φ_{noise} is the phase contribution due to the noise in the system. The phase wrapping operator is given by W.

The variable φ_{defo} can be split in a part for the deformation of the foundations and a part for the deformation of the monument carrying the reflector. This leads to

$$\varphi_{\text{defo}} = W\{\varphi_{\text{foundation}} + \varphi_{\text{monument}}\}. \tag{5.2}$$

For the test site, the assumptions can be made that φ_{orb}, φ_{dtopo} and φ_{atmo} are negligibly small due to the small baseline. Furthermore it is assumed $\varphi_{\text{foundation}}$ negligibly small based on earlier data from the test site[46]. This leaves

$$\varphi_{\text{interferogram}} = W\{\varphi_{\text{monument}} + \varphi_{\text{clutter}} + \varphi_{\text{noise}}\}, \tag{5.3}$$

which opens the opportunity to evaluate $\varphi_{\text{monument}}$ and φ_{clutter} for a specific reflector.

Derivation of results The standard deviation of $\varphi_{\text{interferogram}}$, is given in this chapter as the observed σ_{LOS}. It is derived as the root mean square error of the data fitted to a linear trend. Similar to Eq. 5.3, σ_{LOS} can be split into σ_{monument} and σ_{clutter} and a noise factor of the radar instrument that will be neglected. It is assumed that σ_{monument} and σ_{clutter} are not correlated. This leads to

$$\sigma^2_{\text{monument}} = \sigma^2_{\text{LOS}} - \sigma^2_{\text{clutter}} \tag{5.4}$$

in which all σ's represent double difference values. In this equation, σ_{clutter} will be derived based on the maximum likelihood estimate of the clutter (4.4dB) and the signal model presented in Sec. 2.4.1 in which the experimental values for the RCS are used for the IGRS, and a fixed value of 39 dB is used for the reference reflectors.

Strictly speaking, σ_{monument} is the standard deviation of $\varphi_{\text{monument}}$ which is a double difference value between the IGRS and a reference reflector. For the experiments presented here, the assumption has been made that the reference reflector is perfectly stable, and therefore has a single measurement standard deviation of 0. This will lead to a pessimistic estimate for the IGRS monument stability.

5.2. Data processing

The processing of the Sentinel-1 SAR data of the test site follows a semi-automated processing chain that has been in use for multiple experiments. Several steps can be distinguished. Figure 5.12 shows the processing chain. The numbers are explained in the text below.

1. Download of the data

   The SLC data is downloaded automatically from the ESA API hub. If a new SLC is present, it is downloaded during an hourly check.

2. Partly InSAR processing

   The Sentinel-1 SLC's (Single-Look-Complex or simply radar images) are processed by the DORIS interferometric software. This software package is developed and made available to the scientific community by TU Delft. The SLCs are processed in a single master stack configuration. That is, all images are co-registered to a unique master image geometry, to enable comparison of the data in the time domain.

   Sentinel-1 has a so-called TOPS acquisition mode in which several bursts are compiled to get one standard image. One of these bursts would be adequate. However, more bursts are used to enable high precision co-registration of the images based on Enhanced Spectral Diversity (ESD). At least three burst overlaps before and after the test site are used.

3. Sentinel-1 burst selection

   After co-registration, only the burst that includes the point-of-interest (POI) is selected based on the outline of the bursts. An alternative approach would be to merge all bursts into one image first. However, this would eliminate the possibility to use multiple bursts in the case of a POI within a burst overlap. Burst overlaps do not occur at the test site, but future projects may be within these regions.

4. Radarcoding POI coordinates

   The radar coordinates of the POIs are calculated per stack based on the orbit data, timing parameters and their ITRF2008 (or WGS84) coordinates. Also, the location of the mid-point between all POIs in the radar image is calculated for further use in the processing chain.

5. Extraction of 200 m window around test site location in the radar image

   Based on the radar coordinates of the mid-point between devices, a square window of 200 m is extracted from the SLC stacks for each co-registered image.

6. Oversampling of data window

   The extracted window is up sampled with the help of sinc interpolation up to a ground pixel spacing of 20 cm. This is done to get a better estimate of the peak value of the corner reflector's signal. Furthermore, it results to square pixels which lead to better visualisations. An oversampling factor of 96 in azimuth and 16 in slant range direction is used for the data on the test site.

7. Maximum peak search based on radar coordinates

   There are two modes that can be exploited during processing. The most basic method works as follows: 1.) all useful (the ones which show a reasonable high response for the POI) clipped SLC's are averaged into one multilook complex (MLC). 2.) A small search window is clipped around the priori calculated radar coordinate. This radar coordinate may be off due to small errors in the radar image (like errors in geolocation of the radar image or errors due to a imperfect co-registration). Therefore, 3.) a search for a local intensity maximum is performed. When the local maximum has been found on the edge of the search window, there is a probability that it is no real local maximum. When this happens, step 2 is updated with a slightly larger search window. 4.) The radar coordinates of the POI are updated to the coordinates of the found maximum. These coordinates are used to extract the complex values from the clipped and up-sampled SLCs.

   The second method is mostly the same but updates the coordinates of the maximum at sub pixel level for each individual SLC instead of only once for the MLC.

   In this report, results of the second method are shown.

8. Conversion to RCS (dBm2)

   Now that all data points are found in and extracted and isolated from the larger database, the process is focussed on the conversion of complex values (I and Q) from the SLCs into RCS and phase values.

   The RCS is calculated in a multiple step process. The first step is to calculate Beta naught (β^0). β^0 can be found by:

$$\beta_{S1}^0 = \frac{DN^2}{k_{S1}^2} \tag{5.5}$$

   Where $DN = \sqrt{I^2 + Q^2}$ and k_{S1} is a constant for radiometric calibration of the Sentinel-1 data.

   The RCS in dBm^2 is given by

$$RCS = 10 \cdot log_{10}(\beta^0 \cdot \Delta_{Az} \cdot \Delta_{SR}) \tag{5.6}$$

   where Δ_{Az} and Δ_{SR}) are the (original, not the oversampled) azimuth and slant range resolution, respectively.

9. On/off detection

   When working with active transponders, it may happen that a transponder does not work for some reason. Therefore, an algorithm is checking for a RCS threshold. This step is not of great importance for corner reflector experiments like this one.

10. RCS time series analysis

    The RCS time series is checked on inconsistencies and off-sets from the expected value. Results on this step are presented in the conclusions of this chapter.

11. Phase extraction

    The same Q and I values as used with the RCS calculation are used to get the phase data per POI and per SLC. The phase is given by:

$$\phi = arctan(\frac{Q}{I}) \tag{5.7}$$

    The phase information per POI is stored in a time series of all available SLCs.

12. Phase stability time series analysis

    The phase stability analysis is performed as a double difference analysis due to the relative nature of the data. The time series (difference in time) of two different POIs (difference in location, for this test one experimental reflector and one of the large square based reference corner reflectors at this test field) are compared by extracting one from the other.

$$\phi_{remainder} = \phi_{POI_1} - \phi_{POI_2} \tag{5.8}$$

    Due to the wrapped nature of the phases (phase values in an interval between $-\pi$ and $+\pi$), phase unwrapping over time is required.

    The wavelength of Sentinel-1 is approximately 5.5cm [36]. As the radar measures a 2 way travel time there is a phase ambiguity of approximately 2.75cm. If, for example, a POI would have a LOS deformation of 2.75cm per acquisition, it would stay unnoticed by the observer. If a POI has a linear up or down motion relative to the reference point, the phase values linked to this POI will have a shape of a saw tooth if plotted in a time series. This wrapped linear trend is unwrapped during the phase unwrapping step. Eg.

$$\phi_{remainder} = \begin{bmatrix} .5\pi \\ .0\pi \\ 1.6\pi \\ 0.75\pi \\ 1\pi \end{bmatrix} - \begin{bmatrix} .5\pi \\ 1.25\pi \\ 0.1\pi \\ .5\pi \\ 0\pi \end{bmatrix} = \begin{bmatrix} 0\pi \\ -1.25\pi \\ 1.5\pi \\ -.5\pi \\ 1\pi \end{bmatrix} \rightarrow unwrap \rightarrow \begin{bmatrix} 0\pi \\ .75\pi \\ 1.5\pi \\ 2.25\pi \\ 3\pi \end{bmatrix} \tag{5.9}$$

    A second reason to unwrap in time even if a trend is not suspected is to prevent the following effect:

$$\begin{bmatrix} .5\pi \\ 1\pi \\ -.5\pi \\ 0\pi \end{bmatrix} - \begin{bmatrix} 0\pi \\ .5\pi \\ 1\pi \\ -.5\pi \end{bmatrix} = \begin{bmatrix} .5\pi \\ .5\pi \\ -1.5\pi \\ .5\pi \end{bmatrix} \rightarrow unwrap \rightarrow \begin{bmatrix} .5\pi \\ .5\pi \\ .5\pi \\ .5\pi \end{bmatrix} \tag{5.10}$$

    Which shows the importance of careful handing of phase values. If phasors are constructed with the given phase and intensity values, they can be subtracted in the form of:

$$A = Ae^{i\theta_a}$$
$$B = Be^{i\theta_b}$$
$$Ce^{i\phi_{remainder}} = Ae^{i\theta_a} * Be^{-i\theta_b} \tag{5.11}$$

The deviation from a fitted trend in $\phi_{remainder}$ is a measure for the quality of the signal as high frequency effects are not expected at the spatial scale of the test site (atmospheric signal and orbital errors can be neglected at small distances).

To interpret the phase stability better, a conversion is made from radians to mm displacement in the Line-of-Sight (LOS) according to Eq. 2.15.

As a last step, the mean phase for a time series is subtracted to present the deformation data around 0.

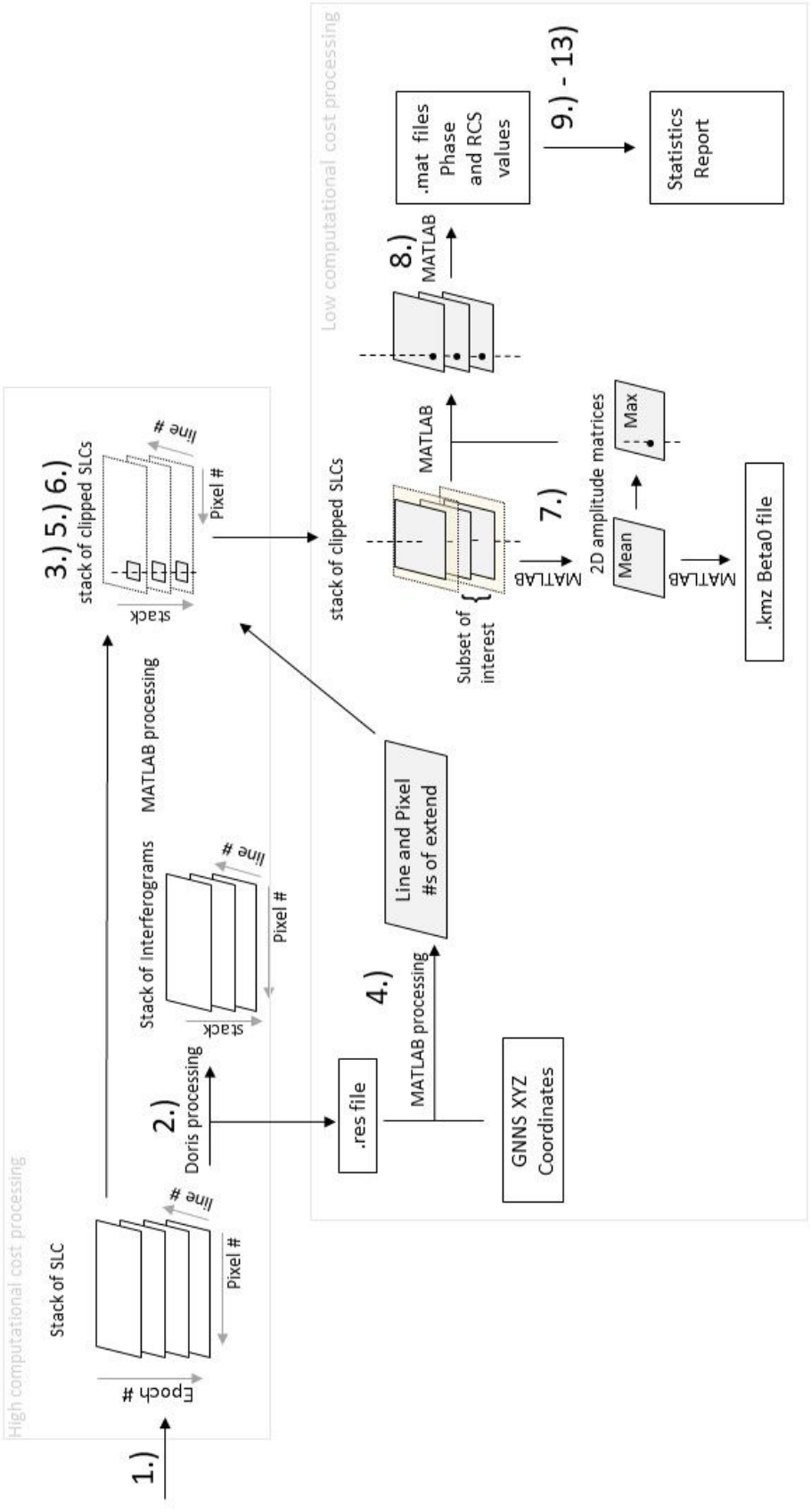

Figure 5.12: The processing chain used for processing the Sentinel-1 data of the test site

5.3. Results on RCS

5.3.1. Reference data

The initial data during the experiments is shown in table 5.3.

Table 5.3: Acquisitions descending reference reflector.

	Ascending		Descending	
Track	**88**	**161**	**110**	**37**
Incidence angle	33.25	41.77	36.68	44.64
Azimuth	11.16	9.54	10.54	8.92
Frame azimuth offset	-0.2	1.5	-.5	-2.1
Mock up				
Tilt planned	2.2		5.4	
Tilt realised	2.6		5.6	
Alignment error Tilt	4.6	-3.9	4.2	-3.8
Theoretical RCS	29.37	29.40	29.39	29.39
Tilt planned	6.5		-	
Tilt realised (19-8-2017)	6.4		-	
Alignment error Tilt	8.4	-0.1	-	-
Theoretical RCS	29.03	29.50	-	-
DBF90T				
Tilt planned	2.2		5.4	
Tilt realised	2.2		5.4	
Misalignment with respect to the incidence angle	4.3	-4.3	4.0	-4.0
Theoretical RCS	29.39	29.38	29.40	29.38
DBF90X				
Tilt plannedl	2.2		5.4	
Tilt realised	2.2		5.4	
Alignment error Tilt	4.3	-4.3	4.0	-4.0
Theoretical RCS	36.48	36.32	36.49	36.36

5.3.2. RCS Time series

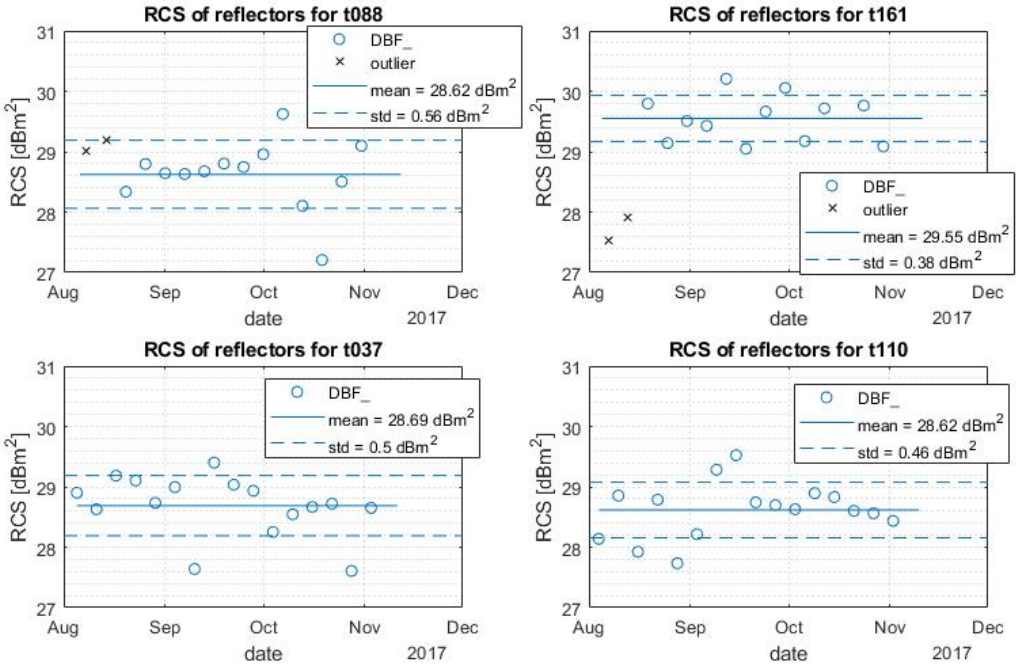

Figure 5.13: RCS values of the mock-up. Outliers are the two acquisitions of the ascending tracks before the intended realignment of the ascending reflector on 19-8-2017.

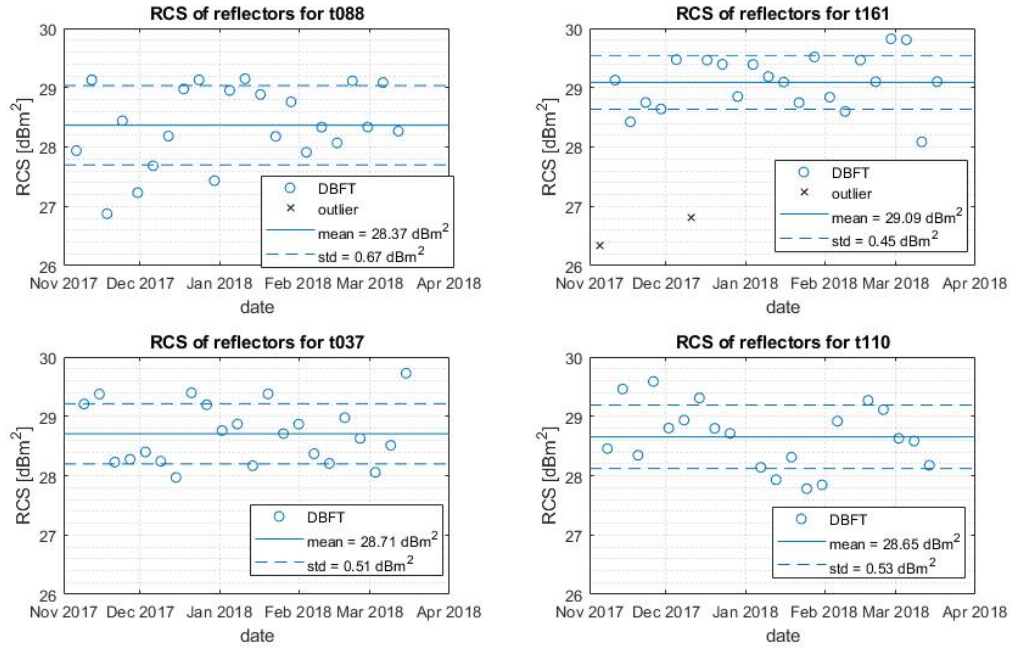

Figure 5.14: RCS results of the DBF90T.

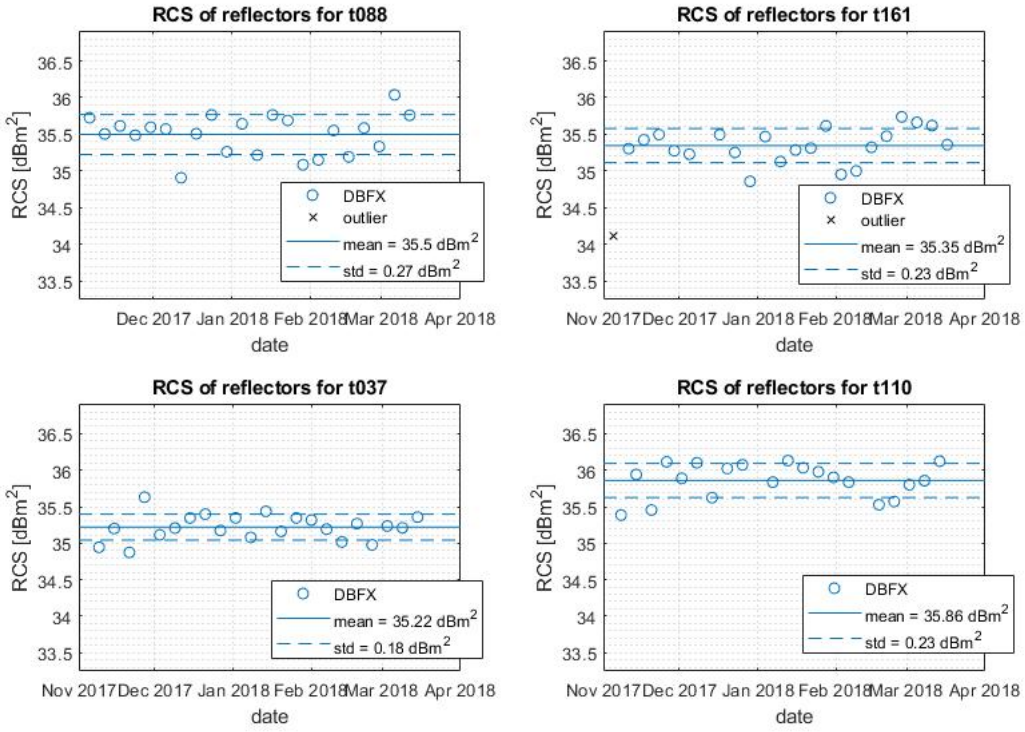

Figure 5.15: RCS results of the DBF90X.

5.3.3. Statistics on RCS results (Mean value, Std, Offset)

Table 5.4: RCS results for the mock up.

	Ascending		Descending	
Track	**88**	**161**	**110**	**37**
Theoretical RCS (first)	29.37	29.40	29.39	29.39
Experimental RCS	29.10	27.71	28.62	28.69
Offset RCS	0.27	1.69	0.77	0.70
Standard deviation	0.13	0.26	0.46	0.50
No. of observations	2	2	16	16
Theoretical RCS (second)	29.03	29.50	-	-
Experimental RCS	28.62	29.55	-	-
Offset RCS	0.41	-0.05	-	-
Standard deviation	0.56	0.38	-	-
No. of observations	13	12	-	-

Table 5.5: RCS results for the DBF90T-GNSS prototype.

	Ascending		Descending	
Track	**88**	**161**	**110**	**37**
Theoretical RCS	29.39	29.38	29.40	29.38
Experimental RCS	28.37	29.09	28.65	28.71
Offset RCS	1.02	0.29	0.75	0.67
Standard deviation	0.67	0.45	0.53	0.51
No. of observations	22	21	20	22

Table 5.6: RCS results for the DBF90X-GNSS prototype.

	Ascending		Descending	
Track	**88**	**161**	**110**	**37**
Theoretical RCS	36.48	36.32	36.49	36.36
Experimental RCS	35.50	35.25	35.86	35.22
Offset RCS	0.98	1.07	0.63	1.14
Standard deviation	0.27	0.23	0.23	0.18
No. of observations	22	21	20	22

5.3.4. Interpretation of the RCS statistics

Table 5.4 till 5.6 and the graph in Figure 5.16 show the actual differences between the experimental and theoretical RCS. Although slightly bigger, the differences are similar to the differences modelled by Zajc et. al. in [48] who presents results on simulated sources of RCS computation errors. Remarkable is the larger offset of the prototype DBF90T-GNSS compared to the offset of the mock-up, as it would be expected to have a better fit with theoretical values due to an improved production method. Overall, the results of both the mock-up and prototypes fit reasonably well with the theoretical derived values.

Both the DBFT and the DBFX time series show outliers. These data points are marked as outlier, as they coincide with low RCS values for the reference reflector as well. Therefore, a external effect (like snow or heavy rainfall) is the source for these RCS dips.

From the sensitivity analysis shown in Figures 2.29 and 4.8 it can be concluded that alignment and sizing errors are not likely to be the only sources of the observed bias as their likely magnitudes do not add up to the seen differences in the results.

Other sources of bias may be the non-orthogonality of the reflector[19], the calibration constant (design requirements of Sentinel-1 calibration: 3σ = 1 dB, [49]), the derivation of experimental RCS with the Doris software or deviations from the geometric optics model[48].

The standard deviation does not correspond to the theoretical value purely based on clutter (Eq. 2.8). Calculated results show 0.012-0.0024 dB while the experimental results show 0.2-0.5 dB. So, other unreported and/or quantified sources contribute to the standard deviation of RCS.

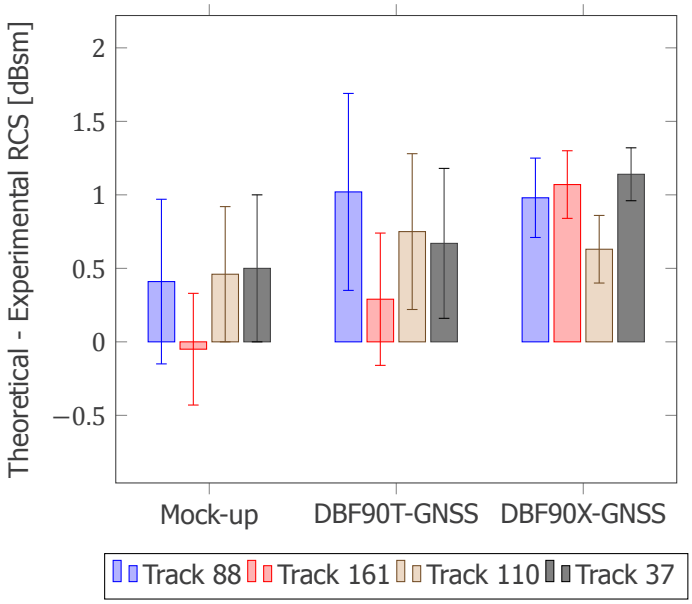

Figure 5.16: The differences for theoretical - experimental RCS for all tracks and reflectors tested. Error bars depict the standard deviation around the mean value. A smaller standard deviation is seen at the DBF90X-GNSS. However, this may be an artefact due to its higher values on the logarithmic scale.

5.3.5. Interpretation of the Top-hat experiment

The part of the design of the IGRS that has been designed to hold the GNSS antenna in place also functions as a radar reflector. The shape corresponds to a so-called top-hat reflector (figure 5.17). It consists out of a flat plate with a cylinder on top. The RCS is azimuth independent as the reflector is symmetrical in all directions trough its centre z-axis.

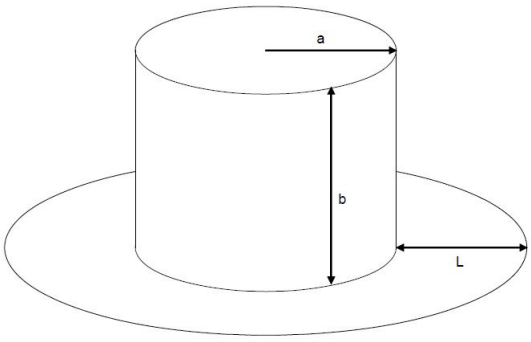

Figure 5.17: Geometry of the tophat reflector. From: [33]

Figure 5.18: Tophat reflector at the IGRS

As a secondary (unwanted) reflector on the IGRS, the phase centre of its reflection differs from the phase centre of the bigger intentional radar reflector. Depending on the geometrical relations in the scene, it will have a different range to the satellite. Depending on the difference in range, the signal will interfere with the main signal, either constructively or destructively.

The theoretical maximum impact of this noise signal on the phase values can be estimated with the help of its magnitude. The magnitude of a top hat reflector can be found with the help of[33]:

$$RCS_{tophat}(\theta) = \frac{8\pi a}{\lambda cos\theta} min(b^2 cos^2\theta, L^2 sin^2\theta) \quad L, a, b >> \lambda \tag{5.12}$$

in which θ is the incidence angle relative to the flat base plate, a is the radius of the cylinder, b the height of the cylinder, L the span of the flat surface below the cylinder and λ is the wavelength of the incoming signal.

For the IGRS this makes:

Table 5.7: RCS values for both reflections.

	Ascending		**Descending**	
Track	**88**	**161**	**110**	**37**
Theoretical RCS top hat reflector $[m^2]$	1.13	0.93	1.04	0.88
Theoretical RCS trihedral corner reflector $[m^2]$	864	870	869	869

From table 5.7 we can see that the influence of the top hat is really small. This corresponds to a maximum phase error of 0.07 degree what is a LOS value of 0.0055 mm for a signal 90 degree out of phase. This value is too small to have any measurable effect as the standard deviation of the phase value in mm LOS is around 0.6-0.8 mm. For constructive or destructive interference of the signal it results in $RCS = RCS_{CR} \pm RCS_{tophat}$. This results in a gain or loss of 0.005 dB for the IGRS. Again, to small to notice as the standard deviation of the RCS is around 100 times higher.

So, the hypothesis will be that no significant differences occur. The results in table 5.8 show no unexpected differences in the RCS or its standard deviation.

Table 5.8: Measured RCS results before and after placement of a pole on the IGRS mock-up. The pole was placed on the mock-up on 31-8-2017

	Ascending		**Descending**	
Track	**88**	**161**	**110**	**37**
RCS without pole $[dBm^2]$	28.53	29.41	28.23	28.88
Std. without pole $[dBm^2]$	0.39	0.45	0.48	0.24
RCS with pole $[dBm^2]$	28.56	29.57	28.80	28.65
Std. with pole $[dBm^2]$	0.69	0.41	0.41	0.51

5.4. Results on the double difference interferometric phase

5.4.1. Interferometric phase time series

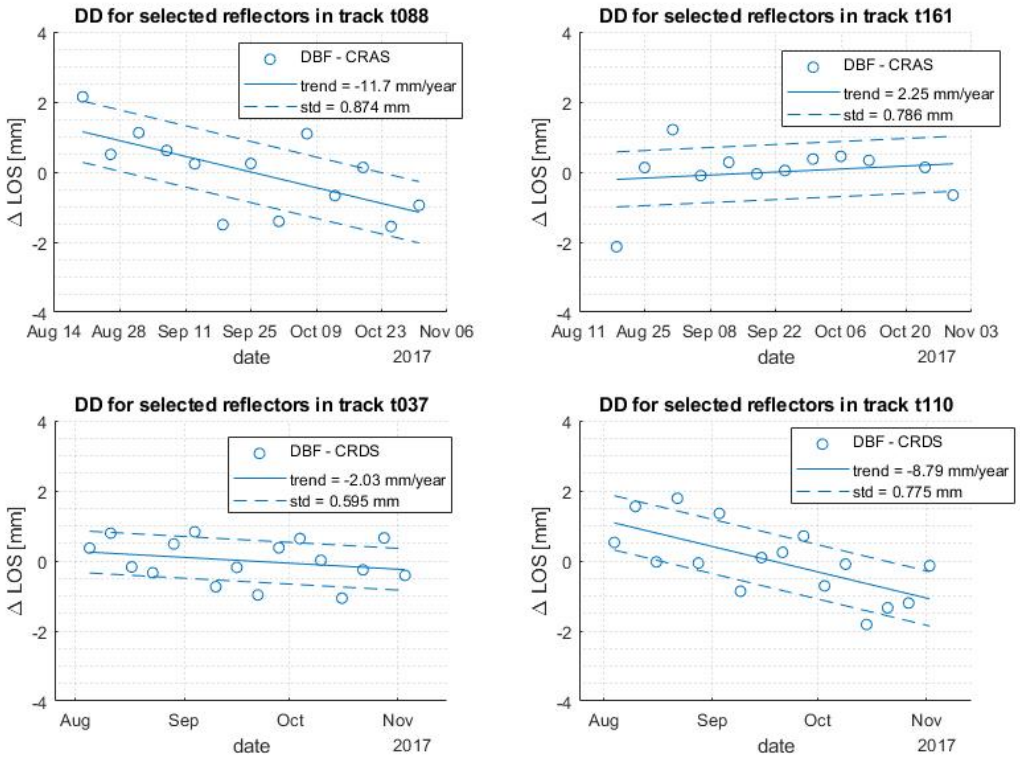

Figure 5.19: Double difference (DD) phase values of the mock-up.

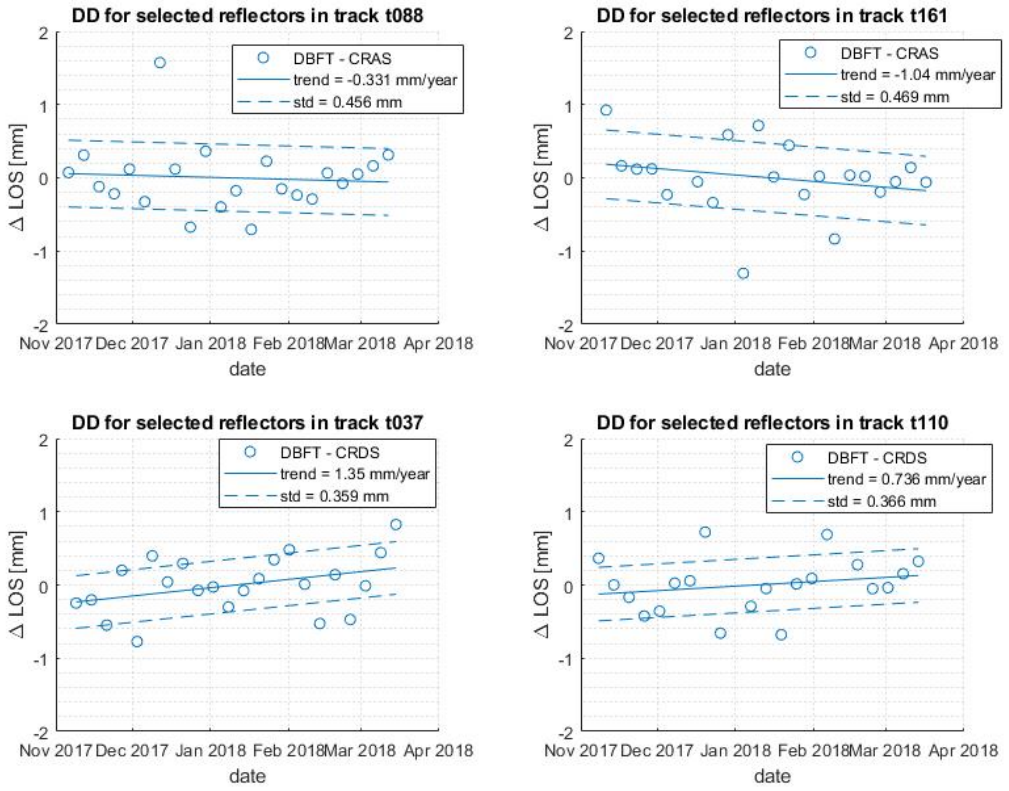

Figure 5.20: Double difference phase results of the DBF90T.

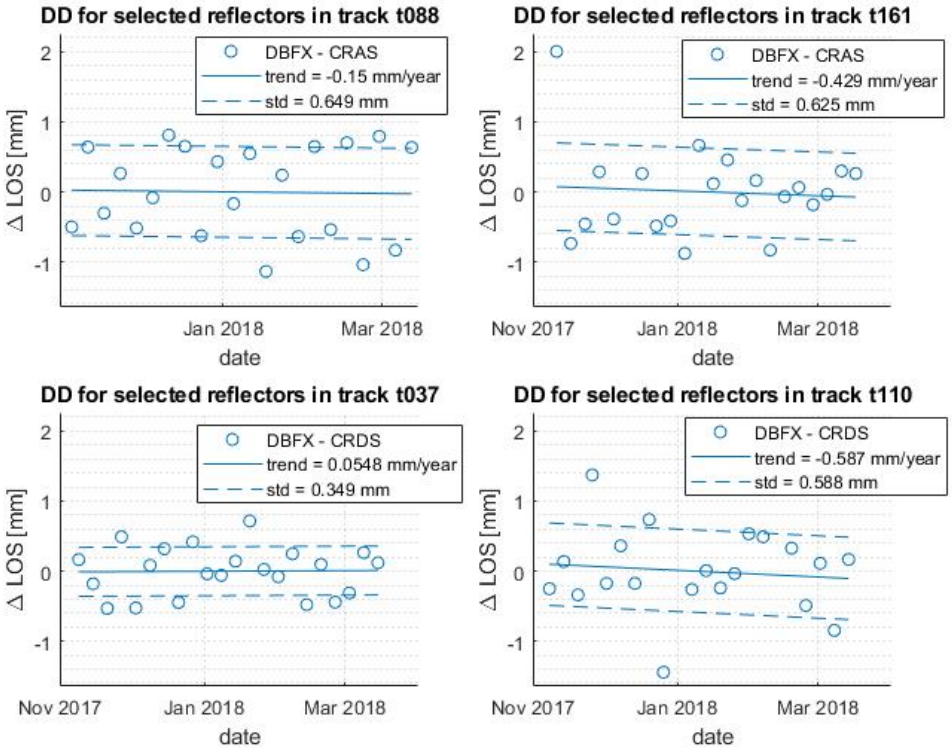

Figure 5.21: Double difference phase results of the DBF90X

5.4.2. Interferometric phase statistics (Trend, Std)

Table 5.9: Phase results for all three tested IGRSs. The clutter has been estimated to be 4.4 dB. All values show double difference results and estimates

		ascending		descending	
Track	**mean**	**88**	**161**	**110**	**37**
Mockup: Trend [mm/year]		-11.7	2.25	-8.79	-2.03
Mockup: Observed σ_{LOS} [mm]	0.758	0.874	0.786	0.775	0.595
Mockup: $\sigma_{clutter}$ [mm]	0.287	0.270	0.313	0.284	0.282
Mockup: $\sigma_{monument}$ [mm]	0.699	0.831	0.721	0.721	0.524
DBF90T: Trend [mm/year]		-0.331	-1.04	0.736	1.35
DBF90T: Observed σ_{LOS} [mm]	0.413	0.456	0.469	0.366	0.359
DBF90T: $\sigma_{clutter}$ [mm]	0.282	0.292	0.270	0.283	0.281
DBF90T: $\sigma_{monument}$ [mm]	0.297	0.351	0.383	0.232	0.223
DBF90X: Trend [mm/year]		-0.15	-0.429	-0.587	0.055
DBF90X: Observed σ_{LOS} [mm]	0.553	0.649	0.625	0.588	0.349
DBF90X: $\sigma_{clutter}$ [mm]	0.149	0.148	0.151	0.144	0.151
DBF90X: $\sigma_{monument}$ [mm]	0.531	0.632	0.607	0.570	0.315

5.4.3. Interpretation of the phase results

The phase results in Table 5.9 show the different contributions to the double difference observed RMSE of the phases of the different reflectors. The values for $\sigma_{clutter}$ are calculated based on the observed RCS values of the IGRSs and the Wassenaar clutter estimate of 4.4 dB, which opens up the opportunity to study $\sigma_{monument}$. However, if the clutter is estimated to low, which will happen in 60% of the cases, this will lead to an actual $\sigma_{clutter}$ which is higher than the estimated $\sigma_{clutter}$.

The results show a clear sign that the $\sigma_{monument}$ of the mock up is the highest, indicating its poor ability to carry the reflectors in a stable manner. The $\sigma_{clutter}$ is similar for the mock-up and the DBF90T-GNSS. This is expected as they have similar RCS values. This indicates that the DBF90T-GNSS has improved on structural stability.

The DBF90X-GNSS has the lowest $\sigma_{clutter}$ due to its high RCS. However, the size of the reflectors takes its toll, as the structural stability of the reflectors is lower than that of the DBF90T-GNSS. This might be due to the less rigid construction or to a less stable phase centre of the reflection due to bending of the plates.

In the case of low clutter conditions, the DBF90T-GNSS will perform better. However, with higher values of clutter, $\sigma_{clutter}$ will rise faster for the DBF90T-GNSS whereas $\sigma_{monument}$ will stay the same for both IGRSs. This effect is shown in Fig. 5.22, showing there is a turn over point, where the DBF90X-GNSS will have better performance.

For the mock-up, the trends are remarkably steep. The steep trend might be partly due to actual deformation of the IGRS during the short measuring period as the construction was already slightly curved after the short time series. This deformation resulting a downward displacement of the reflectors. However, no before and after measurements are taken of the apex height to check this.

The 2D deformation results based on the trends found at the mock-up is shown in Figure 5.23 (see Appendix A for the methodology). It can clearly be seen that the resulting displacement vectors both point in the direction of insensitivity as presented in Fig. 2.41. This clearly indicates the importance of a stiff physical connection between ascending and descending aimed reflectors so they can be assumed to undergo the same displacement making the inverse model less ill-conditioned and thus the estimate more robust.

The deformation trend of the DBF90T-GNSS seems to indicate a tilt towards the west (see Fig. 4.25 for a visual help of the interpretation). This corresponds to earlier measurements at the test field[46]

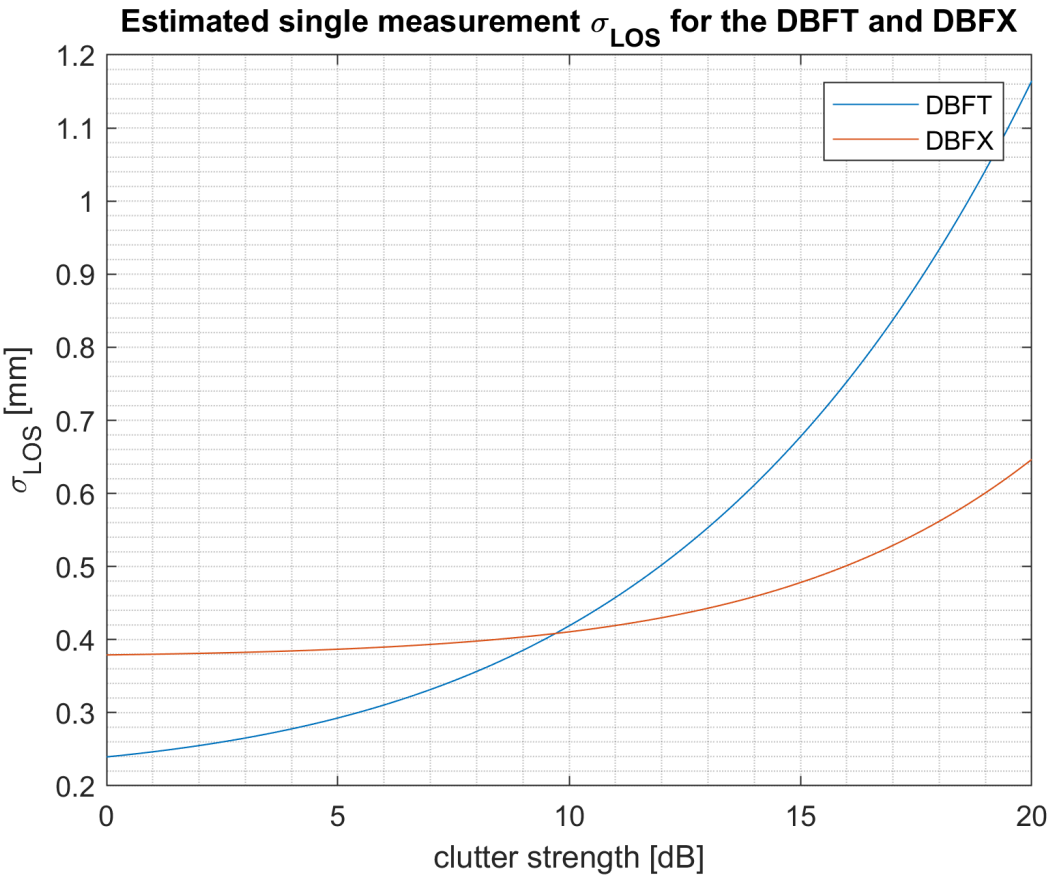

Figure 5.22: The single measurement σ_{LOS} under changing clutter conditions for both the DBF90T-GNSS as the DBF90X-GNSS. As the two lines meet, there is a point where the most optimal choice based on phase precision shifts from one IGRS to the other.

and can be explained by the bank of the canal nearby.

Overall, σ_{LOS} is within bounds for InSAR datum connection set in Section 4.6 as $\sigma_{monument}$ is in the same order as $\sigma_{clutter}$, and based on the observed values of the RCS, $\sigma_{clutter}$ is well within bounds for a double difference 1-σ value of 1 mm. Therefore, the performance is validated for both prototypes.

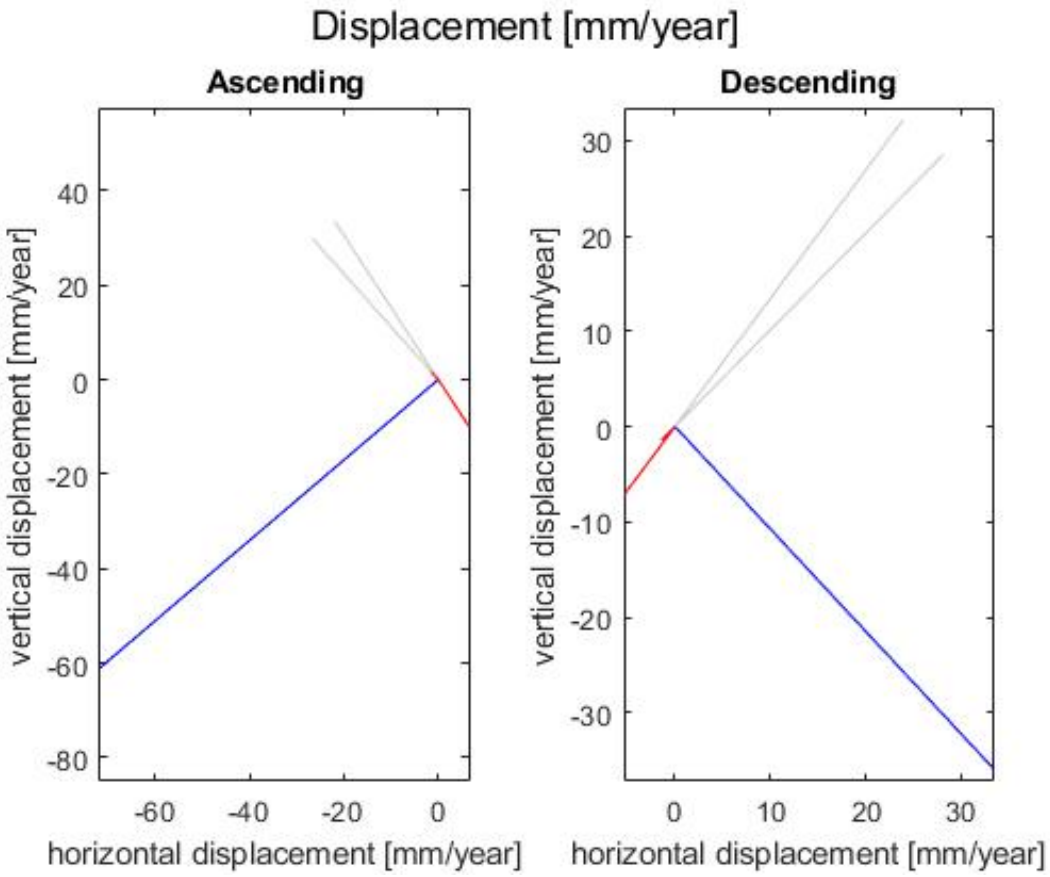

Figure 5.23: 2D deformation signal which suits both estimated trends per reflector for the mock up. Red shows the measured signal, the blue lines are the simulated 2D deformation vectors and the grey lines mimic the LOS direction. They both show a sinking and outward deformation in the direction of low sensitivity as presented in Fig 2.41.

6

Deployment and operational use of the IGRS

This chapter gives information on the deployment of one or multiple IGRSs. Information is given about the workflow from reconnaissance to placement as well as strategies for alignment of the corner reflectors.

Fig 6.1 shows the process of deploying an IGRS. This process can be split in 3 phases:

- Reconnaissance

  This phase is used to gather information about the project. Information on i. a. clutter, visibility for the GNSS and soil characteristics for the foundations is gathered. Finally, it will be decided on which locations the IGRSs will be placed. The CPT soil test and the legal procedures are not part of the scope of this report. The clutter analysis is described in Section 6.1.

- Design and preparation

  Once a location is chosen, parallel steps can be taken. The GNSS receiver at the IGRS needs electrical power, which should be provided. Furthermore, the IGRS has to be mounted on a stable foundation which resembles the deformation characteristics of interest. Both aspects of power supply and foundation are outside the scope of this report.

  The location of the IGRS has influence on the geometry of the satellite - IGRS system. Once all locations of all IGRSs are fixed, an alignment strategy can be formulated based on the calculated geometrical parameters. This process is described in Section 6.2.

- On-site processes

  The last step is placing the IGRS on the foundation. Step-by-step guides of the installation, alignment and baseline measurements survey are given in Section 6.3. Making a foundation and connecting the IGRS to a power supply is work for a contractor.

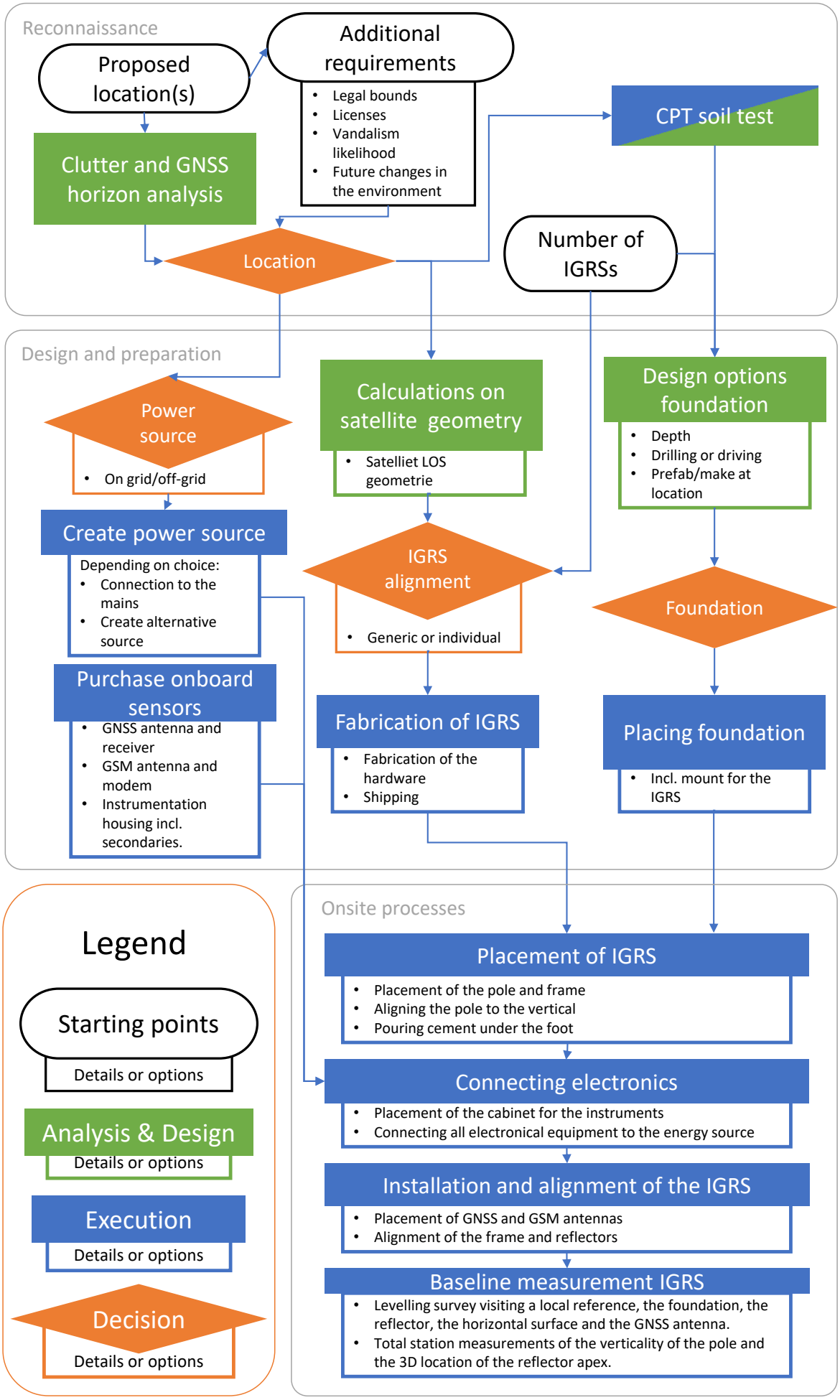

Figure 6.1: Deployment scheme IGRS.

6.1. Location selection

This section describes the steps that are made in the location selection procedure regarding the background signal for radar and the visibility for GNSS measurements.

6.1.1. Local radar clutter

Clutter interferes with the signal of the IGRS as explained in Section 2.4.1. Therefore, a location with low clutter conditions is favourable. Finding this location can be done by analysing the scene of interest on a calibrated amplitude images of the radar SLCs. Fig. 6.2 shows the mean of a series of such images. It shows clutter conditions presented as β_0, projected onto Google Earth imagery. Low values can be seen on some flat tarmac present in the scene, while higher values are seen around objects like fences, trees, and the pump in the middle of the tarmac. When planning a location for an IGRS, the high values should be avoided.

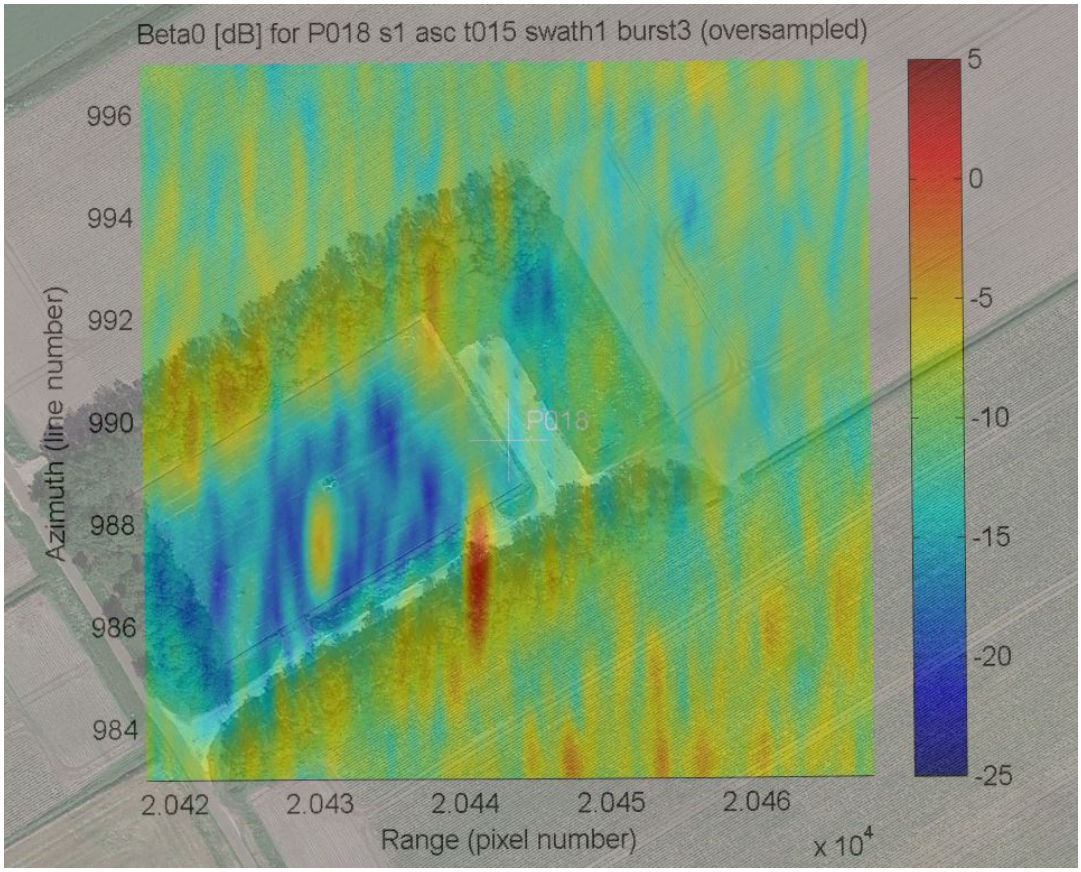

Figure 6.2: Clutter strength presented as β_0, projected onto Google Earth imagery. Low values can be seen on the flat tarmac, while higher values are seen around objects like fences, trees, and the pump in the middle of the tarmac. (Note the shift of one pixel in both range and azimuth direction between signal and source.)

6.1.2. Local GNSS horizon

To get maximum coverage of GNSS satellites, a low horizon is beneficial. Trees, buildings or elevated ground masses can block the signal to low passing satellites. If available, local or regional LiDAR products such as AHN [39] can be used to determine the elevation cut-off angle in all directions from a point of interest. Figure 6.3 and 6.4 show the local horizon elevation angle of such a point of interest derived from AHN. The cut-off angle is commonly set to 10° by GNSS experts, but often exceptions are made to be able to find a suitable location.

The same tool is used to find obstructions in the SAR signal, although fulfilment of the GNSS requirement implies an obstruction-free LOS for the SAR instrument.

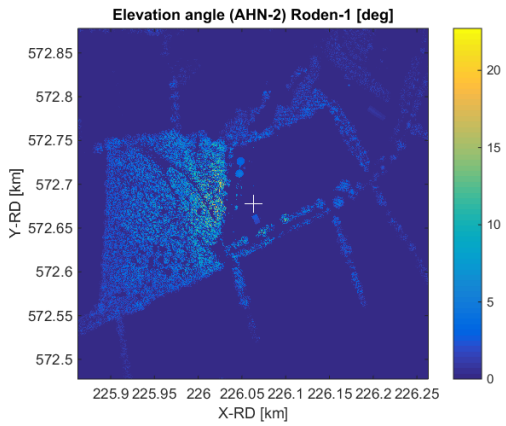

Figure 6.3: Elevation angle from the point of interest for every object visualised as a map. [50]

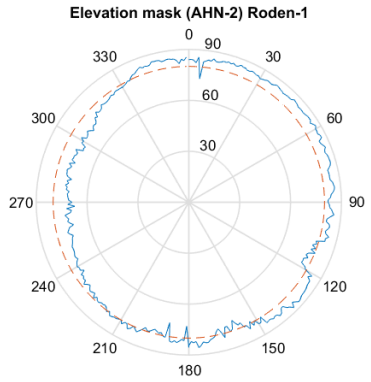

Figure 6.4: 360 degrees horizon elevation angle from the point of interest. Red dotted line shows the cut-off angle. [50]

6.2. Alignment strategy

The alignment strategy of a project with multiple IGRSs is not straight forward. As a case study, this section reports on the result for an investigation on possible alignment strategies for the Groningen field case.

The IGRS that will be deployed in Groningen will be of the type DBF90T-GNSS (see Figure 6.5). It has two corner reflectors; one should be aligned to the ascending tracks and one for the descending tracks. The corner reflectors tilt by moving the apex; the upper edge is fixed to the frame.

6.2.1. Aligning the reflectors of the DBF90T-GNSS

The reflectors of the DBF90T-GNNS can be modelled like shown in figure 6.6. The figure shows the angle definitions that are needed to be able to work with the reflector.

The boresight angle θ and the incidence angle have been defined in section 2.4.3. θ is a parameter of the reflector design (Figure 2.38), the incidence angle is a property that depends on the location of the reflector. Please note that, due to the alternative positioning of the CRs, the z axis points to the ground, while the x and y axis now point mostly upwards.

The tilt angle is defined as the angle between the backplate of the corner reflector and the vertical. As a result of the orthogonal geometry, it can also be measured between the z-axis and the horizontal. Figure 6.6 shows the that the incidence angle can be represented by the summation of the tilt angle and the complementary angle of θ minus the misalignment:

$$\angle_{\text{Incidence}} = \angle_{\text{Tilt}} + (90 - \theta) - \angle_{\text{misalignement}} \tag{6.1}$$

To find the ideal $\angle_{\text{Tilt}}$ we assume $\angle_{\text{misalignement}} = 0$ and get:

$$\angle_{\text{Tilt}} = \angle_{\text{Incidence}} - 35.26 + \angle_{\text{misalignement}} \tag{6.2}$$

To find $\angle_{\text{misalignement}}$ when a $\angle_{\text{Tilt}}$ is chosen you can use:

Figure 6.5: DBF90T-GNSS

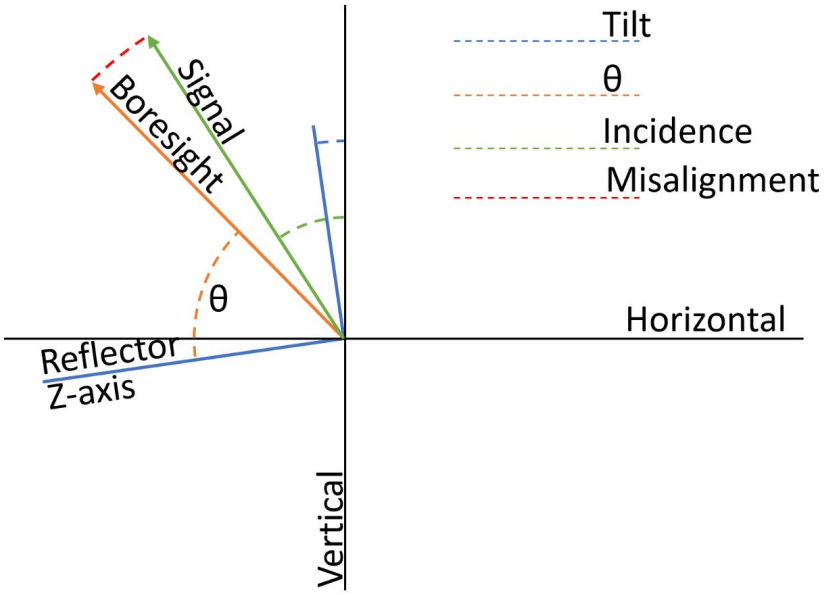

Figure 6.6: Angle definitions in a 2D cross section of a corner reflector in the vertical plane.

$$\angle_{\text{misalignement}} = 35.26 + \angle_{\text{Tilt}} - \angle_{\text{Incidence}} \tag{6.3}$$

Typically, the incidence angle is larger than 35.26 in Groningen (Figure 2.37). This will lead to a positive tilt angle. As seen in figure 6.6, the apex is moved away from the satellite[1].

A second interpretation of the tilt angle can be found using the standard geological notation of a dip angle, in which the dip of an earth layer is given in the range of 0 till 90°. A dip is always pointing downwards, so a positive dip leads to a downward pointing direction. For the reflector this dip would be given by the angle that the z-axis makes with the horizontal plane. As noted before, a tilt of the backplate with respect to the vertical is the same as a dip of the z-axis with respect to the horizontal.

6.2.2. Alignment strategies for the Groningen field study

For the Groningen field study, the reflectors will be optimally aligned to Sentinel-1 track. This decision has been made based on the fact that Sentinel-1 is a widely available system operating with a 6 day repeat[36]. Sentinel-1 operates in C band[36]. Systems operating in X band are not taken into account as their higher frequency makes alignment of the reflectors less critical. Each reflector is within the viewing geometry of two Sentinel-1 tracks with different incidence angles. The difference in incidence angle is 8°.

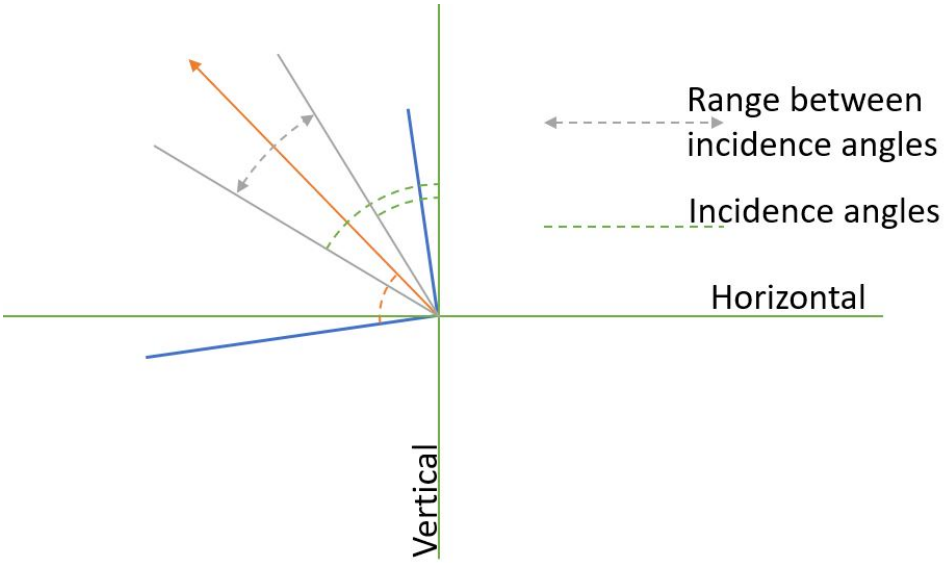

Figure 6.7: Conceptual visualisation of the range between two different incidence angles

To assess which strategy would be the best for the NAM to use, 5 possible scenarios were investigated on how to select the tilt angle of the reflector such that the boresight has the most optimal direction in the range spanned by the two satellite tracks. The 5 possible scenarios are given below:

1. Aim all reflectors for one track only.

   The alignment intended error for one track is 0°, for the other it is about 8°.

2. Aim all reflectors for the exact middle between the two tracks.

   The alignment error for both tracks is about 4°. The $\angle_{\text{Tilt}}$ values vary between 3.25° to 6.13° for the ascending tracks, and between 3.97° and 6.60° for the descending tracks.

[1]The standard mathematical convention for angles describes an anti-clockwise rotation to be positive. This is not applicable as it would need to be defined whether the observer looks to the North or to the South. Furthermore, the definition would be opposite for the ascending and descending reflector.

3. Aim all ascending reflectors to the overall mean ascending incidence angle, and aim all descending reflectors to the overall mean descending incidence angle.

   $\angle_{\text{Tilt}} = 4.76°$ for the ascending tracks and $\angle_{\text{Tilt}} = 5.42°$ for the descending tracks.

4. Use the overall mean incidence angle.

   $\angle_{\text{Tilt}} = 5.09°$

5. Use an integer value for the tilt angle which leads close to the overall mean value .

   $\angle_{\text{Tilt}} = 5.0°$

6.2.3. Simulated results

Table 6.1 shows the simulated mean SCR_{loss} per strategy due to the inevitable misalignment. From the table it becomes clear that the main difference occurs between strategy 1 and the other strategies. With strategy 1 the alignment is optimized for one track only, but because the loss in SCR is not linear with the misalignment angle, the total loss will be much bigger than e.g. scenario 2 in which the losses are divided over both tracks. Figure 6.8 shows a histogram of the SCR_{loss} for the different scenarios. The same data is presented in Table 6.2. The inhomogeneity for the first strategy is immediately apparent from the clear separation of two regions. For strategy 2 to 5 we see that most acquisitions fall in the bins with lower SCR loss, but none in the optimal boresight bin. For strategy 3 to 5 the acquisitions are spread over more bins than for strategy 2, this is also as expected as there is a larger spread of misalignments due to a higher degree of generalisation.

Table 6.1: Mean SCR_{loss} per strategy.

Strategy	SCR_{loss} **(dB)**
1: Aim for 1 track	0.2173
2: Aim in the middle of 2 tracks	0.1133
3: Aim for mean Asc and mean Dsc	0.1175
4: Aim for overall mean	0.1182
5: Aim for integer value for the tilt angle	0.1182

Table 6.2: Number of acquisition per bin per strategy.

	Strategy				
Upper limit SCR_{loss} [dB]	**1**	**2**	**3**	**4**	**5**
0.02	62	0	0	0	0
0.07	0	0	12	14	14
0.12	0	60	40	47	47
0.17	0	64	48	34	36
0.22	0	0	24	25	20
0.27	0	0	0	4	7
0.32	0	0	0	0	0
0.37	0	0	0	0	0
0.42	1	0	0	0	0
0.47	59	0	0	0	0
0.52	2	0	0	0	0

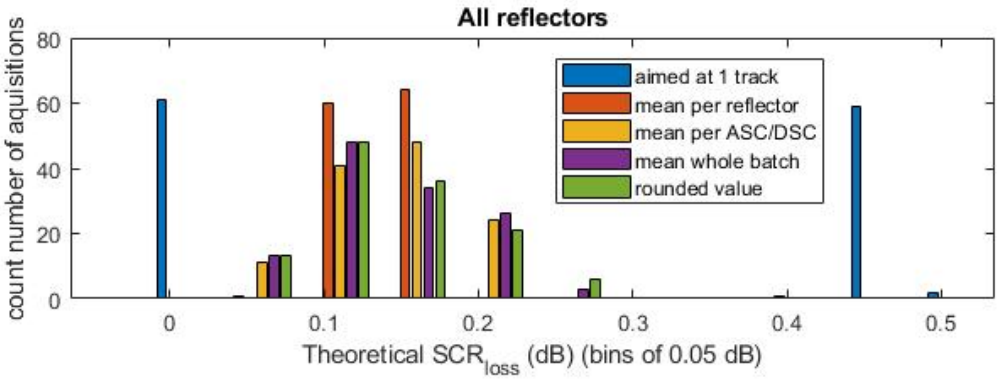

Figure 6.8: Amount of reflectors within the SCR groups with a spacing of 0.05 dB.

σ_{LOS} depends on the SCR as discussed in section 2.4.1. The results only describe a loss in the SCR until now. The exact SCR is not known as it is also dependent on the background clutter, which is not known exactly. However, based on earlier reconnaissance some scenarios are evaluated here.

Eq. 2.10 repeated from section 2.4.1 gives,

$$SCR\ [\text{dB}] = RCS_{\text{cr}} - (\beta_0 + A_{\text{res}}).$$

The RCS of the corner reflectors is just below 30 dB. For the clutter three scenarios, related to Sentinel-1, are investigated:

- low clutter with $\beta_0 = -13\text{dBm}^2$
- nominal clutter with $\beta_0 = -5\text{dBm}^2$
- high clutter with $\beta_0 = 5\text{dBm}^2$

These three scenarios can all be found in 6.2. Low clutter is found on the square area which is a flat tarmac surface. The nominal clutter can be found in the meadows surrounding the tarmac. High clutter values can be found around structures like metal fences and buildings, indicated in the figure by the bright red spot.

$A_{\text{res}} \approx 18 \pm 1$ dBm^2 for Sentinel-1 in its Interferometric Wide swath mode, the exact number depends on the swath number which is site specific. So, simplifying to 18 dB, these scenarios would lead to SCRs of:

$$SCR_{\text{low clutter}} \approx 30 - (-13 + 18) \approx 25\text{dB}$$
$$SCR_{\text{nomimal clutter}} \approx 30 - (-5 + 18) \approx 17\text{dB}$$
$$SCR_{\text{low clutter}} \approx 30 - (5 + 18) \approx 7\text{dB}$$

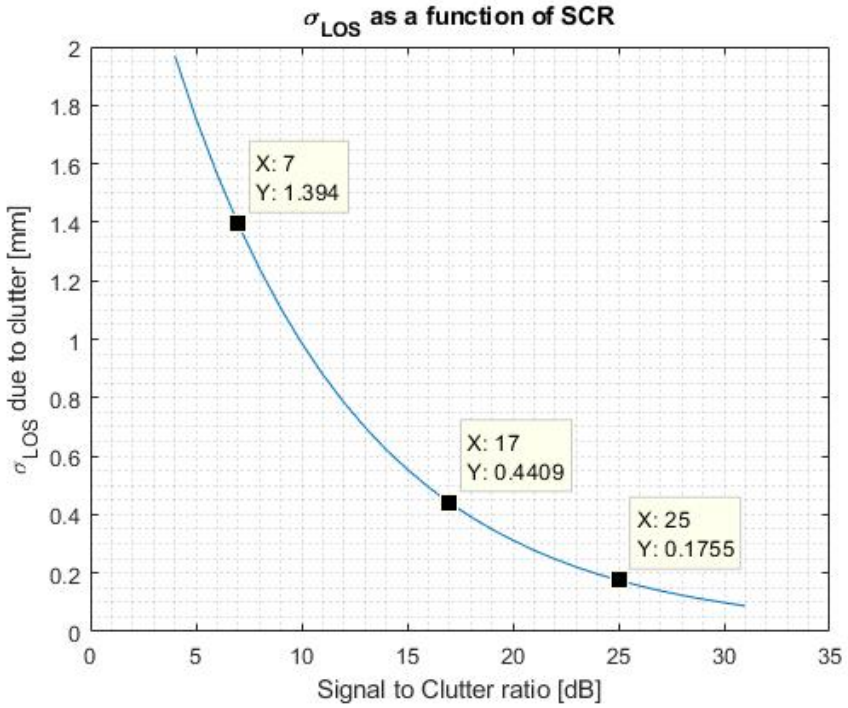

Figure 6.9: Error in the Line-of-Sight with respect to the Signal-to-Clutter ratio, based on Fig. 2.27

Table 6.3 gives the SCR after the correction has been applied due to misalignment. A brief look already shows the different strategies have minor impact compared to the different clutter scenarios. It also shows the values for σ_{LOS}, which, as are related, show the same pattern.

Table 6.3: Mean SCR_{loss} and per strategy.

		Clutter			Clutter		
		High	Medium	Low	High	Medium	Low
Strategy	SCR_{loss}	SCR [dB]			σ_{LOS} [mm]		
0: Arbitrary Initial Scenarios	0	7	17	25	1.394	0.441	0.176
1: Aim for 1 track	-0.217	6.783	16.783	24.783	1.429	0.452	0.180
2: Aim in the middle of 2 tracks	-0.113	6.887	16.887	24.887	1.412	0.447	0.178
3: Aim for mean Asc/Dsc	-0.117	6.8830	16.883	24.883	1.413	0.447	0.178
4: Aim for overall mean	-0.118	6.882	16.882	24.882	1.413	0.447	0.178
5: Aim for integer value	-0.118	6.882	16.882	24.882	1.413	0.417	0.178

6.2.4. Conclusion and recommendation on alignment strategies for deployment of multiple stations

In this section different options were evaluated for the alignment of double backflip corner reflectors for the Groingen field study. The differences in terms of LOS error (σ_{LOS}) between these strategies is very small, except for one strategy which is clearly worse than the others. The results for the other four strategies, which all aim at aligning the reflectors somewhere in the middle of two tracks, are very similar.

Therefore, the advise for a project in which multiple reflectors are involved, is to choose the strategy that gives the least rise to confusion and the best possible long term reliability. For the long term reliability the stability and repeatability of the apex position is of paramount importance; any change in apex position over time will result in an error in the LOS of the InSAR measurement and therefore this bias will be included in the deformation signal of interest.

Likewise it would be useful to use the same value for the tilt angle for all reflectors, corresponding to strategy 4 or 5. Using the same value everywhere avoids confusion during the installation. It prevents mistakes and last but not least, it assists in the verification afterwards during inspections by simply remeasuring the tilt angle and checking against the nominal value. It also means that special tools for the alignment can be developed that are generic for a whole project area.

To conclude, the best strategy in this field study is strategy 4, in which all corner reflectors are installed with one optimal tilt angle.

6.3. On-site placement protocol

The on-site processes start after the site has been prepared by creating a suitable foundation for the IGRS. The placement, installation and alignment of an IGRS follows the following protocol:

1. Slide the pole trough the tube in the frame (2 - 3 persons).
   (a) Place the frame on the side of the cabinet on the ground. Make sure to use protection when working on a rough surface.
   (b) Tilt the frame towards a vertical position of the flat surface. A second person slides the pole trough the tube of the frame. If this process requires a lot of force, then you should loosen the four bolts on the flat surface connecting it to the tube. When the pole has slid all the way trough, re-tighten the four bolts.
   (c) Tighten the clamps on the frame around the main pole to fix the combination temporarily.
2. Place the IGRS on the foundation (2 to 3 persons).
   (a) place one nut and spacer on each bolt roughly 4 cm above the concrete.
   (b) place all nuts roughly horizontal with the help of a level.
   (c) place the IGRS on the bolts with the cable holes to the most North option. 2 persons are needed for carrying the weight. An optional third person can aid with manoeuvring the IGRS on the bolts.
   (d) place a spacer and nut on each bolt
3. Put the pole in a vertical position.
   (a) Turn the bolts in the foot to get a vertical position of the pole. This should lead to a horizontal position of the flat surface.
   (b) Turn the frame with the long edge to the North. Check if its horizontal. If this is not the case, then check for damage to the frame.
   (c) Check if all nuts are equally tight touching the foot, and tighten the nuts above the foot.
   (d) Check the pole again on its verticality. Restart this part if tightening changed the position.
4. Rotate the frame towards north.

   this step involves aligning the centreline of the horizontal surface with the geographic north-south line. The long empty edgy should be turned towards north, and the empty short edge towards south.

   4.1. Place a monument (tripod, ranging rod, fence) 10 meters north from the IGRS with the help of a RTK-GNSS set. Repeat the process with a second monument 10 meters south of the IGRS in exactly the same longitude as the first.
   4.2. Place a rope in between the two monuments. If the rope runs trough the pole, repeat te process slightly to the east or to the west.
   4.3. loosen the nuts on the frame that secure the frame against rotation.

4.4. Rotate the frame until the centre line runs parallel to the north-south line. This can be checked by measuring the distance between the rope and the centre marker on the edge of the horizontal plate.

4.5. Re-tighten the nuts on the frame.

4.6. Check the verticality of the pole and start again when it is not vertical.

4.7. Check the horizontality of the frame. If it is not horizontal, while the pole is vertical, note it down in the installation report.

4.8. Check the nuts on the frame, if tight, continue with drilling a 4.5 mm hole in the pole trough the pre-drilled hole in the frame. Cut M5 thread in the hole. Apply appropriate cutting oil during the drilling and cutting. Place a M5 bolt in the newly made hole to secure the frame against rotation.

5. Adjusting the tilt angle of the reflectors.

   This step asks for specific information about the alignment strategy. A tilt angle should be chosen based on a motivation taking Section 6.2 into account. For the Groningen field case it is decided to tilt all the reflectors 5.1 degree inward and develop a specific Groningen tool to make alignment of the reflectors easier. A work around would be to use an inclinometer (found on smart phones) or work with geometric relations, a level and a ruler. Here we describe the protocol for use with a project specific tool.

   (a) Place the tool in the apex of the corner reflector.

   (b) Place a level which is at least as long as the height of the reflector against the tool and upper edge of the reflector.

   (c) On the tilt mechanism, tighten the nut closest to the frame and readjust the other two nuts until the level is in a vertical position.

   (d) Secure them tight. Measure the distance between the two nuts closest to the frame with a calliper and note it down on the installation form.

   (e) Mark all nuts with paint for future change detection.

6. Mount the cabinet.

   (a) Mount the cabinet by screwing the four bolts from the inside of the cabinet in the frame.

   (b) Let an expert connect the cabinet to the energy source.

7. Installation of the GNSS antenna should be done after consulting the supplier or by an expert. The following steps will roughly apply.

   (a) Mount the GNSS antenna on top of the pole, aim the north mark to the north.

   (b) Connect the antenna to the receiver in the cabinet.

   (c) Mount a GSM/4G antenna in the direction of the closest GSM/4G-pole.

   (d) Connect the GSM/4G antenna to the data modem.

   (e) Connect the receiver to the data modem.

   (f) Power up all electronics.

8. Last control round.

   (a) Check all bolts.

   (b) Check the installation sheet if all columns are filled.

   (c) Take 3-4 pictures of the IGRS for a 360 view of the IGRS and its surroundings.

6.4. Timing of the on-site processes

This section reports on the time spend on deploying an IGRS in the Groningen field case. It is limited to the work on the hardware of the IGRS itself. So, although part of the deployment, issues on the foundation, electronics and legal matters are beyond the scope op this section.

The steps have been timed during the alignment and installation of three different stations. The learning curve of the people installing the IGRS has levelled out and the times presented here can be seen as standard times for a routine job.

Setting up is done by two people. One mainly focusses on the radar, while the other focusses on installing the GNSS equipment. The timed steps are those that are exclusively part of installing an IGRS. Steps that have to be performed for a normal permanent GNSS station installation are not included in this chapter.

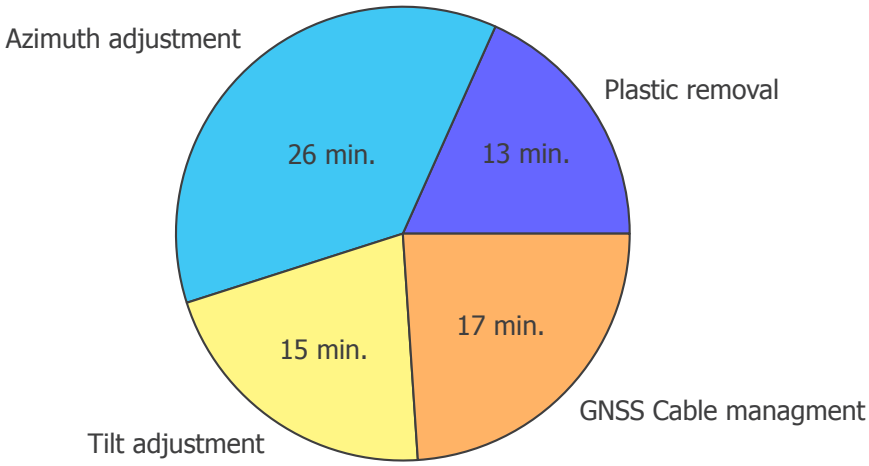

Figure 6.10: Chart with the time spend on different parts of the installation of an IGRS.

Plastic removal The aluminium sheet metal of the IGRSs that are deployed in the Groningen field study are covered in a plastic coating during production, transport and installation. At the start of the alignment procedure, it is removed. This takes roughly 13 minutes.

Azimuth adjustment The azimuth adjustment takes a short half hour. This takes long as it includes setting up an RTK-GNSS set and a north-south line. Once the north south line is set, it takes a couple of minutes to find the proper alignment of the frame as it is easy to overshoot the desired position. The last step is to drill a hole through both the frame and the pole, to fix the set-up with a locking bolt.

Tilt adjustment The adjustment of the tilt takes 15 minutes in which the reflectors are set to the right angle, the nuts on the threaded rod are fixed and locked with paint. The distance between the nuts is measured and noted down.

Cable management GNSS The cables running from the GNSS and GSM antennas to the cabinet run through the pole. This ensures a smooth rotation of the frame around the pole without disturbance of the cables. The cables have to be guided through the pole and some protective casing. This takes approximately 17 minutes.

The whole timed process takes approximately 1 hour and 15 minutes. The full installation (including the installation of the GNSS equipment) of the stations took approximately one and a halve hour. The

extra 15 minutes are spend parking the car, getting all materials ready and cleaning up. Due to travel time to and from stations, a maximum of 3 stations per day could be installed.

6.5. Operational use of the IGRS: Local surveying the IGRS

After deployment of the IGRS the next step is the operational use. This includes measurement campaigns for GNSS, InSAR, LiDAR and levelling. However, this chapter purely focusses on local surveying as:

- GNSS measurements are similar to any permanent GNSS station and are beyond the scope of this thesis.
- InSAR measurements are similar to a PS-analysis and are beyond the scope of this thesis.
- The use in LiDAR campaigns is still unknown.

The IGRS has to be surveyed to measure and check the relative location of the separate parts and to determine the height in NAP of the IGRS as a whole. This is done with levelling measurements and the use of a total station.

6.5.1. Markers

The IGRS has multiple markers that should be measured and checked. The levelling markers are on the GNSS antenna, the radar reflector, the horizontal plate and the foundation. Two additional, temporary levelling markers can be deployed in the apex of the reflector. Markers for the total station should be placed on the pole and on the reflectors if needed

Levelling the GNSS antenna

The GNSS antenna height is measured as seen in figure 6.11 until 6.13. A total of four measurements should be taken on the perimeter of the antenna. One each for north, east, south and west. For the north measurement it is sufficient to measure on one of either sides of the antenna cable. No physical markers are present.

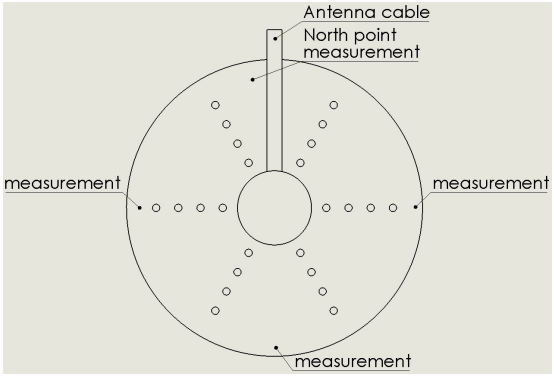

Figure 6.11: Schematic bottom view of GNNS antenna. West and east are not labelled on this bottom view to prevent misinterpretation.

Figure 6.12: GNNS antenna with the levelling rod below.

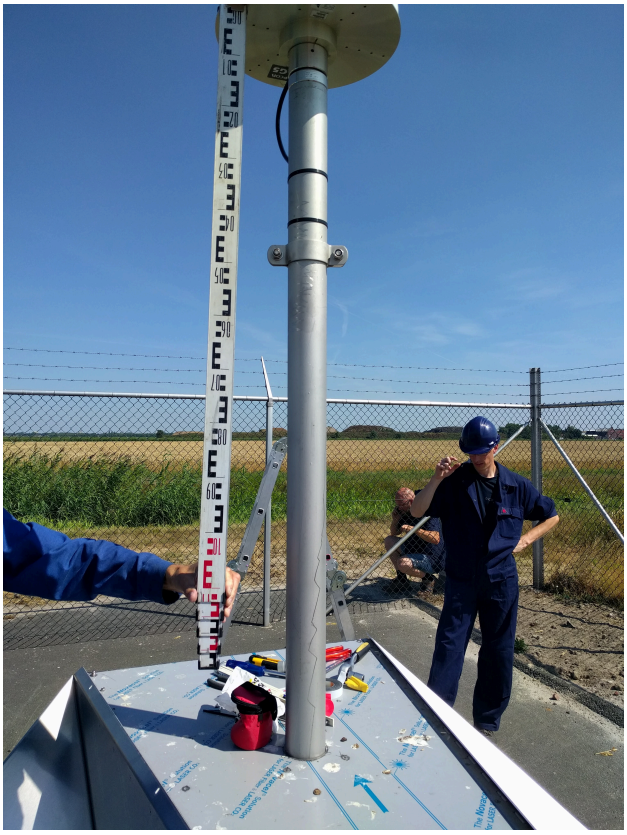

Figure 6.13: The levelling rod should fit under the antenna. Make sure to use a short or adjustable rod.

Levelling the radar reflector and horizontal plate

The radar reflectors and the horizontal plate are levelled using a total of 6 permanent markers, of which 4 are located on the horizontal plate (figure 6.14 till 6.16) and 2 are located at the far tip of either reflector (figure 6.17 and 6.18). The 4 markers on the horizontal plate can be used to detect a tilt of the IGRS in any direction. The 2 markers at the far tips of the reflectors can be used to detect any change in tilt of the reflector with respect to the IGRS. An additional two temporarily markers can be deployed in the apex of the reflector.

Two extra holes are present in the horizontal plate. These may be used to place two extra sets of bolt and nuts as a levelling benchmark. The information gotten from these two bolts may be used to detect a twist in the horizontal plate.

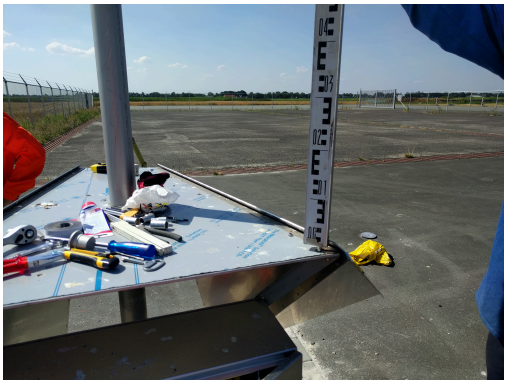

Figure 6.14: Proper way to place the rod on one of the bolts.

Figure 6.15: Close up of the bolt rod connection

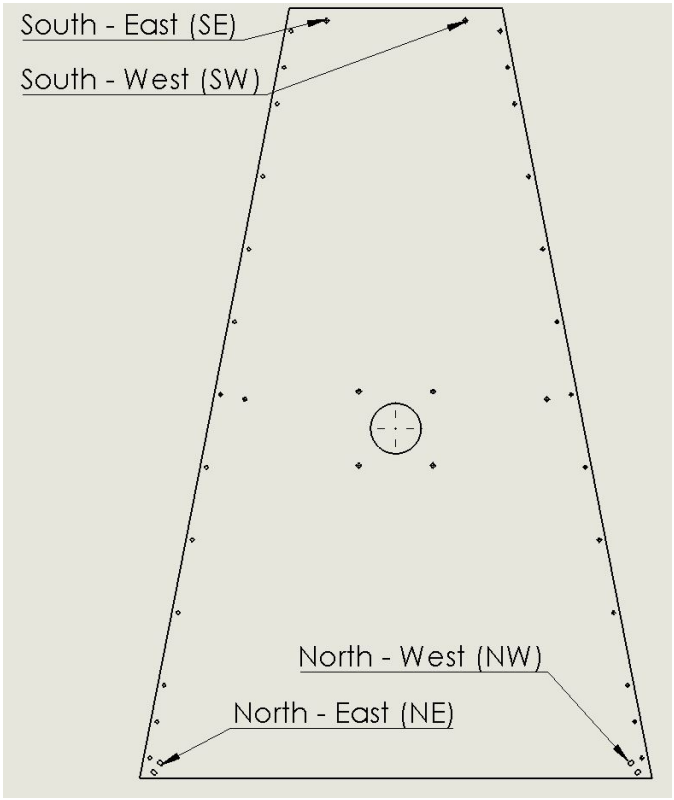

Figure 6.16: Placement of the four measurements on the horizontal plate (Top view).

Figure 6.17: Close up of the bolt rod connection.

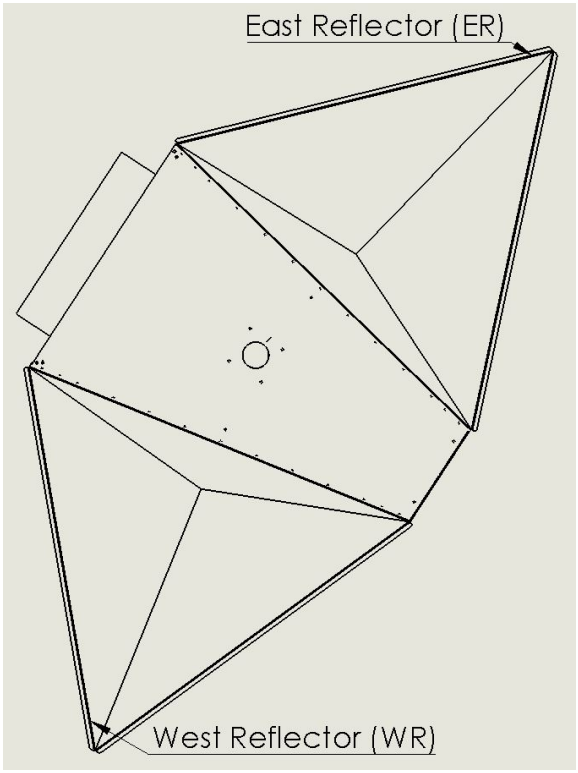

Figure 6.18: Top view of the reflectors.

Foundation

The foundation of the IGRS is a big concrete block. To check if there is any relative motion between the IGRS and the foundation, as many corners as possible of the block should be surveyed. Because the IGRS has a larger footprint than the foundation, it can be difficult to reach all corners of the foundation. Care should be taken to find an appropriate solution. Levelling markers are not yet present and should be made in the field the first time a levelling survey is conducted. As the foundation has a variable orientation, the points have been named in a specific order. C1 is the first corner clockwise from north. C2 is the second corner clockwise form north, etc. If a corner is not suitable for a marker, it is still named 'C#'. It may happen that for example only levelling markers C1 and C4 can be measured.

Nomenclature

The names of the markers represent their cardinal direction and where they can be found. This will be easy to check in the field and will be interpretable once the data is back at the office. The markers have a short and a long name, depending on what is more convenient to use. As the foundation has a variable orientation, the points have been named in a specific order. C1 is the first corner clockwise from north. C2 is the second corner clockwise form north, etc.

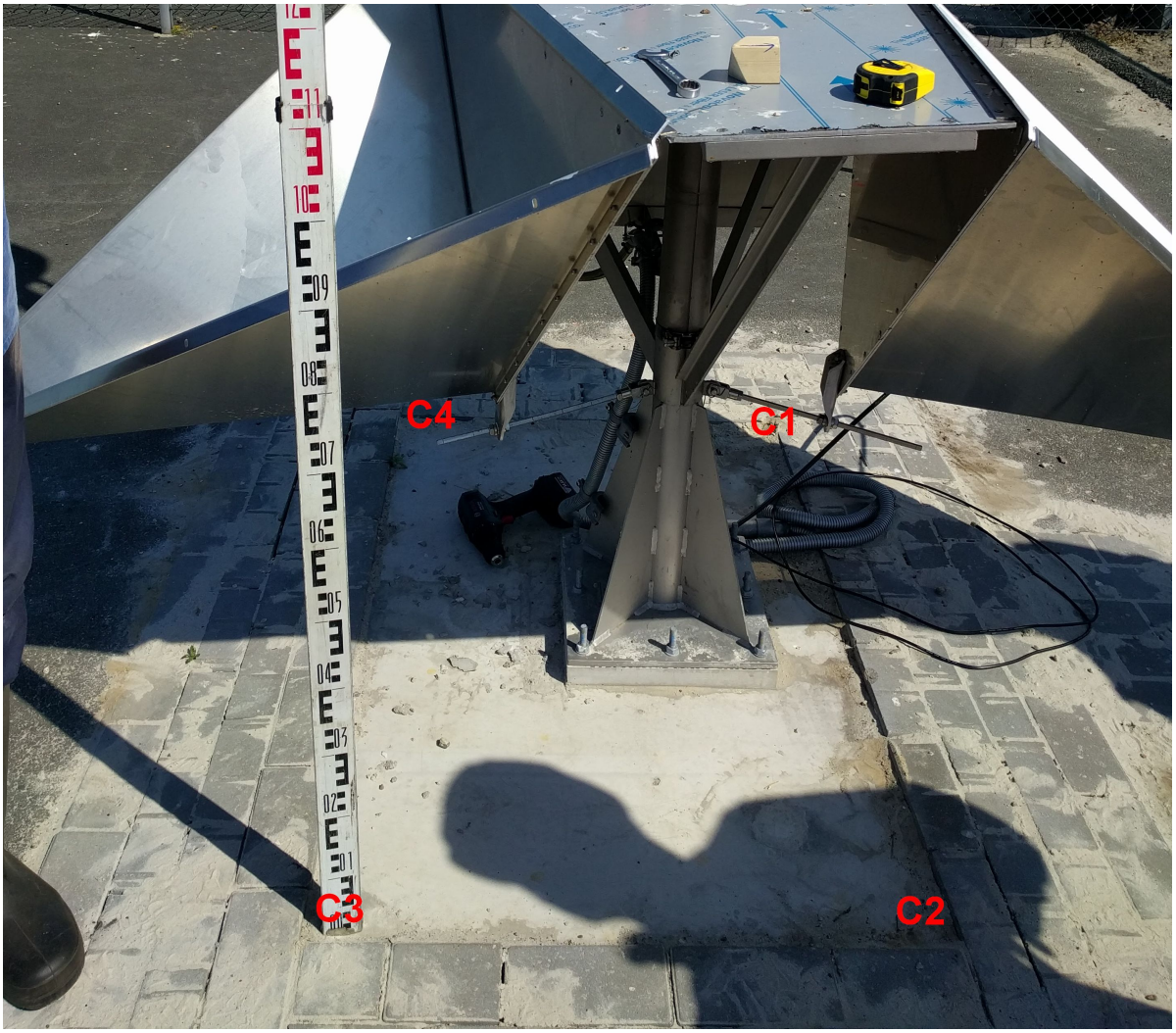

Figure 6.19: Foundation of the IGRS with corner names.

Table 6.4: Acquisitions descending reference reflector.

Part	Long name	Short name
GNSS antenna	GNSS North	GN
GNSS antenna	GNSS East	GE
GNSS antenna	GNSS South	GS
GNSS antenna	GNSS West	GW
Reflector	Reflector East	RE
Reflector	Reflector West	RW
Reflector	Reflector Apex East	RAE
Reflector	Reflector Apex West	RAW
(Optional) Horizontal plate	Plate East	PE
(Optional) Horizontal plate	Plate West	PW
Horizontal plate	Plate North West	PNW
Horizontal plate	Plate North East	PNE
Horizontal plate	Plate South West	PSW
Horizontal plate	Plate South East	PSE
Foundation	Corner 1	C1
Foundation	Corner 2	C2
Foundation	Corner 3	C3
Foundation	Corner 4	C4

6.5.2. First visit, standard campaign & change detection

In this section we elaborate on the three different levelling campaigns that have to be performed.

First visit Depending on the way of deployment, on the first visit there might be no suitable levelling markers yet. Then, it is up to the surveyor to install these. The four bolts on the horizontal plate (see figure 6.16, make sure to swap the inner bolts from the set) should be swapped with 15 mm long M6 stainless steel bolts (DIN 912) , secured with round headed nuts (DIN 1587) as shown in figure 6.20 and 6.21 and should be fixed with appropriate thread locking paste (like Lock-Tight).

Figure 6.20: Bolts not suitable for levelling.

Figure 6.21: Levelling marker after changing bolts.

The remaining two markers are made from 10mm m5 bolts and nuts (again, DIN 912 and DIN 1587) which can be placed in existing empty holes at the far tip of the reflector (Figure 6.17 and 6.18).

A maximum of four levelling markers should be placed in the concrete foundation. These can be round headed screws that should be permanently fixed to the concrete. Only if the IGRS is blocking the possibility to measure the levelling marker, it may be skipped.

Furthermore, a local reference point for the levelling needs to be selected. Ideally, this reference point should be close to the IGRS, but preferably not on the IGRS itself. The reference point could for instance be on a nearby building or structure which has a good stable foundation and is presumably stable. In case no such point can be found, then one of the points on the concrete foundation of the IGRS can be assigned to this role. In case there is a very nearby NAP benchmark this point can serve the role as local reference point.

The next step of the initial survey is to carry out a standard levelling campaign. This comprises a local levelling loop between the reference point and markers on the IGRS, and a levelling loop between the local reference marker and nearest NAP benchmark.

Standard levelling campaign A standard levelling campaign would involve a visit to the IGRS during a levelling loop that originates from one of the NAP benchmarks nearby. During this campaign, a levelling loop between the NAP benchmark and local reference point is measured using standard levelling procedures. At the end of the loop near the IGRS, all local markers are levelled with respect to the chosen local reference point.

The local markers are measured in two cycles, forward and backwards, which both start and end on the local reference point.

Corner reflection alignment inspection A corner reflector alignment inspection may be necessary when the data shows unexplained behaviour.

The corner reflectors are aligned to an optimal position. This alignment might change over time when the bolts unexpectedly loosen. When the alignment changes, so does the phase centre of the measurement (located in the apex) and as a consequence the observations change. In such a case, the distance between the two bolts (see figure 6.22) on the tilt angle mechanism should be checked with the documented value. A seal has been placed on the bolts during alignment. Such a seal can be seen in figure 6.23. A broken seal might be due to weathering or erosion and is no solid proof that something changed. An intact seal however, does indicate some other source should be found for the unexpected deformation signal.

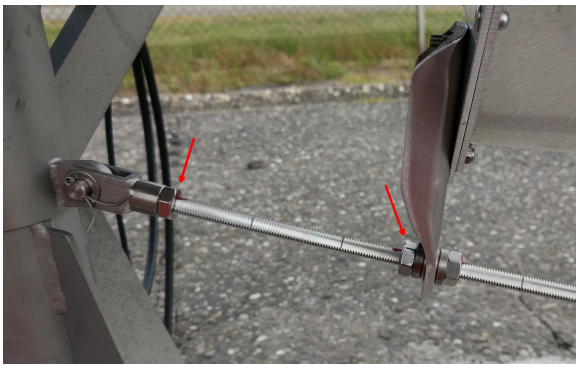

Figure 6.22: The rigger construction for reflector alignment. The distance between the bolts that have been highlighted should be measured.

Figure 6.23: Bolts are sealed with a red seal to indicate change.

When the measurements show unexplained behaviour, or when the seals are broken or when something significant to the structure has happened or was suspected, it is recommend to carry out a local change detection levelling survey or standard levelling survey.

7

Synthesis: Performance in relation to design, deployment strategy and operational use

7.1. Evaluation of the DBF90T-GNSS on the IGRS requirements

The requirements for an IGRS should all be reached by the DBF90T-GNSS to mark it as a successful IGRS. This section describes if the DBF90T-GNSS functions conform all of the requirements. For every individual requirement, a short summary of the work presented in this thesis is given.

7.1.1. Functional requirements

The IGRS shall:

1. **receive and record GNSS signals by using a continuous operating GNSS reference station;**

   This requirement is met. See [38] for a test report including results showing quality standards are met for the current set-up.

2. **reflect radar signals back to SAR satellite constellations (Sentinel-1, TerraSAR-x, Radarsat-2) for both ascending and descending acquisitions;**

   During the development there has been a focus on Sentinel-1 due to lower RCS for targets compared to TerraSAR-X and the higher temporal resolution available compared to Radarsat-2. However, the nature of corner reflectors and their wide range in alignment parameters makes the DBF90T-GNSS compatible to all three constellations.

3. **house levelling benchmarks;**

   The DBF90T-GNSS has levelling benchmarks, as described in Section 6.5. Test results are not yet present and are part of future study

4. **house total station reference points;**

   Total station reference points are not permanently incorporated into the design of the reference station as they are easily made with standard total station stickers which can be mounted on the corner reflectors.

5. **house a LiDAR reference surface; and**

   The flat horizontal plate on top of the frame can be used as a LiDAR reference surface. However, future research should be done to validate this statement. See appendix B for a visualisation of the point cloud of a first test with a terrestrial laser scanner.

6. **integrate all of the above into one physical system.**

   This requirement is met by placing all reference points on a combination of a frame and a pole structure with a single foundation.

7.1.2. Non-functional requirements

The non-functional requirements include performance requirements which are tested on the Wassenaar test site.

The IGRS shall:

1. **make use of geodetic monitoring grade GNSS equipment ensuring ~mm precision;**

   The GNSS equipment can be adjusted to the needs of the owner. State of the art geodetic grade receivers and antennas are used in our set-up ensuring good results. The test report on GNSS multipath shows no significant negative effects of the IGRS itself[38]. The RMS errors for the GNSS errors in the test set-up are 2, 3 and 5 mm for east, north and up respectively [38].

2. **make use of radar reflectors with 1 mm double difference precision in the Line-of-Sight;**

   The RMS error for the interferometric phase are around 0.4 mm in the LOS for the interferometric pair of the DBF90T-GNSS and the reference reflector at the Wassenaar test field (see Fig. 5.20). This corresponds to a 1-σ single measurement precision of the DBF90T-GNSS to be around 0.3 mm in LOS.

   From these results it is clear that both the RCS of the reflectors and the in-situ stability of the DBF90T-GNSS are designed to meet this requirement.

3. **lead to errors associated to the relative location of reference points shall be of the same order or lower than those of the individual sensor errors;**

   For the radar reflectors, the individual sensor error is represented by σ_{clutter} and the errors associated to the relative location of the reference point is represented by σ_{monument}. For the DBF90T-GNSS these values are very similar. For the DBF90X, σ_{monument} is around 3-4 times as large as σ_{clutter}. However, σ_{clutter} is dependent on the clutter conditions. The higher the clutter, the larger the individual sensor error will be while the in-situ stability of the IGRS will stay the same.

   For the GNSS, it is theoretically determined that the in-situ stability is more precise than the measurement precision of the GNSS antenna in Section 4.6.

4. **house equipment for one measurement techniques, which do not significantly lower the signal quality for other measurements;**

   An harming influence of the reflectors on the GNSS results is not found in the test results for the current set-up of the DBF90T/X-GNSS. The influence of the GNSS pole was not significant on the SAR measurements.

5. **be resistant to transport, handling and deployment;**

   Normal care should be taken while transporting the IGRS. In the deployment of 24 IGRSs during the Groningen field study, one IGRS was structurally damaged during transport, handling and deployment. However, this indicates rough treatment as all others only show minor signs of wear and tear exclusively on non-functional parts.

6. **be able to withstand 20+ years of exposure to weather influence (wind, rain, corrosion) with minimum amount of maintenance;**

   It is easy to assume the IGRS will withstand 20+ years of exposure, due to the use of low corrosion metals. This assumption will be tested in the Groningen field study and can be reported in future work.

7. **be affordable, manufacturable and deployable for campaigns with multiple units; and**

   The costs to make the DBF90T are around €4.000,-. Compared to the costs of around €10.000,- of the custom-of-the-shelf GNSS equipment this is reasonable.

8. **not lead to any hazardous situation.**

   Hazardous situations can occur if the bright aluminium reflects the sun into the eyes of passing drivers. However, the aluminium quickly turns pale due to oxidation of the top layer reducing the likelihood of such events. The sharp corners of the far end of the reflector are rounded to ensure little harm is done to people hitting their legs to it.

7.2. Qualitative analysis on IGRS performance

Various aspects of the IGRS have influence on its performance, some of which are trivial, while others have unexpected negative consequences which might be unfavourable. Figure 7.1 shows all the relationships schematically. This section will shortly discuss all relationships.

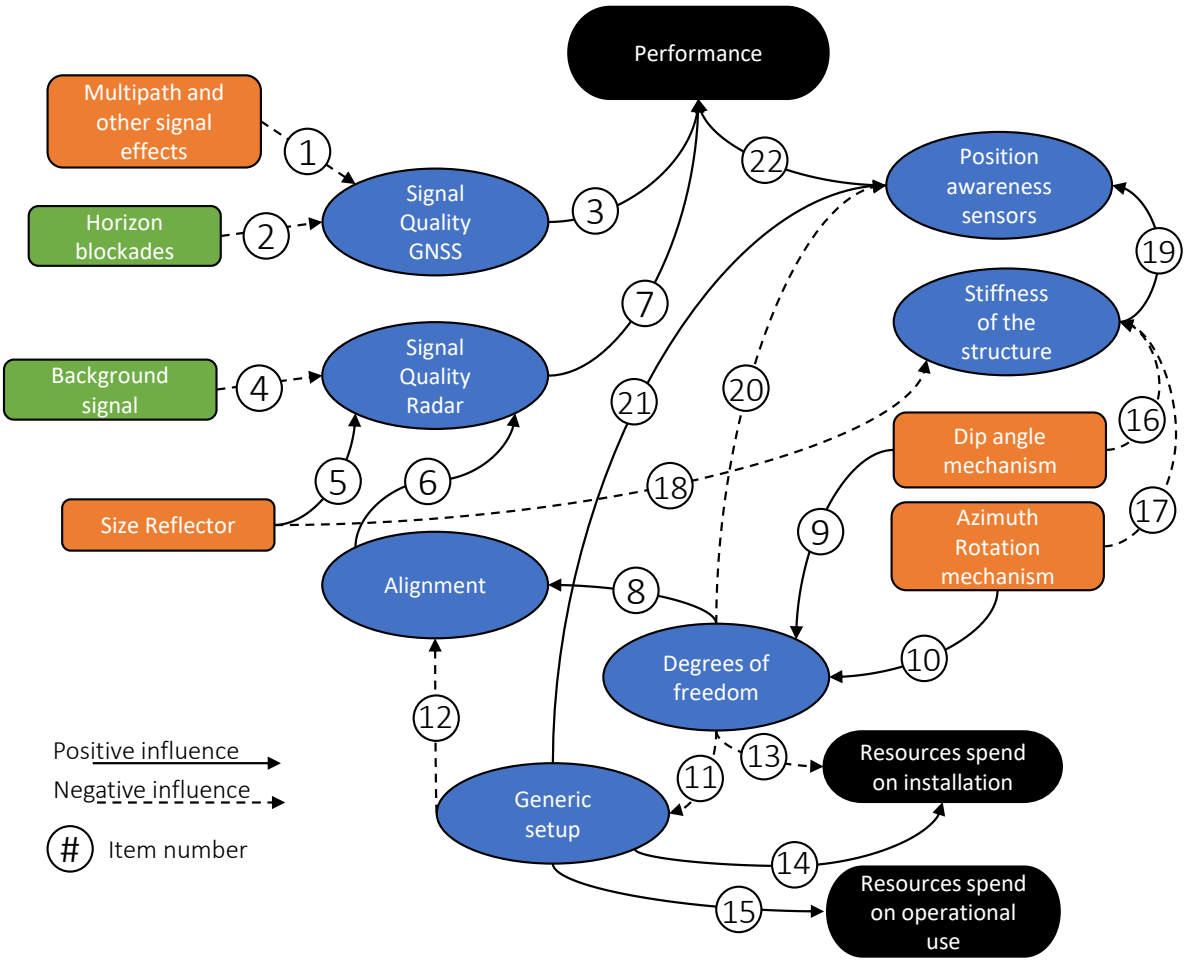

Figure 7.1: Schematic representation of various aspects which influence the performance of the IGRS.

1. Multipath from the environment and the IGRS itself has negative influence on the signal quality of the GNSS. This is reported in [38]. It is concluded that a distance of at least 30 cm between the reflectors and the choke ring GNSS antenna leads to acceptable levels of error for a permanent GNSS station.

2. Objects blocking the view between GNSS satellites and the GNSS antenna can result in lower quality results. Generally, rural areas are suited for a permanent GNSS station, whereas a low placement in a build environment will lead to poor quality result (Section 6.1).
3. The overall signal quality of the GNSS location estimate of the GNSS reference point is directly translated to the performance of the IGRS[7].
4. The background signal, or clutter, has a direct negative effect on the SCR which is a measure for the signal quality of the reflector. Details on this effect are given in section 2.4.1.
5. The size of the reflector has positive impact on the signal strength of the reflector, or RCS, which has a direct effect on the SCR. The influence of the size (effective aperture) on the RCS can be found in Eq. 2.9 and Fig. 4.8.
6. Like the size, aligning the reflector has a positive influence on the signal quality of the reflector. The influence of the alignment on the RCS can be found in Fig. 2.29.
7. Just like GNSS signal quality, a high signal quality and thus a low variance on the estimate of the location of the radar reference point has a positive influence on the quality of the co-location capabilities of the IGRS.
8. For ideal alignment of a corner reflector, two degrees of freedom are needed. If those degrees of freedom are present in the design, it has a positive influence on the alignment capabilities.
9. To obtain the first degrees of freedom, a dip angle mechanism can be constructed which dips/tilts the corner reflector in the vertical plane.
10. The second degree of freedom can be obtained by implementing an azimuth rotation mechanism, to rotate the corner reflector in the horizontal plane.
11. For a project with multiple IGRSs, it may be convenient to have a generic set-up as shown in Section 6.2. When the reflectors have multiple degrees of freedom, this has a negative impact on a generic set-up. A generic set-up with variations due to installation imperfections will result in a less generic set-up.
12. However, a generic set-up has negative influence on the alignment, as it implies that not all reflectors are aligned to their ideal position.
13. The degrees of freedom have a negative impact on the resources spend on installation, since adjustments to the alignment of the reflector have to be made. However, if no azimuth rotation mechanism is implemented at all, this will lead to need of a more sophisticated planning of the foundation to ensure an optimal placement of the IGRS which will probably be more time consuming than adjusting a basic azimuth rotation mechanism.
14. A generic set-up will have a positive effect on the resources spend on installation, as a generic set-up will lead to easier methods for both planning and implementing.
15. For the same reason, a generic set-up will have a positive effect on the resources spend on operational use, since the set-up can be checked against a nominal set-up instead of a specific one.
16. Applying mechanisms to obtain certain degrees of freedom to the reflector while still providing a stiff mounting structure can lead to more sophisticated mounting options which might be more complex or more expensive to implement. This might not pose a problem if a proper design is found.
17. Similar to the the previous item.
18. Large corner reflectors need a more sophisticated design to reach appropriate levels of stability. Not only the reflectors itself are deformed easier, also the whole structure needs to cope with higher forces. Forces due to the increased weight, but moreover higher forces due to weather phenomena like wind and snow.

19. A non-stiff structure, will deform under minor wind loads. This might lead to errors in the position awareness of the reference points, as the assumed sensor offset might not hold under those deformed conditions. In the scale of whole time series this might not pose a problem due to the dynamic and random behaviour of the movement, but single measurements will be effected if the structure moves. Therefore, a stiff structure has a positive influence on the local position awareness of the sensors.
20. Multiple degrees of freedom have a negative influence in the case of malfunctioning locking mechanisms. If locked properly, this negative influence is most likely not happening if designed appropriate. Nevertheless, the risk is present.
21. A generic set-up helps in estimating the off-sets of the reference points, as it opens the possibility to have a rough estimate ready for all stations without making extra measurement.
22. The position awareness of the individual sensors in a local XYZ-reference frame determines the quality of the used offset between sensors. This offset is used in the application of the IGRS and therefore this influences the overall performance.

7.3. Alternative solutions for future generations of IGRSs

As earlier noted in the introduction this work has the objective to gain insight in and knowledge on the practical problem of connecting geodetic datasets in the physical world. This insight and knowledge can be used as a stepping stone in the development of a next generation IGRS. This section reports on the main insight based on the process of writing this thesis which might provide a solid basis for a next generation IGRS.

The DBF90T-GNSS has proven to be the best design presented in this thesis for deployment in low clutter conditions. It fulfils the requirements as presented in Section 7.1. Therefore, in the light of the research question of this thesis, it can be called an adequate design. However, it can be argued that more practical designs are possible.

For the DBF90T-GNSS, the azimuth alignment angles of the corner reflectors are fixed. The tilt angle can be adjusted to the site specific incidence angle of the incoming signal. However, if no site specific tilt angle would be chosen, but instead the azimuth angle is set to either 90 for DSC or 270 ASC and the tilt angle is set to 0, the RCS of a 0.9m does not drop below 26.8 dB for latitudes lower than 70°N as can be seen in Fig. 7.2.

Fig. 7.2 is based on Section 2.4.1 which reports on both the effect of aligning the reflector in azimuth and tilt angle. Fig. 2.29 shows a large range of alignment angles which do not harm the signal of the reflector by more than 1-2 dB. Redesigning the reflector to have a RCS of 2 dB larger is done by making the corner reflector only 10% larger. This is shown in Fig. 4.8.

For future projects this would potentially simplify the design, production and operational aspects of the IGRS related to levelling. Furthermore it would eliminate the alignment procedure of the reflectors, the computation of desirable tilt angles and the risks of undesirable tilt changes. In terms of practicality and simplicity, it can be argued that such a design would be more practical since similar results could potentially be reached with less or simpler tasks.

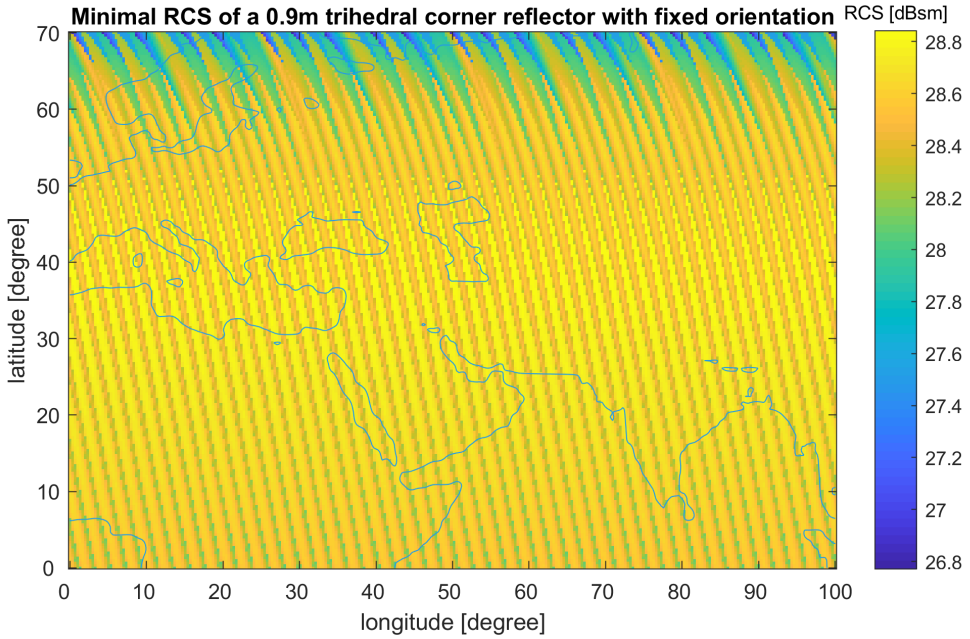

Figure 7.2: Minimum RCS for an ascending trihedral corner reflector with an inner leg length of 0.9cm mounted back to back in a reflector pair as presented in [27] plotted for geographical location.

8

Conclusions and Discussion

This work is written to answer the main research question:

How to design a device, that couples InSAR, GNSS, levelling, and possibly other geodetic measurements, with the main goal to integrate InSAR measurements into a well defined geodetic datum?

This thesis presents the work needed to answer this question. It is shown in this thesis that it is possible to design and build a device that houses reference points for InSAR, GNSS, levelling and local total station surveys with fixed or known relative offsets without significant negative side effects. The answers to the sub-questions are the main conclusions of the work. While some lessons learned are clear conclusions stemming from the work, some lessons learned are open for discussion. Both the conclusions and the discussion about these conclusions are given below.

8.1. Conclusions and Discussion

- **What are the requirements for the device such that it can fulfil its main goal?**

  The wish to place all reference points on a single foundation to ensure one common deformation trend is observed, leads to the the main functional requirement being the one that the IGRS shall integrate all the used reference points in one physical system. This requirement is not yet met by alternative solutions presented in literature, making this research and development process desirable. The total set of requirement are presented in Chapter 3. The fact that the DBF90T-GNSS meets all these requirements is described in Chapter 7.

- **What is good and practical design for such an instrument that fulfil the requirements?**

  For a design to be adequate, it has to meet the set requirements at least. For a design to be good, it has to be better than adequate. For a design to be practical, it should not lead to unnecessary work.

  It can be concluded from the fact that all requirements are successfully met, that the design of the DBF90T-GNSS is adequate at least. It can be argued that the design of the DBF90T-GNSS is a practical design, as it leads to easy deployment of multiple reference points at a single foundation and eliminates the need for frequent repetitive local measurements. It eliminates the need for methodologies to estimate the differences between observations stemming from different monitoring methodologies. Furthermore, it eliminates the need for regular maintenance of the CRs.

  However, it can also be argued that the possibility to make a more practical design is plausible. As described in 7.3 the ability of the DBF90T-GNSS to adjust its tilt angle is at the cost of simplicity of the design, production and operational aspects of the IGRS while only gaining 1-2 dB on RCS/SCR. A similar gain can be obtained by enlarging the reflectors by only 10%. An extra benefit of the latter strategy is that the gain is obtained throughout all systems while proper alignment only benefits systems with the aligned geometry of choice.

Overall, the DBF90T-GNSS is a good IGRS as it performs well within the set requirements without major impractical quirks.

- **What is the error budget and performance of this design?**

  As presented in Section 4.6, the error budget of the IGRS depends on the application which the IGRS is used for. This thesis focusses on the use of the IGRS as a device to integrate InSAR measurements in a well defined geodetic reference frame. For this application, the major aspects influencing the errors are on one hand the individual measurement errors of the InSAR system and GNSS set-up, and on the other hand the stability of the physical connection between the reference points of the measuring systems.

  The errors expected due to the design choices are described in Section 4.6. The main conclusion in this section is that all the contributions to the total error budget are evenly spread. This indicates that the resources to enhance performance are allocated evenly.

  From the experiments has been learned that the actual performance of the DBF90T-GNSS is well within the expected error budget, given its 1-σ value of 0.4mm for the double difference phase observations. However, it must be noted that this is partly due to low clutter conditions at the Wassenaar test site. It should be noted that the performance of the corner reflectors are heavily influenced by the clutter conditions.

- **Which strategies and procedures should be followed for deployment of this design?**

  An example on how to determine an alignment strategy is given in Section 6.2. Procedures on deployment and operational use are given in Sections 6.3 and 6.5.

  The main conclusion is that if IGRSs are deployed in large numbers in an area with IGRS baselines of several tens of kilometres, it is wisely to choose an alignment strategy based on operational reasons instead of signal quality reasons. This is due to marginal gains in signal quality for an individually derived set of alignment parameters.

8.2. Recommendations

Future research on the IGRS itself could benefit from the following recommendations:

- **Evaluation of an extended time series.**

  The two prototypes placed in Wassenaar (Chapter 5) are still present at the test site and have been installed for over a year by the moment of writing. Therefore, the time series is continuously growing, leading to potential better interpretations of the trends. With the currently available dataset, only 3 months of data have been interpreted. Interpreting a full year would possibly improve the interpretation of the results as a yearly trend might be visible.

  The DBF90T-GNSS tested in Wassenaar showed some signs of tilting. Performing a levelling survey to gain some ground truth data on the foundation would be desirable. If available, this would validate or tackle the assumption of a stable foundation and thereby give more information about the stability of the DBF90T-GNSS itself.

- **Further development of the design.**

  As written in the objective of this work, this thesis should be able to provide a stepping stone for future development of a next generation IGRS. Possible further development in the direction of simplicity in terms of design, deployment and operational use is given in Section 7.3. This can be a start to the development of a simpler, more practical next generation IGRS design with similar performance.

- **Development of applications for the use of the IGRS.**

  Now that the IGRSs have been deployed in Groningen, it is time to actually develop the tool-boxes and methodologies using the co-located observations of multiple IGRSs. The other way around, the development of such applications may lead to new requirements for a future design. Applications might be focussed on:

- Atmospheric phase estimation.
- Improved geolocation estimates of scatterers by using GNSS observations.
- Cross-track radar datum connection.
- Integration with LiDAR point clouds (AHN).
- Any other application exploiting the possibility of co-located observations for GNSS, InSAR, levelling, LiDAR and or Gravimetry.

Furthermore there are recommendation on the operational side of the IGRS stations:

- **Create a wider area covered by IGRS stations.**

  This will lead to a wider coverage of connected radar images. A national coverage of the Netherlands as a starting point would be a desirable project as a case study for further implementation of the concept of co-located reference points.

- **Locate the IGRSs in the point cloud of AHN.**

  The IGRS has not yet been tested in an airborne LiDAR measurement set-up. For it to be applicable in an application to integrate its coordinates in the LiDAR point cloud, it is needed to be detected. Therefore, it is desirable how the IGRS looks like in the AHN dataset to see if using the IGRS will enhance the quality of the point cloud.

A

Example: 2D deformation inverse problem

This example shows a method to derive the 2D deformation vector of a single reflector in the vertical plane parallel to the LOS.

A deformation signal in any direction can be decomposed in 3 orthogonal vectors. The deformation signal is projected on the line of sight, resulting in a 1D measurement. Detailed information on this process is given in [6] and [18]. To retrieve the full 3D signal, at least 3 different measurement geometries are needed. For a corner reflector in the Netherlands, typically it can be measured with 2 measurement geometries. With the method below, the deformation in the up and azimuth direction can be be found.

The two different incidence angles of the two different tracks available per reflector, lead to two different line of sight (LOS) measurements (D_a and D_b) of for same in-situ deformation (D). The corresponding geometries are shown in figure A.1.

Assuming high precision, the two measurements D_a and D_b give enough information to get a values for D_{up} and D_{az} in the vertical plane in the azimuth direction. Per side, it is possible to set up the following set of equations for the LOS measurements:

$$\begin{aligned} D_a &= cos(\theta_a) \cdot D_{up} + sin(\theta_a) \cdot D_{az} \\ D_b &= cos(\theta_b) \cdot D_{up} + sin(\theta_b) \cdot D_{az} \end{aligned} \tag{A.1}$$

. This can be rewritten into the form of $y = Ax$:

$$\begin{bmatrix} D_a \\ D_b \end{bmatrix} = \begin{bmatrix} cos(\theta_a) & sin(\theta_a) \\ cos(\theta_b) & sin(\theta_b) \end{bmatrix} \begin{bmatrix} D_{up} \\ D_{az} \end{bmatrix}, \tag{A.2}$$

which can be solved by regular linear least squares:

$$\hat{x} = (A^T A)^{-1} A^T y. \tag{A.3}$$

However, it must be kept in mind that this set of equations is very unfavourable, as the model matrix A is ill-conditioned. This means that a small error in one of the measurements will result in a large error in the estimate. This is shown with actual results in Figure 5.23. To solve this, a combination of both ascending and descending tracks can be used. However, if this is done, it must be ensured that both reflectors under go the exact same deformation.

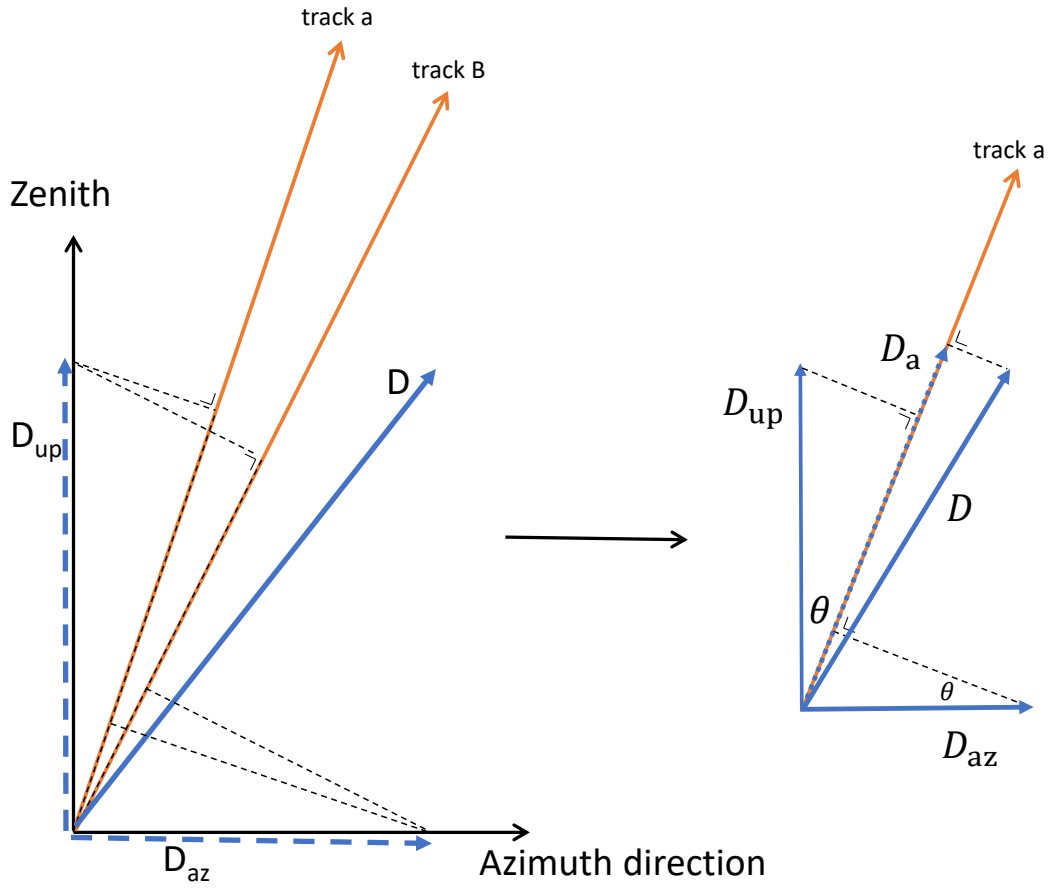

Figure A.1: Geometry of two different different measurements (D_a and D_b) of one single deformation signal (D). On the right there is shown a schematic view of the relation between measurement and deformation signal as a whole and as its two decoupled orthogonal parts. The assumption is made that both geometries of track a and b have a constant azimuth, while they actually have a difference of 1,62 degree for sentinel 1 at the Wassenaar test site.

B

Terrestrial LiDAR test

To get a first impression of how the IGRS would show up in a terrestrial laser scan, a simple quick scan has been made of the mock-up. The results show multi-bounce reflections around the actual geometry of the reflector. This indicates the aluminium plates act like mirrors creating false reflections. The effect is especially present at rays hitting the aluminium at high incidence angles (70° - 90°). For the use of the IGRS in airborne LiDAR campaigns, it is likely that due to the lower incidence angels, this will not be a problem.

Figure B.1: Frontal view of a reflector on the mock-up. False reflections are present outside the geometry of the corner reflector. They are caused by the mirroring properties of the aluminium side panels. The LiDAR instrument assumes a straight Line-of-Sight while in fact the signal has reflected on the way back and forth.

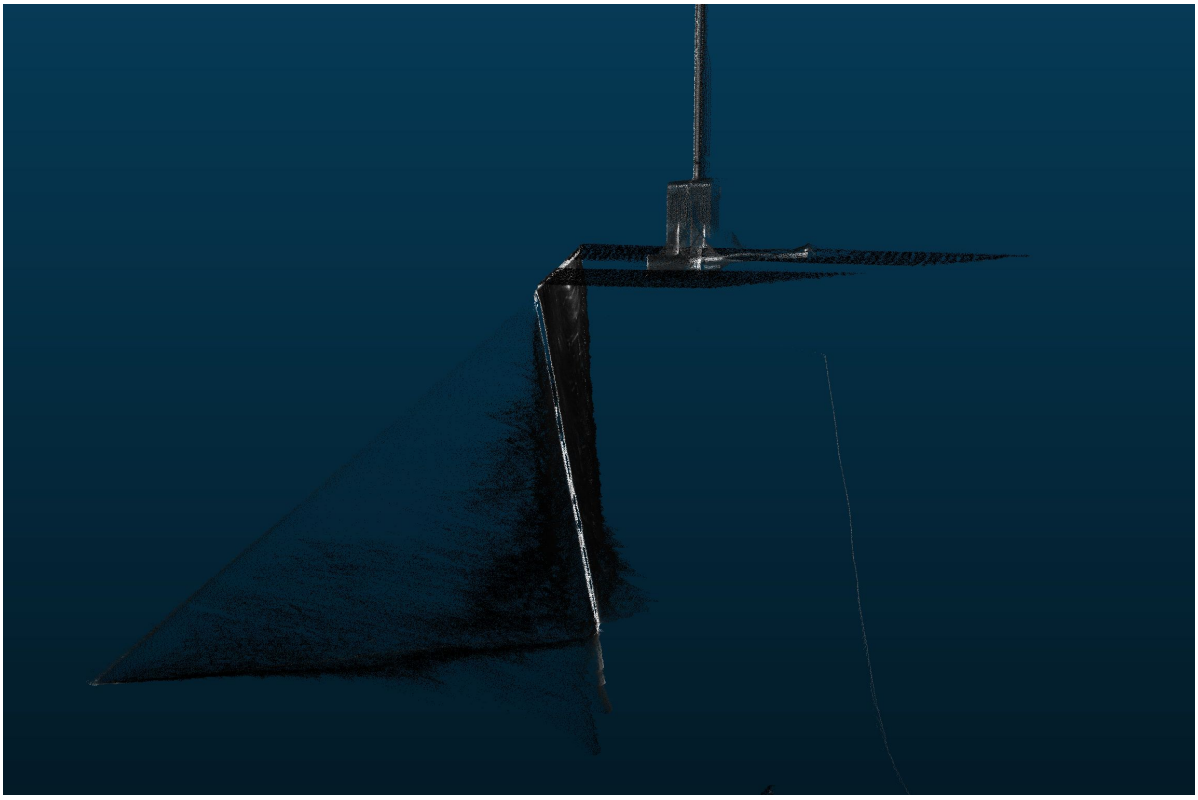

Figure B.2: Side view of a reflector on the mock-up. False reflections are present behind the aluminium backplate while the instrument is physically not able to measure at these positions.

References

[1] G. Bomford, *Geodesy*, Oxford science publications (Clarendon Press, 1980).

[2] S. Wdowinski and S. Eriksson, *Geodesy in the 21st century,* Eos, Transactions American Geophysical Union **90**, 153 (2011).

[3] P. Vanicek, R. O. Castle, and E. I. Balazs, *Geodetic leveling and its applications,* Reviews of Geophysics **18**, 505 (1980).

[4] P. J. Paul Guyer, *An Introduction to Total Station Topographic Survey Procedures* (Guyer Partners, 2018).

[5] B. Hofmann-Wellenhof, H. Lichtenegger, and E. Wasle, *GNSS - Global Navigation Satellite Systems : GPS, GLONASS, Galileo and more* (Springer, 2008).

[6] R. F. Hanssen, *Radar Interferometry* (Springer Netherlands, 2001).

[7] P. Mahapatra, H. van der Marel, F. J. van Leijen, S. Samiei-Esfahany, R. Klees, and R. F. Hanssen, *Insar datum connection using gnss-augmented radar transponders,* in *2016 IEEE International Geoscience and Remote Sensing Symposium (IGARSS)* (2016) pp. 6867–6870.

[8] T. Fuhrmann, M. Garthwaite, S. Lawrie, and N. Brown, *Combination of GNSS and InSAR for future australian datums,* (2018).

[9] M. Garthwaite, S. Lawrie, J. Dawson, and M. Thankappan, *Corner reflectors as the tie between insar and gnss measurements: Case study of resource extraction in australia,* (2015).

[10] Various, *Study and data acquisition - plan induced seismicity in groningen - update post-winningsplan 2016,* report (2016).

[11] H. van der Marel, *Reference systems for surveying and mapping (lecture notes ctb3310),* (2016).

[12] P. Teunissen, *Zero order design: Generalized inverses, adjustment, the datum problem and s-transformations,* in *Optimization and Design of Geodetic Networks*, edited by E. W. Grafarend and F. Sansò (Springer Berlin Heidelberg, Berlin, Heidelberg, 1985) pp. 11–55.

[13] P. Fokker, F. Van Leijen, B. Orlic, H. Van Der Marel, and R. Hanssen, *Subsidence in the dutch wadden sea,* Netherlands Journal of Geosciences: Geologie en Mijnbouw **97**, 129 (2018).

[14] J. Baecker, *Levelling,* `https://en.wikipedia.org/wiki/Levelling/media/FileNivellementExample.svg` (2005).

[15] G. Young, *Geodetic levelinggeodetic leveling,* in *Geophysics* (Springer US, Boston, MA, 1989) pp. 470–474.

[16] A. de Bruijne, J. van Buren, A. Kősters, and H. van der Marel, *Geodetic reference frames in the netherlands,* report (2005).

[17] S. Samiei-Esfahany, *Exploitation of distributed scatterers in synthetic aperture radar interferometry*, Ph.D. thesis, Delft University of Technology (2017).

[18] F. Van Leijen, *Persistent Scatterer Interferometry based on geodetic estimation theory*, Ph.D. thesis, Delft University of Technology (2014).

[19] M. C. Garthwaite, *On the design of radar corner reflectors for deformation monitoring in multi-frequency insar,* Remote Sensing **9** (2017), 10.3390/rs9070648.

[20] V. B. H. Ketelaar, *Satellite Radar Interferometry: Subsidence Monitoring Techniques* (Springer Netherlands, 2009).

[21] P. Dheenathayalan, D. Small, A. Schubert, and R. F. Hanssen, *High-precision positioning of radar scatterers,* Journal of Geodesy **90**, 403 (2016).

[22] W. Jacoby and P. L. Smilde, *Gravity Interpretation* (Springer-Verlag Berlin Heidelberg, 2009).

[23] J. Dakin and R. Brown, *Handbook of Optoelectronics: Concepts, Devices, and Techniques (Volume One)*, Series in Optics and Optoelectronics (CRC Press, 2017).

[24] M. Caro Cuenca, R. Hanssen, A. Hooper, and M. Arikan, *Surface deformation of the whole netherlands after psi analysis,* FRINGE 2011 Workshop, ESA SP-697 , 1 (2011).

[25] A. L. Parker, W. E. Featherstone, N. T. Penna, M. S. Filmer, and M. C. Garthwaite, *Practical considerations before installing ground-based geodetic infrastructure for integrated InSAR and cGNSS monitoring of vertical land motion,* Sensors **17** (2017), 10.3390/s17081753.

[26] NGU, *Measurments of deformation,* https://www.ngu.no/en/topic/measurements-deformation (2019), accessed: 2019-01-24.

[27] G. Quin and P. Loreaux, *Submillimeter accuracy of multipass corner reflector monitoring by ps technique,* IEEE Transactions on Geoscience and Remote Sensing **51**, 1775 (2013).

[28] P. Marinkovic, V. Ketelaar, F. J. van Leijen, and R. F. Hanssen, *Insar quality control: Analysis of five years of corner reflector time series,* in *Fifth International Workshop on ERS/Envisat SAR Interferometry, 'FRINGE07', Frascati, Italy, 26 Nov-30 Nov 2007* (ESA Communication Production Office, 2008) pp. 1–8, niet eerder opgevoerd.

[29] T. Strozzi, P. Teatini, L. Tosi, U. Wegműller, and C. Werner, *Land subsidence of natural transitional environments by satellite radar interferometry on artificial reflectors,* Journal of Geophysical Research: Earth Surface **118**, 1177 (2013), https://agupubs.onlinelibrary.wiley.com/doi/pdf/10.1002/jgrf.20082 .

[30] N. Adam, B. Kampes, and M. Eineder, *Development of a scientific permanent scatterer system: Modifications for mixed ers/envisat time series,* Proceedings of the 2004 Envisat and ERS Symposium(ESA SP-572) (2004).

[31] G. Ketelaar, P. Marinkovic, and R. Hanssen, *Validation of point scatterer phase statistics in multipass insar, European Space Agency, (Special Publication) ESA SP*, (2004).

[32] J. Groot, *Letter: Cross section computation of trihedral corner reflectors with the geometrical optics approximation,* Emerging telecommunications technologies **3** (1992).

[33] A. W. Doerry, *Reflectors for sar performance testing,* report (2008).

[34] S. D. Robertson, *Targets for microwave radar navigation,* Bell System Technical Journal **26**, 852 (1947), https://onlinelibrary.wiley.com/doi/pdf/10.1002/j.1538-7305.1947.tb01325.x .

[35] H. v.d. Marel, *creaq.m,* Matlab script (2017).

[36] *Sentinel-1,* https://sentinel.esa.int/web/sentinel/missions/sentinel-1 (2018), accessed: 2018-09-06.

[37] N. Roozenburg and J. Eekels, *Product Design: Fundamentals and Methods* (1995).

[38] H. v.d. Marel, *Double back-flip corner reflector gnss antenna test result,* report (2017).

[39] N. van der Zon, *Kwaliteitsdocument ahn2,* http://www.ahn.nl/binaries/content/assets/hwh---ahn/common/wat+is+het+ahn/kwaliteitsdocument_ahn_versie_1_3.pdf (2013), accessed: 2018-09-06.

[40] *Ingeklemde balk puntlast in midden,* http://www.designerdata.nl/calculatoren/Doorbuiging/Ingeklemde+balk2C+puntlast+in+midden (2019), accessed: 2019-02-11.

[41] *Ingeklemde balk puntlast op eind,* http://www.designerdata.nl/calculatoren/Doorbuiging/Ingeklemde+balk2C+puntlast+op+eind (2019), accessed: 2019-02-11.

[42] R. Hibbeler, *Engineering Mechanics: Statics*, Engineering Mechanics No. v. 1 (Prentice-Hall, 1995).

[43] N. Hall, *The drag equation,* https://www.grc.nasa.gov/www/k-12/airplane/drageq.html (2015), accessed: 2019-02-14.

[44] KNMI, *Uurgegevens van het weer in nederland - download,* https://projects.knmi.nl/klimatologie/uurgegevens/selectie.cgi, accessed: 2019-02-12.

[45] E. ToolBox, *Linear thermal expansion,* https://www.engineeringtoolbox.com/linear-thermal-expansion-d_1379.html (2008), accessed: 2019-02-11.

[46] H. v.d. Marel, F. J. v. Leijen, and R. F. Hanssen, *Multiple frequency radar compact transponder (mute),* Report (2017).

[47] *Dinoloket,* https://www.dinoloket.nl/ (2018), accessed: 2018-06-18.

[48] T. Zajc, M. Azcueta, J. Ferreyra, and M. Thibeault, *A precise corner reflector characterizationtechnique,* Comision Nacionalde Actividades Espaciales (CEOS, 2017) presented at the CEOS WGCV SAR Subgroup.

[49] M. Schwerdt, K. Schmidt, G. Castellanos, N. T. Ramon, B. Dőring, P. Prats, and M. Zink, *Independent verification of the sentinel-1 system calibration,* (DLR, 2013) aSAR/CEOS Workshop 2013.

[50] H. v.d. Marel, *ahnview.m,* Matlab script (2017).